

Aus dem Fachbereich Medizinische Physiologie
Theoretische Medizin und Biowissenschaften der Medizinischen Fakultät
der Universität des Saarlandes, Homburg/Saar

**Functional Analysis of the Calcium-Dependent
Activator Protein for Secretion 1 and 2 in Primary
Mouse Dorsal Root Ganglion Neurons**

DISSERTATION

zur Erlangung des Grades eines Doktors der Naturwissenschaften der
Medizinischen Fakultät der UNIVERSITÄT DES SAARLANDES
2020

vorgelegt von Angelina Staudt
geboren am 21.10.1990 in Birkenfeld

Tag der Promotion: 16. April 2021
Dekan: Univ.-Prof. Dr. med. Michael D. Menger
Berichterstatter: PD Dr. rer. nat. Ute Becherer
Univ.-Prof. Dr. med. Frank Schmitz

Eidesstattliche Erklärung

Erklärung gemäß § 7 Abs. 1 Nr. 2

Ich erkläre hiermit an Eides statt, dass ich die vorliegende Arbeit ohne unzulässige Hilfe Dritter und ohne Benutzung anderer als der angegebenen Hilfsmittel angefertigt habe. Die aus anderen Quellen direkt oder indirekt übernommenen Daten und Konzepte sind unter Angabe der Quelle gekennzeichnet.

Bei der Auswahl und Auswertung folgenden Materials haben mir die nachstehend aufgeführten Personen in der jeweils beschriebenen Weise unentgeltlich geholfen:

1. Die Klonierung der CAPS1/2 Chimäre erfolgte durch Dr. Olga Ratai.
2. Der Western Blot von Chromaffinzellen transfiziert mit CAPS2-HA oder CAPS1/2-HA wurde von Dr. Hawraa Bzeih durchgeführt.
3. Die Kapazitätsmessungen an Chromaffinzellen wurden von Dr. Ahmed Shaaban im Labor von Jun.-Prof. Dr. Ralf Mohrmann (Physiologie, Zentrum für Human- und Molekularbiologie (ZHMB), Universität des Saarlandes) ausgeführt.
4. Die Virusproduktion erfolgte zusammen mit Margarete Klose.
5. Die Herstellung des Halo Liganden CA-ATTO590 wurde von Alexander Horn im Labor von Prof. Dr. Uli Kazmaier (Organische Chemie, Universität des Saarlandes) durchgeführt.
6. Die STED Mikroskopie wurde zusammen mit PD Dr. Ute Becherer durchgeführt und Aicha Bouzouina hat bei der Datenanalyse geholfen.
7. Die Bildbearbeitung der STED Daten erfolgte durch Jun.-Prof. Dr. Marcel Lauterbach.
8. Die Massenspektrometrie-Experimente wurden von Dr. Claudia Fecher-Trost im Labor von Prof. Dr. Veit Flockerzi (Experimentelle und Klinische Pharmakologie und Toxikologie, Präklinisches Zentrum für Molekulare Signalverarbeitung (PZMS), Universität des Saarlandes) durchgeführt.

Weitere Personen waren an der inhaltlich-materiellen Erstellung der vorliegenden Arbeit nicht beteiligt. Insbesondere habe ich nicht die entgeltliche Hilfe von Vermittlungs- bzw. Beratungsdiensten (Promotionsberater/innen oder anderer Personen) in Anspruch genommen.

Außer den Angegebenen hat niemand von mir unmittelbar oder mittelbar geldwerte Leistungen für Arbeiten erhalten, die im Zusammenhang mit dem Inhalt der vorgelegten Dissertation stehen.

Die Arbeit wurde bisher weder im Inland noch im Ausland in gleicher oder ähnlicher Form in einem anderen Verfahren zur Erlangung des Doktorgrades einer anderen Prüfungsbehörde vorgelegt.

Ich versichere an Eides statt, dass ich nach bestem Wissen die Wahrheit gesagt und nichts verschwiegen habe.

Die Bedeutung der eidesstattlichen Versicherung und die strafrechtlichen Folgen einer unrichtigen oder unvollständigen eidesstattlichen Erklärung sind mir bekannt.

Homburg, 16.10.2020

(Unterschrift der/des Promovierenden)

(Unterschrift der die Versicherung an Eides statt aufnehmenden Beamtin bzw. des aufnehmenden Beamten)

Danksagung

Es gibt eine Reihe von Menschen, ohne deren praktische, theoretische und emotionale Unterstützung diese Arbeit niemals möglich gewesen wäre.

Ich danke **Prof. Dr. Jens Rettig**, dass ich in seinem Labor arbeiten durfte. Es war ein großartiger Ort für mich, um zu lernen und zu wachsen, meine Stärken und Schwächen zu entdecken und erstaunliche Menschen kennen zu lernen. Ganz besonders möchte ich meiner Doktormutter **Dr. Ute Becherer** dafür danken, dass sie mir eine Stelle in ihrer Arbeitsgruppe zur Verfügung gestellt und mich durch meine Doktorarbeit geführt hat. Sie hat es geschafft meinen Geist zu beflügeln und mich für meine Experimente zu begeistern. Ich danke ihr, dass sie mich stets motiviert hat, mir aber auch den Freiraum gegeben hat, meine eigenen Denkweisen zu entwickeln. Ich möchte **Dr. David Stevens, Dr. Claudia Schirra, Dr. Elmar Krause, Dr. Varsha Pattu, Dr. Hsin-Fang Chang** und **Jun.-Prof. Dr. Marcel Lauterbach** für ihre Unterstützung und Hilfe bei der Durchführung der Experimente und für ihren wissenschaftlichen Beitrag zu meiner Arbeit danken. Darüber hinaus möchte ich mich bei **Prof. Dr. Dieter Bruns** und allen seinen Labormitarbeitern für die hilfreichen Diskussionen und die gute Zusammenarbeit bedanken.

Viele weitere phantastische Kollegen waren für meine Doktorarbeit unentbehrlich, indem sie ihr Fachwissen zur Verfügung stellten, technische Ratschläge gaben, Präsentationen kommentierten und den Druck erleichterten. Mein besonderer Dank gilt **Dr. Olga Ratai, Dr. Marwa Sleiman, Dr. Praneeth Chitirala, Keerthana Ravichandran, Nadia Alawar** und **Aicha Bouzouina** für ihre Freundschaft, Unterstützung und ihr Mitgefühl. Außerdem möchte ich mich für die unbegrenzte technische Hilfe und Unterstützung im Labor von **Margarete Klose, Anja Bergsträßer, Nicole Rothgerber, Katrin Sandmeier, Silke Bruns-Engers** und **Tamara Brück** bedanken. Ein besonderer Dank geht an Margarete Klose, für die enorme Unterstützung und herausragende Arbeit in der Zellkultur und bei der Virus-Herstellung. Ebenso bedanke ich mich bei **Bernadette Schwarz** und **Andrea Berger** für ihre Hilfe und Unterstützung, insbesondere bei der Papierarbeit.

Meinen tiefen und aufrichtigen Dank für die Unterstützung möchte ich meiner Familie und meinen wunderbaren Freunden aussprechen. Meinen Eltern, **Volker** und **Margret**, möchte ich dafür danken, dass sie mir immer die Freiheit gegeben haben, meine eigenen Entscheidungen

zu treffen. Ihr Beistand und die Schaffung aller Möglichkeiten haben mir geholfen, dorthin zu gelangen, wo ich jetzt bin. Ein besonderer Dank geht auch an meine Geschwister, **Vivien** und **Julian**, die mir immer hilfsbereit zur Seite stehen. Von ganzem Herzen möchte ich **Jonas** für all seine Ratschläge, seine Geduld und seine Umarmungen danken, als ich sie wirklich brauchte.

Table of Contents

List of Abbreviations	IV
List of Figures	IX
List of Tables	XI
Abstract	XII
Zusammenfassung	XIV
1 Introduction	1
1.1 Spinal cord	1
1.1.1 Dorsal root ganglion neurons	2
1.2 Neuronal communication and exocytosis	4
1.2.1 Synaptic vesicle exocytosis	5
1.2.2 Large dense core vesicle exocytosis	5
1.2.3 Molecular mechanisms regulating vesicle exocytosis.....	6
1.3 Identification and characterization of CAPS proteins	8
1.3.1 CAPS protein domain structure and expression	8
1.3.2 CAPS function.....	10
1.4 Rationale and aims of the project	11
2 Materials and Methods	12
2.1 Materials	12
2.1.1 Chemicals	12
2.1.2 Enzymes	14
2.1.3 Solutions	15
2.1.4 Antibodies.....	20
2.1.5 Oligonucleotides	21
2.1.6 Plasmids.....	23
2.1.7 Bacteria.....	23
2.1.8 Cell lines	23

2.1.9	Mouse strains	23
2.1.10	Kits	24
2.1.11	Consumables.....	24
2.1.12	Devices	25
2.1.13	Total internal reflection fluorescence microscope.....	27
2.1.14	Software.....	27
2.1.15	Companies	28
2.2	Methods	29
2.2.1	Genotyping	29
2.2.2	Cloning	30
2.2.3	Bacterial transformation using heat shock	41
2.2.4	Primary cell culture of adult mouse DRG neurons.....	41
2.2.5	Primary cell culture of embryonic mouse DRG neurons	42
2.2.6	Primary co-culture of DRG/SC neurons.....	42
2.2.7	Lentivirus production	43
2.2.8	Halo ligand chloroalkane-ATTO590 staining.....	45
2.2.9	Immunocytochemistry	45
2.2.10	Double immunocytochemistry	46
2.2.11	Preparing protein lysates	47
2.2.12	Immunoprecipitation	47
2.2.13	Western blot.....	48
2.2.14	Laser scanning microscopy	48
2.2.15	Stimulated emission depletion microscopy.....	49
2.2.16	Total internal reflection fluorescence microscopy	51
2.2.17	Confocal image analysis.....	53
2.2.18	3D STED image analysis.....	53
2.2.19	TIRF image analysis.....	54

2.2.20	Mass spectrometry data analysis	55
2.2.21	Statistics.....	55
3	Results.....	56
3.1	Sequence alignment of CAPS paralogs reveals heterogeneity in the N-terminus.....	56
3.2	CAPS1 is present at synaptic and extra-synaptic sites	59
3.3	Functional analysis of a CAPS1/2 chimera in comparison to CAPS1 and CAPS2...61	
3.4	A role for CAPS1 N-terminal sequence in protein distribution.....	64
3.5	The CAPS1 N-terminal sequence influences localization at synapses.....	65
3.6	STED microscopy indicates a role of the CAPS1 N-terminus in protein localization near active zones.....	68
3.7	Functional analysis of CAPS paralogs in SV and LDCV exocytosis.....	71
3.7.1	The absence of CAPS2 has no effect on SV or LDCV fusion in DRG neurites	72
3.7.2	Both CAPS1 KO and CAPS dKO reduce synaptic transmission but only CAPS dKO decreases the total number of LDCV fusion events in DRG neurites	76
3.8	SV exocytosis is rescued by CAPS1 but not by CAPS2 or CAPS1/2 chimera	80
3.9	Identification of putative CAPS-interacting proteins using immunoprecipitation and mass spectrometry	82
3.9.1	CAPS1 IP and MS analysis	83
3.9.2	CAPS2 IP and MS analysis	86
4	Discussion	89
4.1	Differences in the N-terminus of the CAPS protein family.....	90
4.2	The differential subcellular CAPS localization is determined by its N-terminus.....	91
4.3	The specific function of CAPS in the exocytosis of LDCVs and SVs.....	93
4.4	Identification of putative CAPS-interacting proteins	96
5	Outlook	99
	References.....	XXIII
	Publications and Conferences	XXXII
	Curriculum Vitae.....	Error! Bookmark not defined.

List of Abbreviations

%	Percent
°C	Degrees Celsius
µg	Microgram
µL	Microlitre
µM	Micromolar
µm	Micrometre
2D	Two-dimensional
3D	Three-dimensional
aa	Amino acid
ATP	Adenosine triphosphate
AU	Airy unit
BDNF	Brain-derived neurotrophic factor
BLAST	Basic local alignment search tool
bp	Base pairs
BSA	Bovine serum albumin
<i>C. elegans</i>	<i>Caenorhabditis elegans</i>
CA	Chloroalkane
Ca ²⁺	Calcium ion
CaCl ₂	Calcium chloride
CAPS	Calcium-dependent activator protein for secretion
CGRP	Calcitonin gene-related peptide
CID	Collision-induced dissociation
cm ²	Square centimetre
CNS	Central nervous system
CO ₂	Carbon dioxide
DBD	Dynactin binding domain
DCTN1	Dynactin subunit 1
DCV	Dense core vesicle
DH	Dispase high
DIV	Day(s) <i>in vitro</i>
dKO	Double knock-out
DMEM	Dulbecco's modified eagle medium

DNA	Deoxyribonucleic acid
DNase	Deoxyribonuclease
dNTP	Deoxyribonucleotide triphosphate
DP	Depot pool
DPBS	Dulbecco's phosphate buffered saline
DRG	Dorsal root ganglion
E	Embryonic day
EBSS	Earle's balanced salt sodium
EDTA	Ethylenediaminetetraacetic acid
eGFP	Enhanced green fluorescent protein
EndoFree	Endotoxin-free
EPSC	Excitatory postsynaptic current
ESI	Electrospray ionization
Fab	Fragment antigen-binding
FCS	Fetal calf serum
FDR	False discovery rate
FUDR	Floxuridine
GABA	Gamma-aminobutyric acid
GDP	Guanosine diphosphate
GEP	GDP/GTP exchange protein
GTP	Guanosine triphosphate
H+L	Heavy+light
H ₂ O	Water
H ₂ O _{dd}	Double-distilled water
HA	Hemagglutinin
Halo	HaloTag
HBS	Hepes-buffered saline
HEK	Human embryonic kidney
HEPES	N-2-hydroxyethylpiperazine-N-ethanesulfonic acid
HRP	Horseradish peroxidase
ICC	Immunocytochemistry
IgG	Immunoglobulin G
IP	Immunoprecipitation

kb	Kilobase
KCl	Potassium chloride
Kd	Dissociation constant
kDa	Kilodalton
KIF5B	Kinesin-I heavy chain
KO	Knock-out
L	Litre
LB	Lysogeny broth
LC	Liquid chromatography
LDCV	Large dense core vesicle
LDS	Lithium dodecyl sulfate
LSM	Laser scanning microscope
M	Molar
MAP6	Microtubule-associated protein 6
mg	Milligram
Mg ²⁺	Magnesium ion
MgCl ₂	Magnesium chloride
MgSO ₄	Magnesium sulfate
MHD	Munc13-homology domain
MHz	Megahertz
min	Minute(s)
mL	Millilitre
mM	Millimolar
mm	Millimetre
mmol	Millimole
Munc13	Mammalian uncoordinated-13
Munc18	Mammalian uncoordinated-18
mW	Milliwatt
NA	Numerical aperture
Na ₂ HPO ₄	Disodium phosphate
NaCl	Sodium chloride
NaH ₂ PO ₄	Monosodium phosphate
NaHCO ₃	Sodium bicarbonate

NBA	Neurobasal-A
NEAA	Non-essential amino acids
NF	Neurofilament
NFM	Neurofilament medium polypeptide
ng	Nanogram
NGF	Nerve growth factor
NGS	Normal goat serum
NH ₄ Cl	Ammonium chloride
nm	Nanometre
no.	Number
NPY	Neuropeptide Y
Osm	Osmoles
P	Postnatal day
p	Probability value
PBS	Phosphate buffered saline
PCR	Polymerase chain reaction
PDL	Poly-D-lysine
PFA	Paraformaldehyde
Pfam	Protein families
<i>Pfu</i>	<i>Pyrococcus furiosus</i>
PH	Pleckstrin homology
pH	Potential of hydrogen
pLenti	Lentivirus plasmid
pmol	Picomole
ps	Picosecond
PSF	Point spread function
pSFV	Semliki Forest virus plasmid
rcf	Relative centrifugal force
RIM	RAB3A-interacting molecule
RNA	Ribonucleic acid
ROI	Region of interest
rpm	Revolutions per minute
RRP	Readily releasable pool

RT	Room temperature
SC	Spinal cord
SDS	Sodium dodecyl sulfate
sec	Second
SMART	Simple modular architecture research tool
SNAP	Synaptosomal-associated protein
SNARE	Soluble N-ethylmaleimide-sensitive factor attachment receptor
SRR	Slowly releasable pool
STED	Stimulated emission depletion
STED	Stimulated emission depletion
SV	Synaptic vesicle
SypHy	Synaptophysin-pHluorin
<i>Taq</i>	<i>Thermus aquaticus</i>
TBS	Tris-buffered saline
TBST	Tris-buffered saline + Tween 20
TH	Tyrosine hydroxylase
TIRF	Total internal reflection fluorescence
t-SNARE	Target-soluble N-ethylmaleimide-sensitive factor attachment receptor
U	Units
UNC	Uncoordinated
UniProt	Universal protein
UPP	Unprimed pool
UV	Ultraviolet
V	Volt
VAMP	Vesicle-associated membrane protein
vs.	Versus
v-SNARE	Vesicle-soluble N-ethylmaleimide-sensitive factor attachment receptor
WB	Western blot
WT	Wild-type

List of Figures

Figure 1: Cross-sectional anatomy of the spinal cord.	2
Figure 2: Structure of typical mammalian neurons.	4
Figure 3: Molecules involved in calcium-dependent exocytosis.....	7
Figure 4: The domain structure of mouse CAPS1 protein.	9
Figure 5: Vector maps with restriction enzymes BamHI, ClaI and NheI used for cloning of (A) pLenti-CAPS2b-Halo and (B) pLenti-CAPS1/2 chimera-Halo.....	36
Figure 6: Vector map with restriction enzymes BamHI and NheI used for cloning of pLenti-CAPS1-Halo.	40
Figure 7: The principle of STED microscopy.	50
Figure 8: Sequence alignment of the N-terminus of CAPS paralogs.....	56
Figure 9: Sequence alignment of the N-terminus of CAPS1 between different species.....	58
Figure 10: Sequence alignment of the N-terminus of CAPS1 and Cytohesin-1.	58
Figure 11: CAPS1 clusters are present at synaptic and extra-synaptic sites.	60
Figure 12: CAPS1/2 chimera is correctly expressed and functional.	62
Figure 13: All CAPS-Halo constructs are equally expressed at about twice the endogenous level. (A) Images of DRG CAPS dKO neurons expressing CAPS1-, CAPS2- or CAPS1/2 chimera-Halo co-cultured with SC WT neurons.	63
Figure 14: CAPS1/2 chimera mimics the CAPS1 distribution pattern.	65
Figure 15: CAPS1 N-terminal sequence determines synaptic localization.....	67
Figure 16: 3D STED microscopy resolves CAPS1 N-terminus function in CAPS1 accumulation near active zones.....	70
Figure 17: CAPS2 has no effect on SV fusion in DRG neurons.....	73
Figure 18: CAPS2 KO has no effect on LDCV fusion in DRG neurites.	75
Figure 19: CAPS dKO and CAPS1 KO reduce SV fusion in DRG neurons.	77
Figure 20: CAPS dKO reduces LDCV fusion in DRG neurites.	79
Figure 21: CAPS1 expression rescues SV fusion in DRG CAPS dKO neurons.....	81
Figure 22: IP and MS analysis of CAPS1 from mouse brain.....	83
Figure 23: The CAPS1 protein is detected after IP by nano-liquid chromatography (LC)-MS/MS.	84
Figure 24: Volcano plot of p-value vs. x-fold change of identified peptide spectrum counts displaying enriched proteins after IP with anti-CAPS1 or anti-rabbit IgG antibodies.....	85
Figure 25: IP and MS analysis of CAPS2 from mouse cerebellum.	86

Figure 26: The CAPS2 protein is detected after IP by nano-LC-MS/MS.....87

Figure 27: Volcano plot of p-value vs. x-fold change of identified peptide spectrum counts displaying enriched proteins after IP with anti-CAPS2 or anti-rabbit IgG antibodies.....88

List of Tables

Table 1: PCR mix for CAPS1 genotyping.....	29
Table 2: PCR mix for CAPS2 genotyping.....	29
Table 3: PCR programme for CAPS1 genotyping.	29
Table 4: PCR programme for CAPS2 genotyping.	30
Table 5: PCR mix for pHuji amplification.	31
Table 6: PCR programme for pHuji amplification.....	31
Table 7: Restriction digestion mix for pHuji and pLenti NPY-Venus.....	31
Table 8:Ligation mix for pHuji and pLenti NPY.	32
Table 9: Mix for A-tailing of Halo PCR product.	33
Table 10: Ligation mix for Halo and pGEM-T.	34
Table 11: Restriction digestion mix for pGEM-T-Halo, pSFV-CAPS2b-eGFP, pSFV-CAPS1/2 chimera-eGFP and pLenti NPY-Venus.	34
Table 12: Ligation mix for CAPS2b or CAPS1/2 chimera and Halo.....	35
Table 13: Ligation mix for pLenti vector to add to CAPS2b- or CAPS1/2 chimera-Halo.	36
Table 14: PCR mix for CAPS1 amplification.	37
Table 15: PCR programme for CAPS1 amplification.	37
Table 16: PCR mix for Halo amplification.	37
Table 17: PCR programme for Halo amplification.	38
Table 18: Overlap extension PCR mix for CAPS1-Halo amplification.....	38
Table 19: Overlap extension PCR programme for CAPS1-Halo amplification.....	39
Table 20: Restriction digestion mix for PCR CAPS1-Halo and pLenti NPY-Venus.	39
Table 21 Ligation mix for CAPS1-Halo and pLenti.	40

Abstract

The calcium-dependent activator protein for secretion (CAPS) plays a central role in the secretion of neurotransmitters, neuropeptides, trophic factors or hormones in neurons and neuroendocrine cells. Two paralogs, CAPS1 and CAPS2, are expressed in mammals. Despite high sequence identity, they have redundant expression and function in neuroendocrine cells, but are almost mutually exclusive in neurons. In dorsal root ganglion (DRG) neurons, both paralogs are expressed. While CAPS1 is found in the majority of neurons, CAPS2 is expressed in a smaller population, the so-called peptidergic neurons.

In the present work, a detailed analysis of the different subcellular localizations of CAPS1 and CAPS2 was carried out. Accordingly, the studies were designed on CAPS double knock-out (dKO) DRG neurons that exogenously expressed either CAPS1- or CAPS2-HaloTag and were co-cultured with spinal cord (SC) neurons. Live-cell staining of CAPS-HaloTag was subsequently performed with the ATTO590 HaloTag ligand, which was visualized in confocal, 2D and 3D stimulated emission depletion (STED) microscopy. While CAPS2 accumulated in the soma of DRG neurons and showed a weak diffuse distribution in their neurites, CAPS1 was strongly enriched at synapses. More importantly, sequence analysis of CAPS paralogs detected a strong heterogeneity in the N-terminus and revealed a unique CAPS1 domain of eleven amino acids in a putative coiled coil region that is not present in CAPS2. To investigate the function of this unique N-terminal sequence in protein localization, a CAPS1/2 chimera was generated by introducing these 11 amino acids from CAPS1 into CAPS2. The direct comparison of the exogenous expression of CAPS1, CAPS2 and CAPS1/2 chimera revealed a function of this domain in protein localization, because the CAPS1/2 chimera had the same subcellular distribution as CAPS1.

Based on the hypothesis that differential localization also leads to specific functions, the role of CAPS paralogs in the fusion of large dense core vesicles (LDCVs) and synaptic vesicles (SVs) was investigated. The analyses showed that LDCV fusion in DRG neurites can be mediated by either CAPS1 or CAPS2, whereas synaptic transmission is mainly promoted by CAPS1. Both the CAPS1/2 chimera and CAPS2 were not able to rescue synaptic transmission in CAPS dKO DRG neurons to the same extent as CAPS1. Thus, the unique N-terminal CAPS1 sequence does not appear to be involved in SV priming, although a role in the localization of the protein at synapses was shown. By immunoprecipitation and mass spectrometry, putative CAPS1 binding partners could be identified, which are involved in intracellular transport processes and thus might also play a role in the localization of the protein.

Taken together, a new N-terminal sequence in CAPS1 was identified, which induces its specific subcellular localization at synapses. The understanding of the molecular mechanisms of transport and localization of synaptic proteins is of great interest to many scientists working on synaptic transmission and more generally on regulated exocytosis.

Zusammenfassung

Das Protein Calcium-dependent activator protein for secretion (CAPS) spielt eine zentrale Rolle bei der Sekretion von Neurotransmittern, Neuropeptiden, trophischen Faktoren oder Hormonen in Neuronen und neuroendokrinen Zellen. Zwei Paraloge, CAPS1 und CAPS2, werden in Säugetieren exprimiert. Trotz hoher Sequenzidentität haben sie eine redundante Expression und Funktion in neuroendokrinen Zellen, schließen sich jedoch in Neuronen fast gegenseitig aus. In Neuronen des dorsalen Wurzelganglions (engl. Dorsal Root Ganglion, DRG) werden beide Paraloge exprimiert. Während CAPS1 in der Mehrheit der Neuronen vorkommt, wird CAPS2 in einer kleineren Population, den so genannten peptidergen Neuronen, exprimiert.

In der vorliegenden Arbeit wurde eine detaillierte Analyse der unterschiedlichen subzellulären Lokalisationen von CAPS1 und CAPS2 durchgeführt. Die entsprechenden Studien wurden an CAPS Doppel Knockout (dKO) DRG Neuronen konzipiert, die exogen entweder CAPS1- oder CAPS2-HaloTag exprimierten und mit Neuronen des Rückenmarks (engl. spinal cord, SC) ko-kultiviert wurden. Die Lebendzellfärbung von CAPS HaloTag wurde anschließend mit dem ATTO590 HaloTag Liganden durchgeführt, der in konfokaler, 2D- und 3D-Stimulated Emission Depletion (STED)-Mikroskopie visualisiert wurde. Während CAPS2 sich im Soma von DRG Neuronen anreichert und eine schwach diffuse Verteilung in deren Neuriten zeigt, ist CAPS1 an den Synapsen stark angereichert. Darüber hinaus wurde durch eine Sequenzanalyse der CAPS Paraloge eine Heterogenität im N-Terminus identifiziert, die auf eine einzigartige CAPS1 Domäne von elf Aminosäuren in einer mutmaßlichen Coiled-coil-Region hinweist, die in CAPS2 nicht vorhanden ist. Um die Funktion dieser einzigartigen N-terminalen Sequenz bei der Proteinlokalisierung zu untersuchen, wurde eine CAPS1/2-Chimäre erzeugt, indem die spezifischen 11 Aminosäuren von CAPS1 in CAPS2 eingeführt wurden. Interessanterweise wurde bei einem direkten Vergleich der exogenen Expression von CAPS1, CAPS2 und der CAPS1/2-Chimäre eine potentielle Funktion dieser Domäne bei der Proteinlokalisierung bestätigt, da die CAPS1/2-Chimäre die gleiche subzelluläre Verteilung wie CAPS1 aufwies.

Basierend auf der Hypothese, dass eine differentielle Lokalisation auch zu spezifischen Funktionen führt, wurde die Rolle der CAPS Paraloge bei der Fusion von elektronendichten Granula (engl. Large Dense Core Vesicle, LDCV) und synaptischen Vesikeln (SV) untersucht. Die Analysen zeigten, dass die LDCV Fusion in DRG Neuriten in gleichermaßen von CAPS1 oder CAPS2 vermittelt werden kann, wohingegen die synaptische Übertragung hauptsächlich durch CAPS1 gefördert wird. Sowohl die CAPS1/2-Chimäre als auch CAPS2 waren nicht in

der Lage, die reduzierte synaptische Übertragung in CAPS dKO DRG-Neuronen im gleichen Maße zu erhöhen wie CAPS1. Eine Funktion der spezifischen N-terminalen CAPS1 Sequenz bei der synaptischen Übertragung konnte somit nicht beobachtet werden, obwohl eine Rolle bei der Lokalisierung des Proteins an Synapsen gezeigt wurde. Durch Immunpräzipitation und Massenspektrometrie konnten mutmaßliche CAPS1 Bindungspartner identifiziert werden, die unter anderem an intrazellulären Transportprozessen beteiligt sind und somit auch eine Rolle bei der Lokalisation des Proteins spielen könnten.

Zusammengenommen wurde eine neue N-terminale Sequenz in CAPS1 identifiziert, die dessen spezifische subzelluläre Lokalisation an Synapsen induziert. Die Aufklärung der molekularen Mechanismen des Transports und der Lokalisierung synaptischer Proteine ist für viele Wissenschaftler von großem Interesse, die sich mit der synaptischen Übertragung und ganz allgemein mit der regulierten Exozytose befassen.

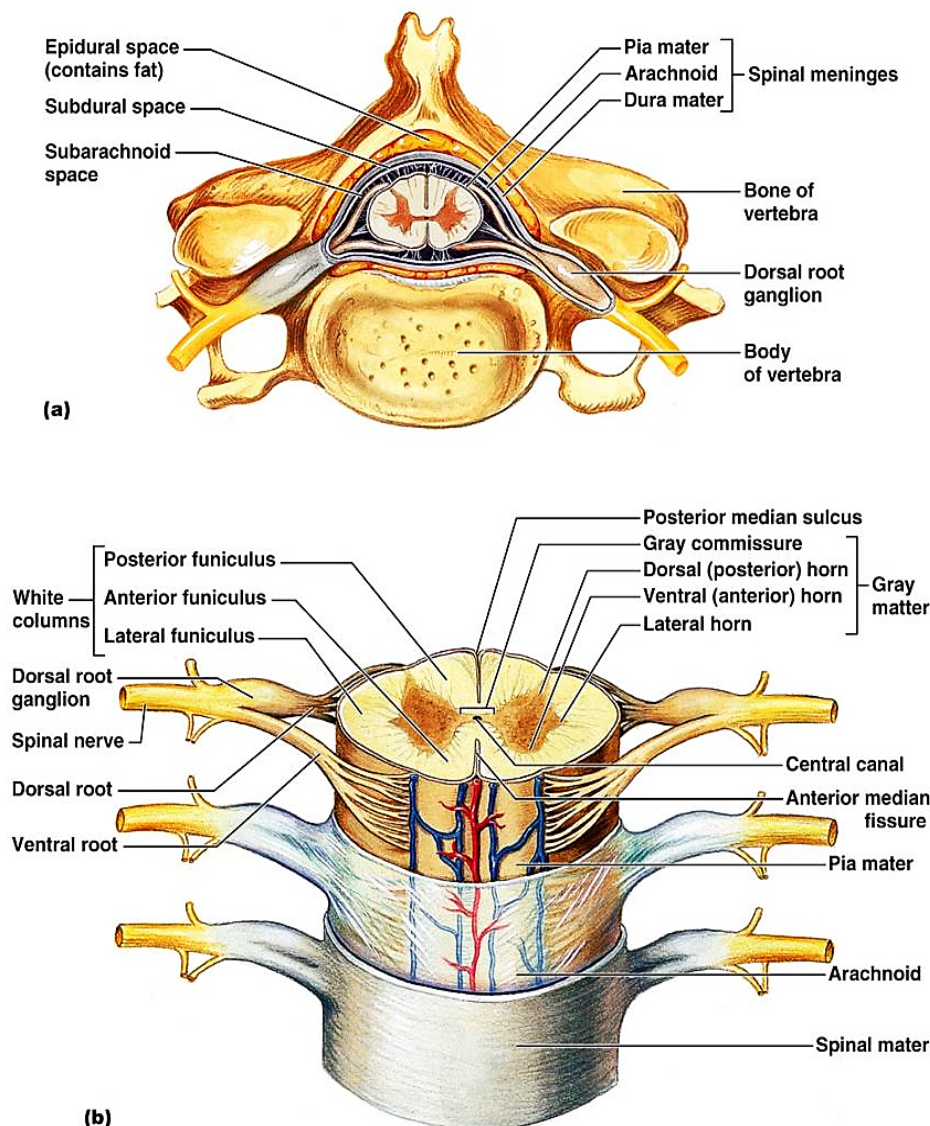
1 Introduction

1.1 Spinal cord

The spinal cord (SC) provides the connection between the brain and the body. In humans, it reaches a length of about 42 cm and a diameter of around 1.8 cm. The SC is protected by bone, meninges and cerebrospinal fluid (Figure 1A). Between the bony walls of the vertebral column and the spinal dura mater is an epidural space filled with fat and a network of veins. The cerebrospinal fluid fills the subarachnoid space between the arachnoid and pia mater meninges. Two consecutive rows of nerve roots emerge laterally from the SC. These nerve roots connect distally and build 31 pairs of spinal nerves (Marieb and Hoehn, 2007). These nerves are divided into 8 cervical, 12 thoracic, 5 lumbar, 5 sacral and 1 coccygeal nerve. The dorsal and ventral roots enter and exit the spinal column through the intervertebral foramen at the vertebral segments. Each segment of the SC innervates a different region of the body. This area of skin supplied by peripheral nerve fibres from a single dorsal root ganglion is called dermatome (Altman and Bayer, 2001).

The dorsal root contains afferent axons that forward visceral and somatic sensory information from peripheral receptors to the central nervous system (CNS). The ventral roots arise from motor neurons in the ventral horn of the SC and innervate skeletal muscles. The ventral and dorsal roots axons merge to form mixed afferent and efferent peripheral nerves (Mills and Marchant-Forde, 2010). A cross section of the SC shows a peripheral mass of white matter, grey matter located medially, and a small central canal (Figure 1B).

The white matter consists mostly of myelinated axons arranged in bundles called tracts or pathways (Solomon et al., 2014). It is divided into the dorsal, lateral and ventral column and contains three different types of nerve fibres: long ascending nerve fibres making synaptic connections to neurons in the brain, long descending nerve fibres that synapse with neurons in the SC grey matter and shorter nerve fibres interconnecting various SC levels (Mills and Marchant-Forde, 2010). The grey matter is divided into dorsal, lateral and ventral horns. The dorsal horns contain somatosensory neurons that receive and process information and transmit it to the brain. The lateral horns contain the preganglionic visceral motor neurons that project to the sympathetic ganglia. The ventral horns contain cell bodies of motor neurons that innervate the skeletal muscles (Purves et al., 2000).



Copyright © 2006 Pearson Education, Inc., publishing as Benjamin Cummings.

Figure 1: Cross-sectional anatomy of the spinal cord. (A) Relationship to the vertebra, meninges, and spinal nerves. (B) Detail of the SC, meninges, and spinal nerves (Marieb and Hoehn, 2007).

1.1.1 Dorsal root ganglion neurons

Dorsal root ganglion (DRG) neurons are sensory neurons located in the dorsal root of a spinal nerve that provide information from the periphery to the CNS. These neurons have a pseudo-unipolar morphology. They contain a peripheral axon, the end of which is located in the skin, muscles or joints, and a central axon, which transmits stimuli to the SC (Pope et al., 2013). The cell bodies of the DRG neurons are tightly associated with satellite glial cells via gap junctions (Ji et al., 2013). According to their sensory perception DRG neurons can be roughly divided into four different groups: nociceptors, thermoreceptors, mechanoreceptors or proprioceptors. Nociceptors and thermoreceptors are rather small sensory neurons with a diameter of less than

30 μm and thinly myelinated ($A\delta$) or non-myelinated (C) axons. Thermoreceptors respond to temperature changes that are considered harmless whereas nociceptors respond to harmful mechanical, chemical or thermal stimuli. Different types of DRG cells can be identified by the expression of different markers, including calcitonin gene-related peptide (CGRP), substance P and tyrosine hydroxylase (TH) (Ju et al., 1987; Li et al., 2011). The expression of neuropeptides is also used to classify nociceptors as peptidergic or non-peptidergic (Le Pichon and Chesler, 2014). The non-peptidergic class can also be distinguished by binding of the histological marker isolectin IB4 (Wang et al., 1994; Averill et al., 1995). Nevertheless, some overlap between these markers exists making them only partially selective (Abraira and Ginty, 2013; McCoy et al., 2013). Large DRG neurons transmit mechanoreceptive and proprioceptive signals and can be distinguished by the expression of neurofilament 200 (NF200) (Goldstein et al., 1991; Fornaro et al., 2008). Though mechanoreceptors typically are larger in diameter ($> 50 \mu\text{m}$) and have thickly myelinated axons ($A\beta$), some have thinly myelinated ($A\delta$) or non-myelinated (C) axons. They innervate the dermal and epidermal regions of the skin where they sense mechanical stimuli, such as vibration and touch (Fleming and Luo, 2013; Le Pichon and Chesler, 2014). Proprioceptors innervate skeletal muscle tissue to provide sensory feedback information on muscle length and tension. They have myelinated fibres ($A\alpha$) with large diameter and high velocity (Ernsberger, 2009; Le Pichon and Chesler, 2014).

More recently, multiple efforts have been made to analyse the transcriptome of DRG neurons. Low-coverage single-cell RNA-sequencing was performed and mouse DRG neurons were further classified into two peptidergic types, three non-peptidergic types, one TH-positive type and five NF200-positive types within the traditional classification framework (Usoskin et al., 2015). A further study used high-coverage RNA-sequencing in combination with *in vivo* patch clamp recording and single-cell PCR to classify mouse DRG neurons. They revealed 10 different types and 14 subordinate subtypes with distinct transcriptional patterns, molecular markers and functional annotations. This approach identified more neuronal types and subtypes than did the previous classifications of DRG neurons and demonstrates the diversity of sensory neurons (Li et al., 2016).

DRG neurons use the excitatory neurotransmitter glutamate, which they release at synapses from synaptic vesicles (SVs) into the synaptic cleft, for signal transduction in the SC (Malet and Brumovsky, 2015). In addition to glutamate, peptidergic neurons release a broad range of neuromodulators via large dense core vesicles (LDCVs) and thus perform autocrine as well as paracrine functions (Landry et al., 2003).

1.2 Neuronal communication and exocytosis

Like all organ systems, the nervous system can fulfil its important functions, because the cells within the nervous system have special properties that allow them to carry out their unique role. These cells are specialized in how they work individually but also how they are connected to each other. Within the nervous system one can distinguish between two cell types. Neurons, which are predominantly responsible for communication and integration in the nervous system, and glia cells, which protect neurons, but also modify their functions (Mason, 2017).

Neurons have distinct regions that carry out the different functions of communication and integration: the cell body or soma, the dendrites, the axon, and the axon terminals. Figure 2 illustrates the structure of some typical mammalian neurons. Multipolar interneurons in (A) have branched dendrites, that receive signals from other cells and transmit them through a single long axon. Most sensory neurons, as shown in (B), are pseudo-unipolar, meaning they have only one axon, which is split into two branches right after it leaves the cell soma. The peripheral branch carries the incoming impulse from the receptor cell and the central branch transmits the signal to the target cell. Both branches are structurally similar except at their terminal portions. In contrast to other neurons, sensory neurons do not have dendrites (Lodish et al., 2000).

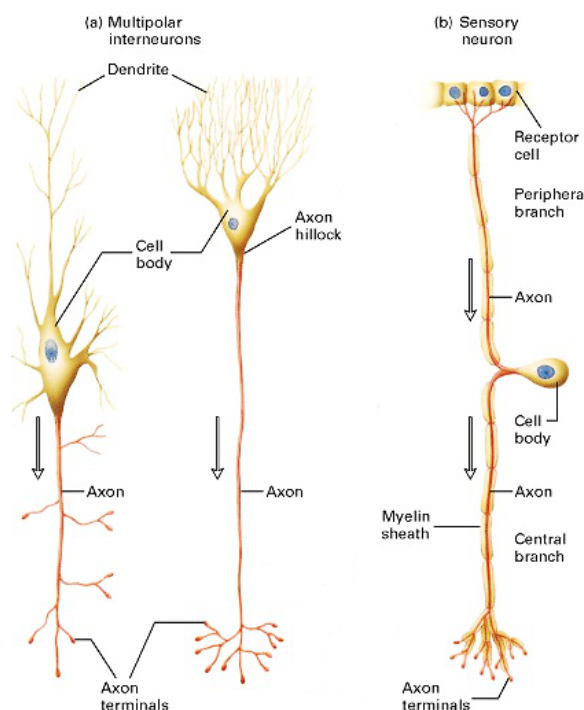


Figure 2: Structure of typical mammalian neurons. (A) Multipolar interneurons with the strongly branched dendrites, a single long axon and the axon terminals. (B) A sensory neuron with an axon that branches immediately after leaving the cell body. The peripheral branch carries the nerve impulse from the receptor cell to the cell body and the central branch carries the impulse from the cell body to the spinal cord or brain. The arrows indicate the direction of the action potentials (modified from(Lodish et al., 2000)).

1.2.1 Synaptic vesicle exocytosis

Neurons communicate with each other via specialized connections called synapses. Two types of synapses have been identified: electrical and chemical. At electrical synapses, gap junctions connect the cytoplasm of adjacent neurons and allow the bidirectional passage of ions between the cells. Electrical synapses are unusual in the adult mammalian nervous system, where most of the synapses transmit chemical signals. A chemical synapse has a complex architecture, but is in general composed of three components, the terminal of the presynaptic axon, the synaptic cleft and the postsynapse of a target cell.

In the axonal terminals of the presynaptic neuron, chemical neurotransmitters are packaged into SVs, and clustered at the active zone, where the release of neurotransmitters occurs. The initial signal is an electric current in the form of an action potential that reaches a chemical synapse and causes the opening of voltage-sensitive calcium channels, which leads to an increase in local intracellular calcium concentration and triggers SV exocytosis. Once the neurotransmitters are released, they diffuse across the synaptic cleft and bind to receptors located on the postsynaptic neuron. The binding of neurotransmitters to their receptors leads to the opening (or closing) of specific ion channels or to the activation of intracellular signals that modify the membrane activity of the postsynaptic cell (Rhoades and Bell, 2009).

1.2.2 Large dense core vesicle exocytosis

Besides SV exocytosis at synapses, LDCV exocytosis of neuropeptides, hormones and amines allows communication in neurons as well (Martin, 1994). In contrast to SVs, LDCVs have no defined region in the cell where they release their contents and can therefore fuse at the cell soma, dendrites or axon.

Conventional neurotransmitter release from SVs occurs close to the site of calcium entry while neuropeptides in LDCVs are released at greater distances from the calcium entry site (Martin, 2003). Thus, it takes longer to reach the intracellular calcium concentration of about 3-10 μM needed to initiate their release (Huang and Neher, 1996). Moreover, the life cycle of LDCVs in the cell is different compared to SVs. While SVs can be locally recycled at the synapse to ensure fast transmission, immature LDCVs are de novo produced in the cell soma and transported to the desired location while undergoing maturation steps. After exocytosis, LDCV membrane components are either destroyed or transported back to the cell soma for reuse. Therefore, no recycling of the LDCV content occurs at their release site (Brady et al., 2012).

1.2.3 Molecular mechanisms regulating vesicle exocytosis

Exocytosis of both SVs and LDCVs is mediated by similar molecular mechanisms. The vesicles filled with neurotransmitters, neuropeptides or hormones translocate to the destined location where they dock with the plasma membrane. During docking the vesicles from the depot pool (DP) transfer to the unprimed pool (UPP). Once docked, vesicles undergo a priming process in which they become fusion competent. Priming corresponds to the transfer of vesicles from the UPP to the slowly releasable pool (SRP) or the readily releasable pool (RRP). A calcium signal then triggers vesicle fusion with the plasma membrane and the release of vesicular content (Becherer and Rettig, 2006).

As shown in Figure 3, the membrane fusion step requires the formation of the soluble N-ethylmaleimide-sensitive factor attachment receptor (SNARE) complex. The SNARE complex consists of proteins located on the target membrane (t-SNAREs) and a protein attached to the vesicle (v-SNARE). All SNARE proteins contain a SNARE motif, which forms a coiled coil structure (Jahn and Sudhof, 1999). For regulated exocytosis, the t-SNARE syntaxin harbours one SNARE motif whereas the t-SNARE of the synaptosomal-associated protein (SNAP) contains two. The v-SNARE from the vesicle-associated membrane protein (VAMP)/synaptobrevin family contains one SNARE motif. During membrane fusion, the four SNARE motifs interact with each other to form a very stable bundle of four coiled α -helices. It is suggested that the progressive N- to C-terminal formation of the SNARE complex could provide the energy required for fusion (Sollner et al., 1993a; Sollner et al., 1993b).

However, SNARE complex formation alone does not mediate fusion. Munc18-1, a member of the Sec1/Munc18-like protein family, is an essential component of the core fusion machinery which binds to the SNARE complex (Hata et al., 1993). Moreover, presynaptic active zones are formed by large proteins that facilitate vesicle fusion. Among these proteins, Munc13s and RIMs play important roles (Rizo and Rosenmund, 2008). Munc13s function in opening syntaxin-1 (Richmond et al., 2001), acting in concert with Munc18-1 to form the syntaxin-1/SNAP-25 heterodimer and thereby promote vesicle priming (Ma et al., 2011; Ma et al., 2013). RIM1 α was first recognised as a Rab3 effector, but RIMs have several functions beyond this role, as only a subset of RIMs contain the Rab-binding site (Kaeser and Sudhof, 2005; Rizo and Rosenmund, 2008). RIMs play a role in vesicle priming by building a Munc13-1/RIM heterodimer and the Munc13-1/RIM/Rab3A complex may help to recruit Munc13-1 at release sites (Betz et al., 2001; Dulubova et al., 2005; Lu et al., 2006; Deng et al., 2011; Camacho et al., 2017).

In addition to the above-mentioned proteins, the fusion machinery requires regulator proteins preventing spontaneous fusion events. These regulators poise the fusion machinery in an active state to allow rapid and synchronous fusion in response to a trigger. By grappling the SNAREs, regulatory proteins can hold the machinery in a ‘cocked’ state that only needs a small triggering stimulus to proceed (Sudhof and Rothman, 2009). Complexin and synaptotagmin are probably the best understood grappling proteins in membrane fusion (Rizo and Rosenmund, 2008). Complexin performs as the grappling protein that promotes zippered SNARE complexes into an activated but stationary state, and releases it only upon calcium entry and binding to synaptotagmin (Reim et al., 2001; Maximov et al., 2009; Dhara et al., 2014). Synaptotagmins are vesicle proteins containing two protein kinase C-like C2 domains which bind to phospholipids (Perin et al., 1990; Brose et al., 1992; Fernandez-Chacon et al., 2001) and to the SNARE complex (Chapman et al., 1995; Li et al., 1995; Pang et al., 2006) in a partly calcium-dependent manner. It is likely that synaptotagmin binds to the SNARE complex in the absence of calcium but switches upon calcium entry to phospholipid binding creating a mechanical force causing the plasma membrane to positively curve and thus promoting fusion (Sudhof, 2004).

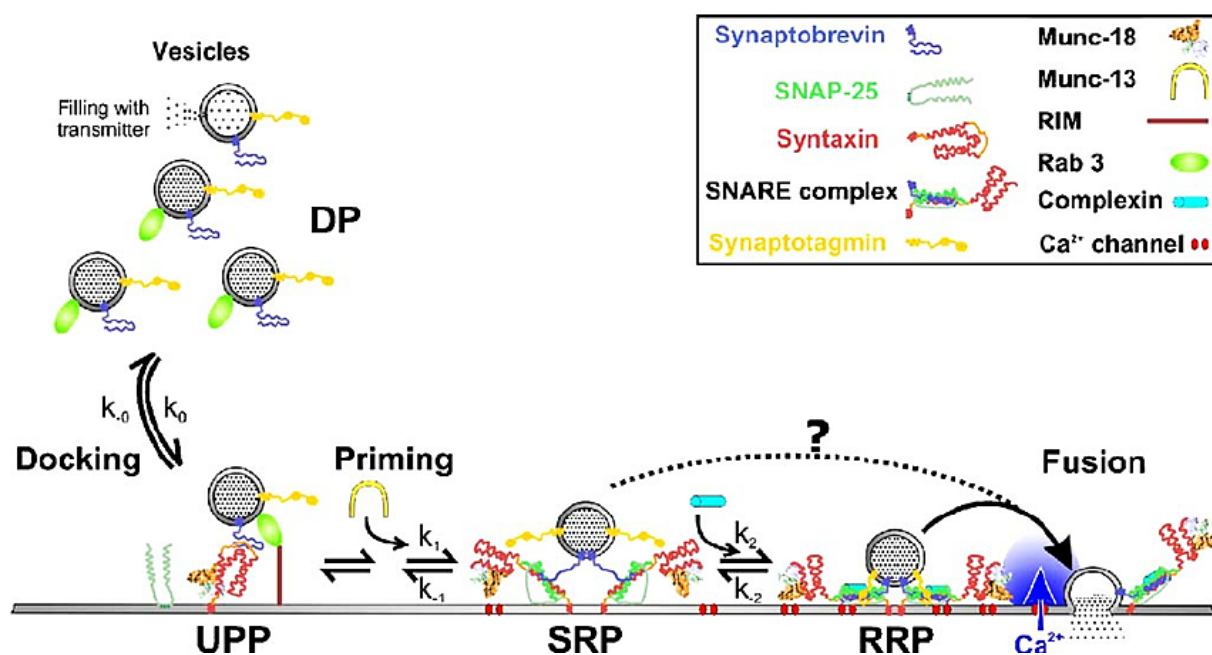


Figure 3: Molecules involved in calcium-dependent exocytosis. A cascade of molecular reactions is required during the major steps of calcium-dependent exocytosis. During docking, the vesicles are transferred from the depot pool (DP) to the unprimed pool (UPP). Molecules like Munc18 stabilize the vesicles in the docked state, most likely by reducing the rate k_0 . During priming, vesicles are transferred from the UPP to the slowly releasable pool (SRP) due to the (partial) formation of the SNARE complex from the individual SNAREs SNAP-25, syntaxin and synaptobrevin. Munc13 acts as a priming factor by increasing the rate k_1 . The balance between SRP and readily releasable pool (RRP) is modulated by complexin, which lowers the rate k_2 . The final fusion of the vesicles is initiated by binding of calcium to synaptotagmin (Becherer and Rettig, 2006).

1.3 Identification and characterization of CAPS proteins

In 1992 the calcium-dependent activator protein for secretion (CAPS) was purified from brain lysate by chromatography. It was identified as a cytosolic 145 kDa protein. The inactivation of the protein with a specific antibody led to a reduced release of norepinephrine. In neuronal cells it acts with other cytosolic components in calcium-dependent secretion (Walent et al., 1992). It has a calcium binding affinity with a dissociation constant (K_d) of 270 μM (Ann et al., 1997). CAPS is highly conserved and homologs have been described in *C. elegans* and *Drosophila*. Mammals express two CAPS paralogs referred to as CAPS1 and CAPS2, which are 80% identical at the amino acid level (Speidel et al., 2003).

1.3.1 CAPS protein domain structure and expression

CAPS paralogs consist of multiple conserved functional domains. The Dynactin binding domain (DBD), the C2 domain, the pleckstrin homology (PH) domain, the Munc13-homology domain (MHD) and the dense core vesicle (DCV) binding domain (Figure 4). The functions of the individual CAPS domains are still partially unclear. The DBD in the N-terminus is proposed to play a role in sorting and transport of vesicles. Dynactin could connect CAPS with Dynein or Kinesin-2, which are used as motor proteins of microtubules for bidirectional transport (Sadakata et al., 2007b). Following the DBD domain, CAPS contains a C2 domain (Grishanin et al., 2002). In general, these domains are common motifs for calcium-binding, which causes a change in the electrostatic potential of the protein and thus its conformational change (Rizo and Sudhof, 1998). Sequence comparisons show that CAPS lacks most of the necessary aspartates important for calcium-binding (Speidel et al., 2005) and therefore the role of the C2 domain is not completely clear. However, studies have shown that a mutation in the C2 domain of CAPS (G476E) has a reduced release rate of norepinephrine (Grishanin et al., 2004) and that the C2 domain is involved in CAPS dimerization (Petrie et al., 2016). The PH domain of CAPS binds to phospholipids and is essential for CAPS interaction with the plasma membrane. Mutations in the PH domain of CAPS led to reduced granule fusion (Kabachinski et al., 2014) and an incomplete PH domain strongly reduces the RRP (Nguyen Truong et al., 2014). In the C-terminus, CAPS contains a MHD for which a similar priming activity is proposed as that shown for Munc13 (Koch et al., 2000). In addition, the binding of CAPS to SNARE proteins is mediated via the MHD (Khodthong et al., 2011). However, the priming function of CAPS is not only facilitated by its SNARE binding via the MHD, but also by its PH domain (Nguyen

Truong et al., 2014). At the C-terminal end of CAPS, the DCV domain is considered necessary for CAPS to bind to dense core vesicles (Grishanin et al., 2002; Grishanin et al., 2004).

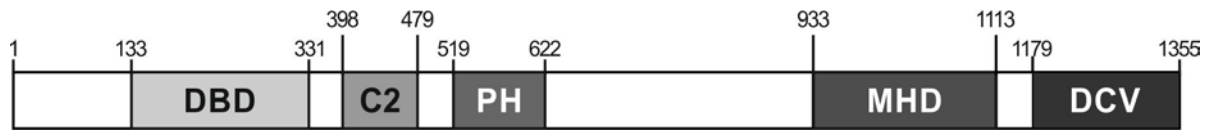


Figure 4: The domain structure of mouse CAPS1 protein. CAPS contains a N-terminal Dynactin binding domain (DBD). The central portion of CAPS contains the C2 domain and the pleckstrin homology (PH) domain. Distal to these domains are a Munc-13 homology domain (MHD) and a C-terminal dense core vesicle (DCV) binding domain. Numbers indicate the positions of the domains within the amino acid sequence.

The CAPS1 and CAPS2 proteins are encoded by two different CADPS genes. The CADPS1 gene is located on chromosome 3 while the CADPS2 gene is found on chromosome 7. In general, both paralogs share the same domain structure, but unlike CAPS1 there are six published splice variants of the CAPS2 paralog, CAPS2a-f. The three long splice variants (CAPS2a-c) contain all of the before mentioned protein domains. In contrast, the three shorter splice variants (CAPS2d-f) lack the C-terminal parts of the protein, including the MHD and DCV domain (Sadakata et al., 2007a).

CAPS proteins are predominantly expressed in neuronal and endocrine cells. Interestingly, CAPS1 is expressed in all brain tissues (Speidel et al., 2003), while CAPS2 is mainly localized in cerebral granule cells (Sadakata et al., 2007a). Additionally, CAPS1 is found in the pancreas, spleen, stomach and adrenal medulla, whereas CAPS2 is present in lungs, thyroid gland, stomach, salivary gland, kidney, spleen, thymus, colon, liver and testes (Speidel et al., 2003). The expression of CAPS depends not only on the tissue type but also on the stage of development. In the embryonic stage, e.g. embryonic day 19 (E19), CAPS2 is predominantly expressed in the brain as well as in the adrenal gland, whereas in the adult stage, e.g. on day 30 postnatal (P30), the expression of CAPS1 dominates (Speidel et al., 2005). The detection of the six naturally occurring splice variants CAPS2a-f allowed the investigation of their specific expression and function. The individual splice variants were detected more or less strongly in different tissues. In the cerebellum, for example, the expression of all splice variants is strongest up to P21 and decreases thereafter. Only the expression of CAPS2b remains constantly high even at P56 (Sadakata et al., 2007a).

1.3.2 CAPS function

CAPS is an important protein involved in regulated exocytosis of LDCVs and SVs. In *C. elegans* null mutants of the CAPS homolog UNC-31, LDCV exocytosis is impaired and LDCV docking decreased (Avery et al., 1993; Speese et al., 2007; Zhou et al., 2007). In *Drosophila* CAPS null mutants, LDCV exocytosis in neuromuscular junctions is reduced and LDCVs accumulate at synapses (Renden et al., 2001).

Deletion of CAPS1 and CAPS2 (CAPS dKO) in mammals significantly reduces exocytosis of LDCVs in chromaffin cells and neurons. In mouse embryonic chromaffin cells, lacking CAPS1 and CAPS2, there was a significant decrease in the fast component of release (RRP), and sustained release was almost eliminated. However, the number of morphologically docked vesicles did not differ significantly between wild-type (WT) and double knock-out (dKO) mice. Therefore, the reduction in secretion was attributed to a deficit in primed vesicles. It was also found that the replenishment of RRP in CAPS dKO was greatly reduced, while SRP filling was similar to that in WT mice. Additionally, expression of CAPS1 and CAPS2 in CAPS dKO returns the secretion to WT levels (Liu et al., 2008; Liu et al., 2010). This indicates that both CAPS1 and CAPS2 promote priming in chromaffin cells.

More than 20 years ago, neuronal CAPS was suggested to localize to LDCVs where it was involved in calcium-activated LDCV exocytosis (Berwin et al., 1998). More recent studies in CAPS dKO hippocampal neurons showed a strong reduction of LDCV secretion, which was restored by overexpression of exogenous CAPS1 (Farina et al., 2015; van Keimpema et al., 2017). In CAPS2 single KO mice, an impairment of the secretion of brain-derived neurotrophic factor (BDNF) was observed in cerebellar granule cells, cerebral cortical neurons and hippocampal neurons that produce gamma-aminobutyric acid (GABA) (Sadakata et al., 2004; Sadakata et al., 2007b; Shinoda et al., 2011).

However, CAPS proteins are not only involved in LDCV exocytosis but also in SV exocytosis. Using glutamatergic autaptic hippocampal cultures of WT, CAPS1 KO, CAPS2 KO and CAPS dKO, it was shown that SV priming and transmitter release was indeed impaired. In CAPS dKO and CAPS1 KO neurons, excitatory postsynaptic current (EPSC) amplitudes and RRP sizes were significantly reduced compared to WT cells. In contrast, CAPS2 KO neurons showed no phenotype (Jockusch et al., 2007) suggesting that only CAPS1 plays a role in synaptic transmission. Thus, the functions of CAPS paralogs appear to differ in discrete neuronal populations, possibly reflecting a differential role for both CAPS paralogs in LDCV and SV exocytosis. Indeed, in DRG neurons, where CAPS1 is present in all cells and CAPS2 expression

is specific to peptidergic neurons, CAPS2 predominantly mediates LDCV release from the cell soma and CAPS1 plays a major role in synaptic transmission (Shaib et al., 2018).

1.4 Rationale and aims of the project

Although the molecular machinery of SV and LDCV exocytosis has already been extensively studied, the proteins involved and their exact function are not yet fully understood. Neurotransmitter release by SV exocytosis is the main mechanism of information processing in neurons, but secretion of neuromodulators by LDCV exocytosis is also important for many neuronal processes, including neuronal development, neuronal plasticity and immunity.

In sensory DRG neurons, where synaptic transmission and neuropeptide release are of equal importance, the secretion machinery has hardly been analysed. Interestingly, the priming factors CAPS1 and CAPS2 are co-expressed in these neurons, which makes them a perfect model system for studying the function of the proteins in LDCV and SV fusion. Analyses from previous studies already indicated a differential function of CAPS paralogs, with CAPS1 supporting synaptic transmission and CAPS2 playing a role in the fusion of LDCVs in the cell soma. However, it remains unclear by which properties of the CAPS paralogs these differential functions are controlled.

Therefore, the main goal of this work is to identify differences in CAPS paralogs and to analyse them with respect to the specific functions of the proteins in mouse DRG neurons. In particular, the protein structure and subcellular localization were studied in detail. In addition, biochemical analyses were used to better understand the molecular processes and to obtain information about the CAPS1- and CAPS2-specific interaction partners.

2 Materials and Methods

2.1 Materials

2.1.1 Chemicals

Product	Company
Abberior Solid Mounting Medium	Abberior Instruments
Agar Agar	Roth
Agarose	Roth
Ampicillin	Roth
B27-Supplement	Thermo Fisher Scientific
β -Mercaptoethanol	Roth
Bovine Serum Albumin (BSA)	Sigma-Aldrich
$\text{CaCl}_2 \times 2\text{H}_2\text{O}$	Merck
Chloroform	Sigma-Aldrich
Coomassie	Merck
cOmplete Mini, EDTA-free Protease Inhibitor	Roche
Cocktail Tablets	
Dulbecco's Modified Eagle Medium (DMEM) + GlutaMAX	Thermo Fisher Scientific
dNTP-Mix	Fermentas
Dulbecco's Phosphate Buffered Saline (DPBS)	Thermo Fisher Scientific
E64 Protease Inhibitor	Sigma-Aldrich
Earle's Balanced Salt Sodium (EBSS) +Ca +Mg	Thermo Fisher Scientific
Ethanol (100%)	Roth
Ethidium bromide	Roth
Fetal Calf Serum (FCS)	Thermo Fisher Scientific
Floxuridine (FUDR)	Sigma-Aldrich
Fluo-4 AM	Thermo Fisher Scientific
GeneRuler 1kb DNA Ladder	Thermo Fisher Scientific
Geneticin	Sigma-Aldrich
Glucose	Merck
GlutaMAX	Thermo Fisher Scientific
Glycerol	Sigma-Aldrich

Glycine	Roth
HEPES	Sigma-Aldrich
Human beta-Nerve Growth Factor (NGF)	Alomone
Isopropanol	Roth
Kanamycin	Sigma-Aldrich
KCl	Merck
λ Marker	Roche
Methanol	Roth
$\text{MgCl}_2 \times 6\text{H}_2\text{O}$	Merck
Mowiol 4-88	Calbiochem
NaCl	Roth
NaHCO_3	Merck
$\text{Na}_2\text{HPO}_4 \times 2\text{H}_2\text{O}$	VWR
$\text{NaH}_2\text{PO}_4 \times \text{H}_2\text{O}$	VWR
Neurobasal-A (NBA)	Thermo Fisher Scientific
Non-Essential Amino Acids (NEAA)	Thermo Fisher Scientific
Non-fat Dried Milk Powder	PanReac AppliChem
Normal Goat Serum (NGS)	Panbiotech
NuPAGE LDS Sample Buffer 4x	Thermo Fisher Scientific
NuPAGE Tris-Acetate SDS Running Buffer 20x	Thermo Fisher Scientific
NuPAGE Transfer Buffer 20x	Thermo Fisher Scientific
Paraformaldehyde (PFA)	PolyScience
PCR Buffer	Sigma-Aldrich
Pefabloc SC	Sigma-Aldrich
Penicillin/Streptomycin (10000 U/mL, 10 mg/mL)	Thermo Fisher Scientific
Pepstatin A	Sigma-Aldrich
Pepton	Roth
<i>Pfu</i> -Polymerase Buffer	Thermo Fisher Scientific
Phenol	Sigma-Aldrich
Phusion Polymerase Buffer	Thermo Fisher Scientific
Poly-D-Lysine (PDL)	Sigma-Aldrich
Ponceau S Solution 0,1%	Sigma-Aldrich
Q5 Polymerase Buffer	NEB

Q5 Enhancer	NEB
Quick Start Bradford Protein Assay	Bio-Rad
Restore Western Blot Stripping Buffer	Thermo Fisher Scientific
Sigma H ₂ O	Sigma-Aldrich
Sodium Pyruvate	Thermo Fisher Scientific
Spectra Multicolor Broad Range Protein Ladder	Thermo Fisher Scientific
Streptomycin	Thermo Fisher Scientific
Sucrose	Merck
SuperSignal West Dura Extended Duration Substrate	Thermo Fisher Scientific
Triton X-100	Roth
Trypsin inhibitor from chicken egg white	Sigma-Aldrich
Tween 20	Roth
Uridine	Sigma-Aldrich

2.1.2 Enzymes

Enzyme	Company
DNase	Roche
Liberase Dispase High (DH) Research Grade	Sigma-Aldrich
Papain	Cell Systems
<i>Pfu</i> Polymerase	Thermo Fisher Scientific
Phusion Polymerase	Thermo Fisher Scientific
Q5 Polymerase	NEB
Quick Extract	Biozym
Red Hot Start <i>Taq</i> 2 × Mix	Biozym
TrypLE Express	Thermo Fisher Scientific
Trypsin-EDTA (0.5%)	Thermo Fisher Scientific

Restriction Enzyme	Company
AgeI	NEB
BamHI	NEB
ClaI	NEB
HincII	NEB
NheI	NEB

2.1.3 Solutions**10/10 medium**

BSA	1 g
Trypsin inhibitor	1 g
EBSS +Ca ²⁺ +Mg ²⁺	up to 100 mL

1/1 medium

DNase	0.01 g
Medium 10/10	10 mL
EBSS +Ca ²⁺ +Mg ²⁺	up to 100 mL

Blocking solution

NGS	5%
in PBS + MgCl ₂ + CaCl ₂	

DRG NBA medium (with FUDR)

FCS	5%
B27	2%
GlutaMAX	1%
Penicillin/Streptomycin	0.4%
(FUDR	10 µL/mL)
in NBA medium	

DRG extracellular solution

NaCl	147 mM
KCl	2.4 mM
CaCl ₂ × 2H ₂ O	2.5 mM
MgCl ₂ × 6H ₂ O	1.2 mM
HEPES	10 mM
Glucose	10 mM
pH: 7.4	
Osmolarity: 300 mOsm/L (with Glucose)	

DRG extracellular solution + 40 mM NH₄Cl

NH ₄ Cl	40 mM
NaCl	105 mM
KCl	2.4 mM
CaCl ₂ × 2H ₂ O	2.5 mM
MgCl ₂ × 6H ₂ O	1.2 mM
HEPES	10 mM
Glucose	10 mM

pH: 7.4

Osmolarity: 300 mOsm/L (with Glucose)

FUDR

FUDR	8.1 mM
Uridin	20.5 mM

in DMEM + GlutaMAX

HBS 2x solution

HEPES	50 mM
NaCl	280 mM
NaH ₂ PO ₄	1.5 mM

pH: 7.04

HEK293FT cell culture medium (with antibiotics)

Sodium pyruvate	1%
NEAA	1%
FCS	10%
Geneticin	1%
(Penicillin/Streptomycin	0.1%)

in DMEM + GlutaMAX

Lysogeny broth (LB)-medium

Pepton	8 g
Yeast extract	4 g
NaCl	4 g
H ₂ O _{dd}	800 mL

LB agar plates (with antibiotic)

Pepton	4 g
Yeast extract	2 g
NaCl	2 g
Bacto agar	6 g
H ₂ O _{dd}	400 mL
(Ampicillin 100 mg/mL	400 µL)
(Kanamycin 30 mg/mL	400 µL)

Loading buffer

Sucrose	4 g
Bromophenol blue	tip of a spatula
Sigma H ₂ O	10 mL

Liberase S solution

Liberase DH	2.3 U
NBA medium	1 mL

Locke's solution (10x)

NaCl	1.54 M
KCl	56 mM
NaH ₂ PO ₄ × H ₂ O	8.5 mM
Na ₂ HPO ₄ × 2H ₂ O	21.5 mM
D-Glucose H ₂ O	100 mM
pH:	6.8

Lysis buffer

HEPES	20 mM
KCl	150 mM
CaCl ₂	100 nM
Tween	0.05%
E64	10 µM
Pefabloc SC	2 mM
Pepstatin A	1 µg/mL
pH:	7.4

Mounting medium

Mowiol4-88	2.4 g
Glycerol	6 g
H ₂ O _{dd}	6 mL
0.2 M Tris buffer pH 8.5	12 mL

Paraformaldehyde (15%)

PFA	1.5 g
H ₂ O _{dd}	10 mL
NaOH	30 µL
pH: 7.4	

Paraformaldehyde (4%)

PFA 15% in H ₂ O _{dd}	2.7 mL
PBS + MgCl ₂ + CaCl ₂	7.3 mL

Permeabilization solution

NGS	5%
Triton X-100	0.1%
in PBS + MgCl ₂ + CaCl ₂	

Phosphate-buffered saline (PBS) + MgCl₂ + CaCl₂

Na ₂ HPO ₄ × 2H ₂ O	58 mM
NaH ₂ PO ₄ × H ₂ O	17 mM
NaCl	83 mM
MgCl ₂	2 mM
CaCl ₂	0.5 mM
pH: 7.4	

Osmolarity: 330 mOsm/L

Poly-D-lysine (PDL)

Poly-D-Lysine hydrobromide 0.5 mg/mL
in Sigma H₂O

Quenching solution

Glycine	50 mM
in PBS + MgCl ₂ + CaCl ₂	

SC NBA medium

FCS	5%
B27	2%
GlutaMAX	1%
Penicillin/Streptomycin	0.4%
FUDR	10 µL/mL
NGF	2 µL/mL
in NBA medium	

SC enzymatic solution

DMEM+ GlutaMAX	5 mL
L-Cysteine	10 mg
100 mM CaCl ₂	0.5 mL
EDTA	50 mM
Papain	20 U/mL

Tris-acetate-EDTA buffer (50x)

Tris Base	242 g
Acetic Acid	57.1 g
0.5 M EDTA	100 mL
pH 8.5	

Tris-buffered saline (TBS)

Tris-Cl	50 mM
NaCl	150 mM
pH: 8.0	

TBS-Tween 20 (TBST) 0.05%

Tween 20	500 µL
TBS	1 L

2.1.4 Antibodies

Antibody	Host	Immunogen	Manufacturer and catalogue no.	Working dilution
Primary antibody				
Bassoon	Mouse	Recombinant protein from rat Bassoon	Enzo ADI-VAM-PS003	1:400 (ICC)
Beta-actin	Mouse	clone AC-15	Merck A1978	1:10,000 (WB)
CAPS1	Rabbit	aa 18 to 107 from mouse CAPS1	Synaptic Systems 262013	5 µg ~ 1:50 (IP) 1:1,000 (WB) 1:500 (ICC)
CAPS2	Rabbit	aa 15 to 89 from mouse CAPS2	Synaptic Systems 262103	5 µg ~ 1:50 (IP)
CAPS2	Rabbit	Full length CAPS2e. This antibody was immunopurified against a CAPS2 specific sequence GSGGGAARPV	Provided by M. Jung	1:1,000 (WB)
HA Tag	Rat	aa 98-106 from the human influenza hemagglutinin protein	Roche 3F10	1:1,000 (WB)
Homer1	Rabbit	aa 1 to 196 from human Homer1	Synaptic Systems 160003	1:1,000 (ICC)
Munc13-1	Rabbit	aa 3 to 317 from rat Munc13-1	Synaptic Systems 126103	1:500 (ICC)
Normal IgG	Rabbit	N/A	Merck 12-370	5 µg ~ 1:50 (IP)
Synapsin	Guinea Pig	aa 2 to 28 from rat Synapsin1	Synaptic Systems 106004	1:1,000 (ICC)
Secondary antibody				
Alexa 488	Goat	Rabbit	Thermo Fisher Scientific A11034	1:1,000
Alexa 647	Goat	Rabbit	Thermo Fisher	1:1,000

Alexa 405	Goat	Mouse	Scientific A21245 Thermo Fisher	1:1,000
Fab fragment	Goat	Rabbit	Scientific A31553 Rockland	1:50
IgG F(ab') ₂ HRP	Goat	Rabbit	811-1102 Merck AQ132P	1:5,000
IgG (H+L) HRP	Goat	Mouse	Thermo Fisher Scientific 32430	1:1,000
IgG HRP	Goat	Rat	GE Healthcare NA935	1:5000
STAR RED	Goat	Mouse	Abberior STRED- 1001-500UG	1:100
STAR 580	Goat	Rabbit	Abberior ST580- 1002-500UG	1:100
STAR 580	Goat	Guinea Pig	Abberior ST580- 1006-500UG	1:100

2.1.5 Oligonucleotides

All oligonucleotides (Primers) were ordered from Eurofins Genomics.

2.1.5.1 Primer for genotyping of CAPS1 and CAPS2

Name	Sequence (5'-3')
Primer 1502	TGCGGTGGGCTCTATGGCTTCT (22 bp)
Primer 1503	CTCGAGTGGCCTGATCTTTGTCA (23 bp)
Primer 1504	TATGAGGAGTTTATGTGCGTGGAT (24 bp)
Primer 5471	GTACCATAGTTCTGTGCCGTGTAATC (26 bp)
Primer 5472	GGAGGCTCGCAGCTCTTCAATG (22 bp)
Primer 4174	CGCATCGCCTTCTATCGCCTTCTT (24 bp)

2.1.5.2 Primer for cloning

Name	Sequence (5'-3')
pHuji fp with AgeI and linker aa (#660)	ATGTATATCCACCGGTCGCCACCATGGTGAG CAAGGGCGAGGAG (44 bp)
pHuji rp with NheI and stop codon (#588)	ATGTATACTAGCTAGCTTACTTGTACAGCTCG TCCATGCCGCCG (44bp)
pHuji fp sequencing (#598a)	GAACTCGGCTTGAAGACCCTGC (22 bp)
pHuji rp sequencing (#599a)	GGAGCAACATAGTTAAGAATACCAGTC (27 bp)
Fp HaloTag with ClaI (#661)	ATATACCATCGATATGGCAGAAATCGGTACTGG CTTTCCATTC (43 bp)
Rp HaloTag with NheI (#603)	ATATACTAGCTAGCGCGGCCGCGGCGGATCCTT AGCCGGAAATCTCGAG (49 bp)
CAPS2-Halo Primer 1 fw sequencing (#727)	GACGCCATCCACGCTG (16 bp)
CAPS2-Halo Primer 2 fw sequencing (#729)	GGCGGAGGACTTCAGG (16 bp)
CAPS2-Halo Primer 3 rv sequencing (#728)	GAATACCAGTCAATCTTTCAC (21 bp)
CAPS2-Halo Primer 4 rv sequencing (#664)	GAAATCATTAGCAGAGCATCC (21 bp)
Fp CAPS1 with BamHI (#652)	ATATACGCGGATCCATGCTGGACCCTTCGTCCA GC (35 bp)
Rp CAPS1 OE (#732)	CCGCTTCCGCCGCTCCCACCGCGCGCCGCATCA TCTTCTTCATCTTCCTCATCACTGTC (59 bp)
Fp Halo OE (#732)	GGAGCGGCGGAAGCGGCGGTACCATCGATATG GCAGAAATCGGTACTGGCTTTCCATTC (59 bp)
Rp Halo with NheI (#734)	TATACTAGCTAGCTTAGCCGGAAATCTCGAGCG TCGACAG (40 bp)
CAPS1-Halo Primer 2 fw sequencing (#598b)	CTGAGCAAGGAACAGCTC (18 bp)
CAPS1-Halo Primer 3 fw sequencing (#599b)	CTACAGCTGGACGGCTAC (18 bp)
CAPS1-Halo Primer 4 fw	GTAGGCCGCTTAATCACTC (19 bp)

sequencing (#600)	
CAPS1-Halo Primer 5 fw	CGAGTCCCACAGTCAATATG (21 bp)
sequencing (#601)	
CAPS1-Halo Primer 6 rv	CAGCTCTCGTCTGATCTG (18 bp)
sequencing (#695)	
CAPS1-Halo Primer 7 rv	CATAGCTTGGACCCAC (16 bp)
sequencing (#736)	
CAPS1-Halo Primer 8 rv	GGTCTTTGACAGTCTG (16 bp)
sequencing (#739)	

2.1.6 Plasmids

Name	Company
#12251 pMDLg/pRRE	Addgene
#12253 pRSV-Rev	Addgene
#12259 pMD2.G	Addgene
#8455 pCMV-dR8.2 dvpr	Addgene
#8454 pCMV-VSV-G	Addgene
#61505 TfR-pHuji	Addgene
#A3600 pGEM®-T Vector Systems	Promega

2.1.7 Bacteria

DH5 α : F- ϕ 80lacZ Δ M15 Δ (lacZYA-argF)U169 recA1 endA1 hsdR17(rk-, mk+) phoA supE44 thi-1 gyrA96 relA1 λ - (Thermo Fisher Scientific)

Stbl3: F mcrB mrr hsdS20(r_B⁻, m_B⁻) recA13 supE44 ara-14 galK2 lacY1 proA2 rpsL20(Str^R) xyl-5 λ leu mtl-1 (Thermo Fisher Scientific)

2.1.8 Cell lines

HEK293FT Thermo Fisher Scientific

2.1.9 Mouse strains

C57Bl/6N Stock number: 005304, The Jackson Laboratory

2.1.10 Kits

Kit	Company
EndoFree Plasmid Maxi Kit	Qiagen
EndoFree Plasmid Midi Kit	Qiagen
Pierce Silver Stain Kit	Thermo Fisher Scientific
QIAprep Spin Miniprep Kit	Qiagen
QIAquick Gel Extraction Kit	Qiagen
QIAquick PCR Purification Kit	Qiagen

2.1.11 Consumables

Product	Company
6-Well Plate	Greiner Bio-One
12-Well Plate	Greiner Bio-One
Amicon Ultra-15 Centrifugal Filter (100,000 NMWL)	Merck
Cell Culture Flask (25 Cm ²)	Sarstedt
Cell Culture Flask (75 Cm ²)	Sarstedt
Cell Culture Flask (150 Cm ²)	Faust
Cell Filter Millex-HV 0.45µm	Merck
Coverslip (25 mm)	Paul Marienfeld
Coverslip (15 mm)	Paul Marienfeld
Cryotube Nalgene (2 mL)	Thermo Fisher Scientific
Dynabeads Protein G	Thermo Fisher Scientific
Gel Blotting Papers Thickness 0.34 mm	Roth
Glass Pasteur Pipette	Roth
Multiply µstrip 0.2 mL Chain PCR Tubes	Sarstedt
Microscope Slide	Roth
Microscope Slide Superfrost Plus	Thermo Fisher Scientific
Needle (18G × 1½, 1.2 × 40 mm)	Braun
Needle (20G × 1½, 0.9 × 40 mm)	Braun
Needle (20G × 2¾, 0.9 × 70 mm)	Terumo
NuPAGE 3-8% Tris-Acetate Gel 1.0 mm	Thermo Fisher Scientific

Petri Dish (35 mm, 92 mm, 150 mm)	Sarstedt
Serological Pipette (2mL, 5mL, 10 mL, 25 mL)	Sarstedt
Pasteur Pipette (2 mL)	Brand
Pipette Tip (200, 1000 μ L)	Sarstedt
Pipette Filter Tip (10 μ L)	Biozym
Pipette Filter Tip (10 μ L, 20 μ L, 200 μ L, 1000 μ L)	Sarstedt
Reaction Tube (0.5 mL, 1.5 mL, 2 mL)	Sarstedt
Syringe Filter 25 mm 0.2 μ m	VWR
Syringe Filter Acrodisc 13 mm, 0.2 μ m	VWR
Syringe Filter Acrodisc 32 mm, 0.2 μ m	VWR
Polypropylene Centrifuge Tube (25 \times 89 mm)	Beckman Coulter

2.1.12 Devices

Device	Company
Axiovert 200 Microscope	Carl Zeiss
Balance BP 1215	Sartorius
Balance BP 4100S	Sartorius
Bath Incubator	Memmert
Biophotometer Plus	Eppendorf
Centrifuge Mini 3-1810	neoLab
Centrifuge 5415 C	Eppendorf
Centrifuge 5415 D	Eppendorf
Centrifuge 5415 R Fast Cool	Eppendorf
Centrifuge 5424	Eppendorf
Centrifuge 5702 R	Eppendorf
Centrifuge 5804 R	Eppendorf
Centrifuge Fresco 17	Thermo Fisher Scientific
Centrifuge Heraeus Labofuge 400 R	Thermo Fisher Scientific
Centrifuge Mini Spin Plus	Eppendorf
Centrifuge small	Eppendorf
Combimag RCT	IKA
Confocal Laser Scanning Microscope LSM 780	Carl Zeiss
Dissection Microscope M3Z	Wild Heerbrugg

Eclipse TS 100 Microscope	Nikon Instruments
FluorChem M System	ProteinSimple
Fridge/Freezer	Liebherr
Glass Potter	B. Braun
Heracell 150i CO ₂ Incubator	Thermo Fisher Scientific
Hera Freeze Heraeus -80°C Freezer	Thermo Fisher Scientific
Herafreeze HFU B -80°C Freezer	Thermo Fisher Scientific
Heraguard Eco	Thermo Fisher Scientific
Herasafe Cell Culture Hood	Thermo Fisher Scientific
KL 1500 Light Source	Schott
Master Cycler Personal	Eppendorf
Master Cycler Gradient	Eppendorf
Microforge	World Precision Instruments Inc.
Microwave	Severin
MS2 Minishaker	IKA
MSC-Advantage Hood	Thermo Fisher Scientific
peqPower300 Power Supply	Peqlab
pH Meter	Schott
Pipettes (2.5 µL, 10 µL, 20 µL, 200 µL, 1000 µL)	Eppendorf
PowerPac300 Basic Power Supply	Bio-Rad
Protran BA 83 Nitrocellulose Membrane	Thermo Fisher Scientific
P-touch 2420 PC	Brother
RCT Basic	IKA
Rotator	neoLab
Stimulated Emission Depletion Microscope (four-color STED QuadScan)	Abberior Instruments
SW 32 Ti Swinging-Bucket Rotor	Beckman Coulter
Thermocycler peqSTAR	Peqlab
Ultracentrifuge Optima XPN-80	Beckman Coulter
UV-Transilluminator	Thermo Fisher Scientific
UV-Chamber	Custom-built
Vortex Mixer 7-2020	neoLab
Wescor Osmometer	Kreienbaum

XCell II Blot Module	Thermo Fisher Scientific
XCell SureLock Mini-Cell Electrophoresis System	Thermo Fisher Scientific

2.1.13 Total internal reflection fluorescence microscope

The TIRF microscope setup is a custom-made device with various components that allow a wide range of electrophysiological experiments to be performed.

Component	Company
IX70 Microscope	Olympus
Valve control VC-6 Valve	Warner Instruments
450, 488 and 514 nm laser 285-FA11	Spectra-Physics
561 nm laser 85-YCA-615	Melles Griot
VisiChrome Polychromator	Visitron Systems
Acousto Optical Tunable Filter VS AOTF-2ahf	Visitron Systems
Filter sets green/red, UV, mTFP and yellow/red	AHF
QuantEM 512SC or Evolve 512 camera	Photometrics
Dual View 565 dcxr dichroic emission filter	Chroma
Isolated Pulse Stimulator 2100	A-M Systems
Micromanipulator SM8	Luigs & Neumann
Field Electrode Platinum/Iridium Blunted Tip PI2ST30.5B10	MicroProbes for Life Science

2.1.14 Software

Software	Company
A plasmid Editor (ApE), version 2.0.49	M. Wayne Davis
CorelDRAW X6 Graphic	Corel
Igor Pro, version 6.37	Wavemetrics
ImageJ, version 1.51u	National Institutes of Health
Imaris, version 9.5.1	Bitplane
Inspector, version 16.3.11815-w2024	Abberioior Instruments
Office 2016	Microsoft
Python Based Relational Animal Tracking (PyRAT), version 4.2	Scionics Computer Innovation

Scaffold Viewer, version 4.8.8	Proteome Software
SigmaPlot, version 11 and 13	Systat Software
SnapGene Viewer, version 4.0.4	GSL Biotech
VisiView, version 4.4.0.4	Visitron Systems
Zeiss Efficient Navigator (ZEN) 2012	Carl Zeiss

2.1.15 Companies

Abberior Instruments: Göttingen, DE. **Abcam:** Cambridge, UK. **AHF Analysentechnik:** Tübingen, DE. **Alomone:** Jerusalem, IL. **A-M Systems:** Sequim, US. **B. Braun:** Melsungen, DE. **Beckman Coulter:** Krefeld, DE. **BD Biosciences:** Heidelberg, DE. **Bio-Rad:** München, DE. **Biozym:** Hessisch Oldendorf, DE. **Bitplane:** Belfast, UK. **Brand:** Wertheim am Main, DE. **Calbiochem:** Mannheim, DE. **Cell Signaling Technologies:** Danvers, US. **Cell Systems:** Troisdorf, DE. **Chroma:** ? **Corel:** Ottawa, CA. **Enzo Life Sciences:** Lörrach, DE. **Eppendorf:** Hamburg, DE. **Faust:** Schaffhausen, CH. **Fermentas:** St. Leon-Rot, DE. **GSL Biotech:** Chicago, US. **Greiner Bio-One:** Frickenhausen, DE. **IKA:** Staufen, DE. **Kreienbaum:** Langenfeld, DE. **Luigs & Neumann:** Ratingen, DE. **Melles Griot:** Bensheim, DE. **Memmert:** Schwabach, DE. **Merck:** Darmstadt, DE. **MicroProbes for Life Science:** Gaithersburg, US. **Microsoft:** Berlin, DE. **Molecular Devices:** San Jose, US. **Eurofins Genomics:** Ebersberg, DE. **neoLab:** Heidelberg, DE. **New England Biolabs:** Frankfurt/M., DE. **Nikon Instruments:** Amsterdam, NL. **Olympus:** Hamburg, DE. **Panbiotech:** Aidenbach, DE. **PanReac AppliChem:** Darmstadt, DE. **Paul Marienfeld:** Lauda Königshofen, DE. **Peqlab:** Erlangen, DE. **Photometrics:** Tucson, US. **Physik Instrumente:** Karlsruhe, DE. **ProteinSimple:** San Jose, US. **Proteome Software:** Portland, US. **QIAGEN:** Hilden, DE. **Roche:** Grenzach-Wyhlen, DE. **Roth:** Karlsruhe, DE. **Sarstedt:** Nümbrecht, DE. **Sartorius:** Göttingen, DE. **Schott:** Mainz, DE. **Scionics Computer Innovation:** Dresden, DE. **Sigma Aldrich:** Steinheim, DE. **Systat Software:** San Jose, US. **Spectraphysics:** Darmstadt, DE. **Sutter Instrument:** Novato, US. **Synaptic Systems:** Göttingen, DE. **Terumo:** Eschborn, DE. **The Jackson Laboratory:** Bar Harbor, US. **Thermo Fisher Scientific:** Schwerte, DE. **Visitron Systems:** Puchheim, DE. **VWR:** Darmstadt, DE. **Warner Instruments:** Hamden, US. **Wavemetrics:** Lake Oswego, US. **Wild Heerbrugg:** Gais, CH. **World Precision Instruments:** Berlin, DE. **Carl Zeiss:** Jena, DE.

2.2 Methods

2.2.1 Genotyping

Mice with a deletion of CAPS1 or CAPS2 were generated as described previously (Speidel et al., 2005; Jockusch et al., 2007). CAPS1/2 dKO mice were generated by breeding the CAPS1 mutation into the CAPS2 mutant background. CAPS1 KO mice and CAPS1/2 dKO mice are lethal and die shortly after birth. Therefore, embryos from CAPS1 heterozygous and CAPS2 KO mice were prepared after caesarean section.

Determination of the CAPS1 or CAPS2 genotype from mice were carried out by polymerase chain reaction (PCR). Tails of mice were digested by 50 μ L Quick Extract for 10 minutes at 65°C and 300 rpm followed by 2 minutes of inactivation at 98°C and 300 rpm. 2 μ L of DNA lysate were used for one PCR reaction. Primers were used at a stock concentration of 50 pmol/ μ L. Primers 1502 and 1504 detect CAPS1 KO, 1503 and 1504 CAPS1 WT. Primers 5471 and 5472 detect CAPS2 KO, 5471 and 4147 CAPS2 WT.

Table 1: PCR mix for CAPS1 genotyping.

reagent	volume
Primer 1502	0.3 μ L
Primer 1503	0.3 μ L
Primer 1504	0.3 μ L
DNA	2 μ L
Sigma H ₂ O	7.1 μ L
Polymerase Mix	10 μ L

Table 2: PCR mix for CAPS2 genotyping.

reagent	volume
Primer 5471	0.4 μ L
Primer 5472	0.2 μ L
Primer 4174	0.2 μ L
DNA	2 μ L
Sigma H ₂ O	7.2 μ L
Polymerase Mix	10 μ L

Table 3: PCR programme for CAPS1 genotyping.

	temperature	time	no. of cycles
1. Initial Denaturation	95°C	3 min	1
2. Denaturation	95°C	30 sec	30
3. Annealing	60°C	30 sec	
4. Elongation	72°C	30 sec	
5. Final Elongation	72°C	2 min	1
6. End	8°C	forever	

Table 4: PCR programme for CAPS2 genotyping.

	temperature	time	no. of cycles
1. Initial Denaturation	95°C	3 min	1
2. Denaturation	95°C	30 sec	
3. Annealing	67°C	30 sec	35
4. Elongation	72°C	30 sec	
5. Final Elongation	72°C	2 min	1
6. End	8°C	forever	

The genotype was determined based on the size of the PCR product. The PCR product of CAPS1 WT was 380 base pair (bp) and CAPS1 KO was 465 bp. For CAPS2 WT a 153 bp amplicon was generated and a 225 bp amplicon for CAPS2 KO. In heterozygous animals both PCR products (WT and KO) were generated. The DNA fragments with different size were separated by a 2% agarose gel for 45 minutes at 80 Volt.

2.2.2 Cloning

2.2.2.1 Lentivirus plasmid Neuropeptide Y-pHuji

To visualize LDCVs in DRG neurons and to investigate LDCV fusion in these neurons, a lentivirus plasmid encoding for the fusion protein Neuropeptide Y (NPY)-pHuji was cloned. In general, NPY can be connected to any fluorophore, but pHuji, a red fluorescent protein with a pH sensitivity is particularly well suited for detection of single exocytosis events. pHuji is a mApple variant with a single mutation of K163Y showing a high pH sensitivity with a pKa of 7.7. It is reported to display a more than 20-fold fluorescent intensity change from pH 5.5 to 7.5 (Shen et al., 2014). For cloning, pHuji was amplified via PCR from the TfR-pHuji plasmid. Afterwards, amplified pHuji and the lentivirus plasmid with NPY-Venus were digested with AgeI and NheI. For right expression and localization of the NPY-pHuji fusion protein it was important to use the same linker sequence as in NPY-Venus, because small changes in the linker sequence between NPY and its fluorophores could lead to mislocalization of the protein. To amplify pHuji a forward primer was used with the AgeI restriction site and part of the linker sequence: 5' ATGTATATCC[^]ACCGGTCGCCACCATGGTGAGCAAGGGCGAGGAG 3'. The reverse primer included the NheI restriction site and a stop codon: 5' ATGTATACTA[^]GC TAGCTTACTTGTACAGCTCGTCCATGCCGCCG 3'.

Table 5: PCR mix for pHuji amplification.

reagent	volume
Forward primer 25 pmol	1 μ L
Reverse primer 25 pmol	1 μ L
DNA (pHuji) 100 ng/ μ L	1 μ L
dNTP mix 10 mmol/ μ L	1 μ L
10 \times Pfu polymerase buffer + MgSO ₄	5 μ L
Pfu polymerase 2.5 U/ μ L	1 μ L
Sigma H ₂ O	40 μ L

Table 6: PCR programme for pHuji amplification.

	temperature	time	no. of cycles
1. Initial Denaturation	95°C	5 min	1
2. Denaturation	95°C	30 sec	
3. Annealing	60°C	30 sec	35
4. Elongation	72°C	1.5 min	
5. Final Elongation	72°C	10 min	1
6. End	4°C	forever	

After PCR the size of the amplified DNA product was checked on a 1% agarose gel (with ethidium bromide). For that, 1 μ L of sample with 1 μ L 6 \times loading dye and 4 μ L Sigma H₂O were loaded together with 6 μ L of the 1 kb GeneRuler DNA ladder and was run for 15 minutes at 160 V. The PCR product was then purified with the QIAquick PCR Purification Kit following the manufacturer's protocol. The DNA purification uses a simple and fast bind-wash-elute procedure. The kit contains silica membrane columns for DNA binding in high-salt buffer and elution with low-salt buffer or water. After purification, the PCR product and the NPY-Venus lentivirus plasmid were digested with the restriction enzymes NheI and AgeI. Restriction enzyme digestion generates compatible ends capable of being ligated together afterwards.

Table 7: Restriction digestion mix for pHuji and pLenti NPY-Venus.

reagent	PCR pHuji	pLenti NPY-Venus
DNA	~ 50 μ L	2 μ L (~ 3.6 μ g)
NheI	2 μ L	2 μ L
AgeI	2 μ L	2 μ L
10 \times Cutsmart	6 μ L	3 μ L
Sigma H ₂ O	-	21 μ L

The mixture was incubated for 2 hours at 37°C. Afterwards loading buffer was added to the linearized DNA and loaded together with the 1 kb GeneRuler DNA ladder on a 1% agarose gel (with ethidium bromide). The gel was run for 45 minutes at 80 V. The DNA bands with the correct size for pHuji (~ 730 bp) and pLenti NPY (~ 6500 bp) were cut under the UV lamp and isolated from the agarose gel by using the QIAquick Gel Extraction Kit according to the

manufacturer's protocol. To check the isolated DNA concentration 1 μL of sample with 1 μL 6 \times loading dye and 4 μL Sigma H₂O were loaded together with 5 μL of 1 kb GeneRuler DNA ladder on a 1% agarose gel (with ethidium bromide). The gel was run for 45 minutes at 80 V. Next, the two digested DNA fragments (pHuji and pLenti NPY) were combined with the T4 DNA ligase. After calculation with a vector to insert ratio of 1:5, 100 ng of vector DNA were used with 56 ng of insert DNA. The ligation control included the digested vector and the same components of the ligation reaction but without the insert. The ligation reaction tube and the control tube were incubated for 45 minutes at 22°C.

$$\frac{100 \text{ ng vector} \times 0.73 \text{ kb insert} \times 5}{6.518 \text{ kb vector}} \approx 56 \text{ ng insert}$$

Table 8:Ligation mix for pHuji and pLenti NPY.

reagent	reaction volume	control volume
Vector DNA (pLenti NPY) 20 ng/ μL	5 μL	5 μL
Insert DNA (pHuji) 35 ng/ μL	1.5 μL	-
T4 DNA Ligase	2 μL	2 μL
10 \times T4 DNA Ligase Buffer	2 μL	2 μL
Sigma H ₂ O	9.5 μL	11 μL

After retransformation, amplification and isolation of the DNA (see 2.2.3 Bacterial transformation using heat shock, page 41) the cloning success was checked by a control digestion with HincII for its triple cutting within the vector and insert. For that, 5 μL DNA after isolation with QIAprep Spin Miniprep Kit were digested with 1 μL HincII in the presence of 3 μL 10 \times Cutsmart buffer and 21 μL Sigma H₂O. The reaction mix was incubated for 1 hour at 37°C. Loading buffer was added and samples were run on a 1% agarose gel (with ethidium bromide) for 40 minutes at 80 V. Clones with the correct digestion pattern were sequenced to eliminate the possibility of mutations.

2.2.2.2 Lentivirus plasmids CAPS2-Halo and CAPS1/2 chimera-Halo

To analyse the localization of CAPS2 vs. CAPS1/2 chimera in DRG neurons, lentivirus plasmids were generated by cutting out CAPS2 or CAPS1/2 chimera from the existing Semliki Forest virus plasmids (pSFV) and attaching a HaloTag to their C-terminus. The HaloTag is a modified haloalkane dehalogenase which binds rapidly, specifically and irreversible to synthetic ligands by covalent bonding. The ligands comprise a chloroalkane linker that can be attached to a variety of useful molecules, such as fluorescent dyes or solid surfaces (Los et al.,

2008). The HaloTag was particularly well suited for our analysis, because it allowed us a greater freedom and flexibility in choosing the excitation source. For cloning CAPS2-Halo and CAPS1/2 chimera-Halo it was important to keep the same linker sequence between the protein and its tag as in the pSFV-CAPS2-eGFP and pSFV-CAPS1/2 chimera-eGFP constructs. The linker sequence comprised a unique ClaI restriction site which was used to ligate CAPS2 or CAPS1/2 chimera with the HaloTag. First, the HaloTag was amplified via PCR from an existing pMAX-Synaptobrevin2-Halo construct to add a ClaI restriction site at the N-terminus with the primer: 5' ATATACCATCGAT[^]ATGGCAGAAATCGGTACTGGCTTTCCATTC 3' and a NheI restriction site to its C-terminus with the following reverse primer: 5' ATATACTA[^]GCTAGCGCGGCCGCGGCGGATCCTTAGCCGGAAATCTCGAG 3'. The PCR mix and programme was the same as for pHuji amplification (see Table 5 and Table 6). After PCR the size of the amplified DNA product was checked on a 1% agarose gel (with ethidium bromide). For that, 1 μ L of sample with 1 μ L 6 \times loading dye and 4 μ L Sigma H₂O were loaded together with 6 μ L of the 1 kb GeneRuler DNA ladder and was run for 15 minutes at 160 V. The PCR product was then purified with the QIAquick PCR Purification Kit following the manufacturer's protocol. Since the HaloTag contains a methylated ClaI restriction site which loses its methylation after the PCR and is then accessible for ClaI cutting, the digestion of the PCR product with ClaI could not be performed directly. To again methylate the ClaI restriction site within the HaloTag it was introduced into a pGEM-t vector via TA-cloning and amplified in DH5 α bacteria. For that, a single 3' A residue was added by incubating the Halo PCR fragment for 20 minutes at 72°C with dATP and a non-proofreading DNA polymerase. After the tailing reaction was completed, the DNA was purified with the QIAquick PCR Purification Kit following the manufacturer's protocol.

Table 9: Mix for A-tailing of Halo PCR product.

reagent	volume
DNA (Halo purified PCR product)	6 μ L
dATP 10 mmol/ μ L	1 μ L
10 \times Red Taq buffer	5 μ L
Red Taq polymerase 1 U/ μ L	2.5 μ L
Sigma H ₂ O	35.5 μ L

The DNA concentration was checked by running a quantitative agarose gel with 1 μ L of sample diluted in 4 μ L Sigma H₂O and 1 μ L 6 \times loading dye together with 5 μ L 1 kb GeneRuler DNA ladder on a 1% agarose gel (with ethidium bromide). The gel was run for 45 minutes at 80 V. By using a molar ratio of 1:3 vector to insert, 45 ng purified DNA was used for ligation with

50 ng pGEM-T vector. The ligation control included the pGEM-T vector and the same components of the ligation reaction but without the insert. The ligation reaction tube and the control tube were incubated for 1 hour at 23°C.

$$\frac{50 \text{ ng vector} \times 0.891 \text{ kb insert} \times 3}{3.0 \text{ kb vector}} \approx 45 \text{ ng insert}$$

Table 10: Ligation mix for Halo and pGEM-T.

reagent	reaction volume	control volume
Vector DNA (pGEM-T) 50 ng/μL	1 μL	1 μL
Insert DNA (Halo) 40 ng/μL	1 μL	-
T4 DNA Ligase	2 μL	2 μL
10 × T4 DNA Ligase Buffer	2 μL	2 μL
Sigma H ₂ O	14 μL	15 μL

After retransformation, amplification and isolation of the DNA (see 2.2.3 Bacterial transformation using heat shock, page 41), the cloning success was checked by a control digestion with ClaI and NheI for cutting at the N- and C-terminus of Halo. Therefore, 5 μL DNA after isolation with QIAprep Spin Miniprep Kit were digested with 1 μL of each enzyme in the presence of 3 μL 10 × Cutsmart buffer and 20 μL Sigma H₂O. The reaction mix was incubated for 2 hours at 37°C. Loading buffer was added and samples were run on a 1% agarose gel (with ethidium bromide) for 40 minutes at 80 V. The clone with the correct digestion pattern was used for cloning of CAPS2- or CAPS1/2 chimera-Halo into a lentivirus plasmid (Figure 5, page 36). For this purpose, the pGEM-T-Halo plasmid was digested with ClaI and NheI, the pSFV-CAPS2b-eGFP and pSFV-CAPS1/2 chimera-eGFP plasmids were digested with BamHI and ClaI, and the lentiviral backbone plasmid was digested with BamHI and NheI. The digestion mixture was incubated for 2 hours at 37°C.

Table 11: Restriction digestion mix for pGEM-T-Halo, pSFV-CAPS2b-eGFP, pSFV-CAPS1/2 chimera-eGFP and pLenti NPY-Venus.

reagent	pGEM-T-Halo	pSFV-CAPS2b-eGFP	pSFV-CAPS1/2 chimera-eGFP	pLenti NPY-Venus
DNA	25 μL (~ 3.5 μg)	1 μL (~ 3.8 μg)	2.5 μL (~ 3.5 μg)	2 μL (~ 3.6 μg)
NheI	1 μL	-	-	1 μL
BamHI	-	1 μL	1 μL	1 μL
ClaI	1 μL	1 μL	1 μL	-
10 × Cutsmart	3 μL	3 μL	3 μL	3 μL
Sigma H ₂ O	-	24 μL	22.5 μL	23 μL

Afterwards loading buffer was added to the linearized DNA and samples were run on a 1% agarose gel (with ethidium bromide) together with the 1 kb GeneRuler DNA ladder for 45 minutes at 80 V. The DNA bands for Halo, CAPS2b or CAPS1/2 chimera and the lentiviral backbone plasmid were cut under the UV lamp and isolated from the agarose gel by using the QIAquick Gel Extraction Kit according to the manufacturer's protocol. To check the isolated DNA concentration 1 μ L of sample with 1 μ L 6 \times loading dye and 4 μ L Sigma H₂O were loaded together with 5 μ L of 1 kb GeneRuler DNA ladder on a 1% agarose gel (with ethidium bromide). The gel was run for 45 minutes at 80 V.

Afterwards, the digested DNA fragments were combined with the T4 DNA ligase. At first, inserts (Halo and CAPS2b or CAPS1/2 chimera) were ligated at a 1:1 molar ratio by incubation for 1 hour at 23°C.

$$\frac{120 \text{ ng CAPS2b} \times 0.917 \text{ kb Halo}}{3.966 \text{ kb CAPS2b}} \approx 27.7 \text{ ng Halo}$$

$$\frac{120 \text{ ng CAPS1/2 chimera} \times 0.917 \text{ kb Halo}}{3.969 \text{ kb CAPS1/2 chimera}} \approx 27.7 \text{ ng Halo}$$

Table 12: Ligation mix for CAPS2b or CAPS1/2 chimera and Halo.

reagent	volume	
	CAPS2b	CAPS1/2 chimera
Insert DNA (CAPS2b) ~20 ng/ μ L	6 μ L	-
Insert DNA (CAPS1/2 chimera) ~20 ng/ μ L	-	6 μ L
Insert DNA (Halo) ~10 ng/ μ L	3 μ L	3 μ L
T4 DNA Ligase	1 μ L	1 μ L
10 \times T4 DNA Ligase Buffer	1.5 μ L	1.5 μ L
Sigma H ₂ O	3.5 μ L	3.5 μ L

Next, CAPS2b-Halo and CAPS1/2 chimera-Halo were ligated with the digested lentiviral backbone plasmid using a 1:3 vector to insert molar ratio. For that, the ligation mixture with vector DNA (15 μ L) was split in half and added to the CAPS2b-Halo or CAPS1/2 chimera-Halo ligation mix and incubated overnight at 16°C.

$$\frac{120 \text{ ng CAPS2b} - \text{Halo} \times 6.682 \text{ kb vector} \times 1}{4.883 \text{ kb CAPS2b} - \text{Halo} \times 3} \approx 54.7 \text{ ng vector}$$

$$\frac{120 \text{ ng CAPS1/2 chimera} - \text{Halo} \times 6.682 \text{ kb vector} \times 1}{4.886 \text{ kb CAPS1/2 chimera} - \text{Halo} \times 3} \approx 54.7 \text{ ng vector}$$

Table 13: Ligation mix for pLenti vector to add to CAPS2b- or CAPS1/2 chimera-Halo.

reagent	volume
Vector DNA (pLenti) ~20 ng/ μ L	6 μ L
T4 DNA Ligase	1 μ L
10 \times T4 DNA Ligase Buffer	3 μ L
Sigma H ₂ O	20 μ L

After retransformation, amplification and isolation of the DNA (see 2.2.3 Bacterial transformation using heat shock, page 41), the cloning success was checked by a control digestion with BamHI for its dual cutting within the vector and insert. For that, 5 μ L DNA isolated with the QIAprep Spin Miniprep Kit were digested with 1 μ L BamHI in the presence of 3 μ L 10 \times Cutsmart buffer and 21 μ L Sigma H₂O. The reaction mix was incubated for 2 hours at 37°C. Loading buffer was added and samples were run on a 1% agarose gel (with ethidium bromide) for 40 minutes at 80 V. Clones with the correct digestion pattern were sequenced to eliminate the possibility of mutations.

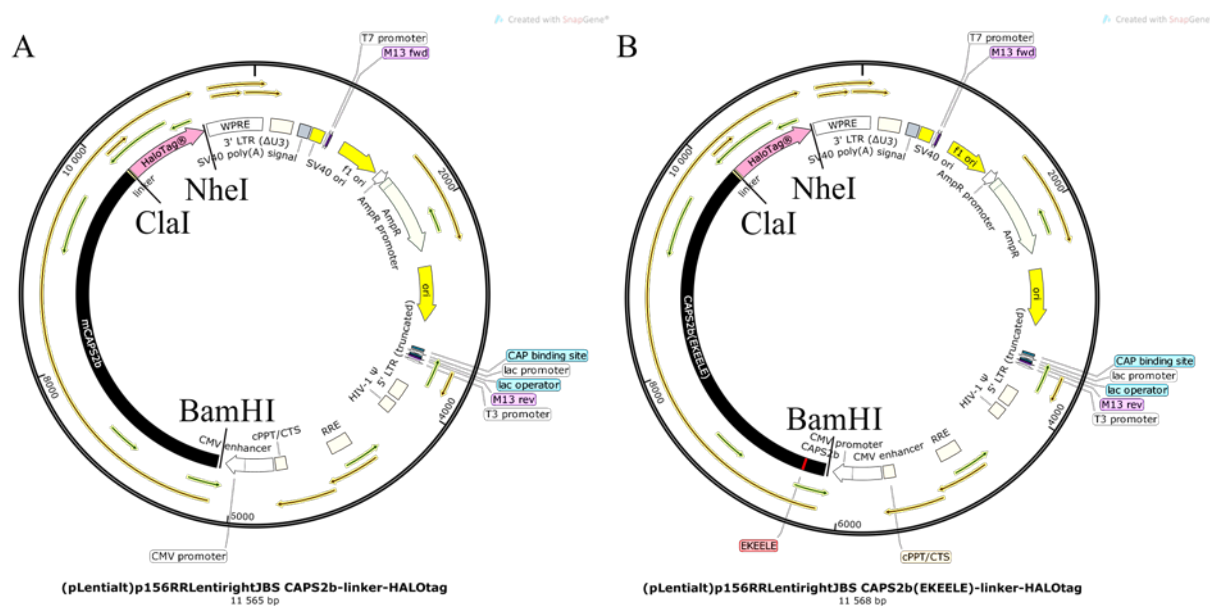


Figure 5: Vector maps with restriction enzymes BamHI, ClaI and NheI used for cloning of (A) pLenti-CAPS2b-Halo and (B) pLenti-CAPS1/2 chimera-Halo.

2.2.2.3 Lentivirus plasmid CAPS1-Halo

CAPS1-Halo cloning differed from CAPS2-Halo and CAPS1/2 chimera-Halo, because there was no plasmid with fitting restriction enzymes. For this reason, CAPS1 and Halo were assembled by overlap extension PCR. The strategy involved designing overlapping primers and two end primers with unique restriction sites to insert the product in the lentiviral vector. The first step was to perform two separate PCRs in which CAPS1 and Halo were amplified. CAPS1

was produced by using a forward primer which included a BamHI restriction site 5' ATATACGCGGATCC[^]ATGCTGGACCCTTCGTCCAGC 3' and a reverse primer to add an overhang for the following overlap extension PCR 5' CCGCTTCCGCCGCTCCCACCGCG CGCCGC[^]ATCATCTTCTTCATCTTCCTCATCACTGTC 3'. Halo was amplified by a forward primer adding the same overhang sequence as in CAPS1 5' GGAGCGGCGGAAGCG GCGGTACCATCGAT[^]ATGGCAGAAATCGGTACTGGCTTTCCATTC 3' and a reverse primer which included a NheI restriction site 5' TATACTAGCTAGC[^]TTAGCCGGAAATCT CGAGCGTCGACAG 3'.

Table 14: PCR mix for CAPS1 amplification.

reagent	volume
Forward primer 25 pmol	1 μ L
Reverse primer 25 pmol	1 μ L
DNA (CAPS1) 25 ng/ μ L	4 μ L
dNTP mix 10 mmol/ μ L	1 μ L
5 \times Q5 polymerase buffer	10 μ L
5 \times Q5 polymerase GC enhancer	10 μ L
Q5 polymerase 2 U/ μ L	0.5 μ L
Sigma H ₂ O	22.5 μ L

Table 15: PCR programme for CAPS1 amplification.

	temperature	time	no. of cycles
1. Initial Denaturation	98°C	30 sec	1
2. Denaturation	98°C	10 sec	
3. Annealing	65°C	30 sec	35
4. Elongation	72°C	2.5 min	
5. Final Elongation	72°C	2 min	1
6. End	4°C	forever	

Table 16: PCR mix for Halo amplification.

reagent	volume
Forward primer 25 pmol	1 μ L
Reverse primer 25 pmol	1 μ L
DNA (Halo) 100 ng/ μ L	1 μ L
dNTP mix 10 mmol/ μ L	1 μ L
5 \times Phusion polymerase buffer	10 μ L
Phusion polymerase 2 U/ μ L	0.5 μ L
Sigma H ₂ O	35.5 μ L

Table 17: PCR programme for Halo amplification.

	temperature	time	no. of cycles
1. Initial Denaturation	98°C	30 sec	1
2. Denaturation	98°C	30 sec	
3. Annealing	60°C	40 sec	30
4. Elongation	72°C	1 min	
5. Final Elongation	72°C	10 min	1
6. End	4°C	forever	

The amplified DNA products (50 μ L) were loaded with 10 μ L 6 \times loading dye and run together with 6 μ L of the 1 kb GeneRuler DNA ladder on a 1% agarose gel (with ethidium bromide) for 1 hour at 75 V. The DNA bands with the correct size (~ 4100 bp for CAPS1 and ~ 800 bp for Halo) were then eluted from the gel with the QIAquick Gel Extraction Kit according to the manufacturer's protocol. The concentration of the isolated DNA was checked by running a quantitative agarose gel. For that, 1 μ L of sample with 1 μ L 6 \times loading dye and 4 μ L H₂O were loaded together with 5 μ L of 1 kb GeneRuler DNA ladder on a 1% agarose gel (with ethidium bromide). The gel was run for 45 minutes at 80 V. The estimated DNA concentration of CAPS1 was 10 ng/ μ L and for Halo 70 ng/ μ L. In a next step, the purified DNA fragments were assembled by overlap extension PCR. First, Master Mix A was prepared to hybridize the common overhang sequence of CAPS1 in the C-terminus and Halo in the N-terminus and extended by DNA polymerase. For a sufficient hybridization, a 1:1 molar ratio of CAPS1 and Halo was used. After 15 cycles without primers Master Mix B with CAPS1 forward primer and Halo reverse primer was added to the overlap extension PCR reaction to amplify the hybridised CAPS1-Halo fragment for another 20 cycles.

Table 18: Overlap extension PCR mix for CAPS1-Halo amplification.

reagent	volume	
	Master Mix A	Master Mix B
Forward primer 25 pmol (CAPS1)	-	1 μ L
Reverse primer 25 pmol (Halo)	-	1 μ L
DNA (CAPS1) 10 ng/ μ L	13.3 μ L	-
DNA (Halo) 70 ng/ μ L	0.45 μ L	-
dNTP mix 10 mmol/ μ L	1 μ L	1 μ L
5 \times Q5 polymerase buffer	5 μ L	5 μ L
5 \times Q5 polymerase GC enhancer	5 μ L	5 μ L
Q5 polymerase 2 U/ μ L	0.25 μ L	0.25 μ L
Sigma H ₂ O	-	11.75 μ L

Table 19: Overlap extension PCR programme for CAPS1-Halo amplification.

	temperature	time	no. of cycles
1. Initial Denaturation	98°C	30 sec	1
2. Denaturation	98°C	10 sec	
3. Annealing	70°C	30 sec	15
4. Elongation	72°C	3 min	
5. Pause	10°C	add Master Mix B	
6. Denaturation	98°C	10 sec	
7. Annealing	70°C	30 sec	20
8. Elongation	72°C	3 min	
9. Final Elongation	72°C	2 min	1
10. End	4°C	forever	

Afterwards the PCR result was verified on a 1% agarose gel (with ethidium bromide). For that, 50 μ L of the sample with 10 μ L 6 \times loading dye were loaded together with 6 μ L of the 1 kb GeneRuler DNA ladder and was run for 45 minutes at 80 V. The PCR product with a size of about 5 kb was then eluted from the gel with the QIAquick Gel Extraction Kit following the manufacturer's protocol. After elution and purification, the CAPS1-Halo PCR product and the NPY-Venus lentivirus plasmid were digested with the restriction enzymes BamHI and NheI in order to generate compatible ends capable of being ligated together.

Table 20: Restriction digestion mix for PCR CAPS1-Halo and pLenti NPY-Venus.

reagent	PCR CAPS1-Halo	pLenti NPY-Venus
DNA	23 μ L	0.75 μ L (~ 1 μ g)
BamHI	2 μ L	2 μ L
NheI	2 μ L	2 μ L
10 \times Cutsmart	3 μ L	3 μ L
Sigma H ₂ O	-	22.25 μ L

The digestion mixture was incubated for 3 hours at 37°C. Afterwards loading buffer was added to the linearized DNA and loaded together with the 1 kb GeneRuler DNA ladder on a 0.8% agarose gel (with ethidium bromide). The gel was run for 45 minutes at 80 V. The DNA bands for CAPS1-Halo and the lentiviral backbone plasmid were cut under the UV lamp and eluted from the agarose gel by using the QIAquick Gel Extraction Kit following the manufacturer's protocol. To check the concentration of the isolated DNA 1 μ L of sample with 1 μ L 6 \times loading dye and 4 μ L H₂O were loaded together with 6 μ L of the 1 kb GeneRuler DNA ladder on a 0.8% agarose gel (with ethidium bromide). The gel was run for 45 minutes at 80 V. Subsequently the DNA concentrations were estimated by comparing with the DNA ladder band intensities. For CAPS1-Halo the evaluated DNA concentration was about 10 ng/ μ L and for the lentiviral backbone plasmid around 30 ng/ μ L. In a next step, the two digested DNA

fragments (lentiviral backbone plasmid and CAPS1-Halo) were combined with the T4 DNA ligase and incubated for 16 hours at 14°C. After calculating a molar ratio of 1:2 vector to insert, 90 ng lentiviral plasmid were used with 135 ng CAPS1-Halo. In addition, a control ligation was prepared with the digested vector but not with the insert to validate the ligation success.

$$\frac{30 \text{ ng pLenti} \times 5.014 \text{ kb CAPS1} - \text{Halo} \times 2}{6.681 \text{ kb pLenti}} \approx 45 \text{ ng CAPS1} - \text{Halo}$$

Table 21 Ligation mix for CAPS1-Halo and pLenti.

reagent	reaction volume	control volume
Vector DNA (pLenti) 30 ng/μL	3 μL	3 μL
Insert DNA (CAPS1-Halo) 10 ng/μL	13.5 μL	-
T4 DNA Ligase	1 μL	1 μL
10 × T4 DNA Ligase Buffer	2 μL	2 μL
Sigma H ₂ O	-	7.3 μL

After retransformation, amplification and isolation of the DNA (see 2.2.3 Bacterial transformation using heat shock, page 41) the cloning success was checked by a control digestion with BamHI for its single cutting within the vector. In addition, clones with positive digestion pattern were send for sequencing to exclude the possibility of mutations.

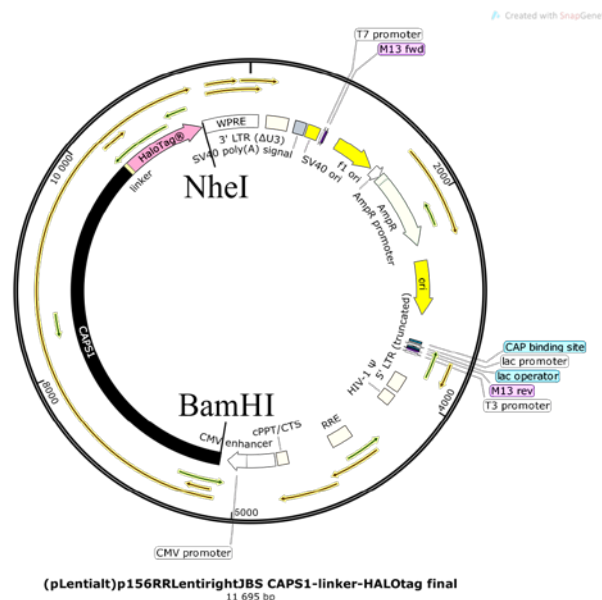


Figure 6: Vector map with restriction enzymes BamHI and NheI used for cloning of pLenti-CAPS1-Halo.

2.2.3 Bacterial transformation using heat shock

An aliquot of the competent bacteria (DH5 α or Stbl3) was thawed on ice for 20 minutes and mixed with either 1 μ g plasmid DNA or the whole ligation mixture (insert DNA attached to plasmid DNA). Afterwards bacteria and DNA were incubated together on ice for 30 minutes. Heat shock was performed at 37°C for 5 minutes. The bacteria were then placed back in the ice for 10 minutes. Subsequently, they were mixed with 300 μ L LB medium under semi sterile conditions and incubated at 37°C with shaking at 600 rpm for 45 minutes. The content was streaked on preheated LB agar plates with appropriate selection medium (LB medium with 100 μ g/mL ampicillin or 30 μ g/mL kanamycin) and incubated overnight at 37°C. Successfully transformed bacteria were picked as colonies and amplified overnight in the liquid LB selection medium. Afterwards, bacteria were harvested and DNA isolation was carried out using QIAprep Spin Miniprep Kit or EndoFree Plasmid Maxi Kit according to the manufacturer's instructions. The quantitative DNA determination was carried out by photometric measurement at 260 nm.

2.2.4 Primary cell culture of adult mouse DRG neurons

Six 25 mm coverslips were placed into the wells of a sterile 6-well plate and coated with Poly-D-Lysine (PDL). For this purpose, 200 μ L of PDL solution (0.5 mg/mL in Sigma H₂O) were added to the centre of each coverslip and incubated overnight at 37°C. On the next day, PDL solution was aspirated and the coverslips were rinsed twice with 300 μ L sterile Sigma H₂O. After washing the coverslips in the 6-well plate were sterilized in a UV-chamber for 20 minutes. After UV radiation coverslips were rinsed again with 300 μ L sterile Sigma H₂O followed by two washes with 500 μ L NBA medium. Each well was then filled with 2 mL DRG cell culture medium and placed in the incubator (37°C and 5% CO₂).

For preparation of the DRG neurons scissors and forceps were disinfected with 70% ethanol. The mouse was killed via decapitation and disinfected with 70% ethanol. The skin above the spine was removed. The surrounding tissue of the spine was also removed. The spine was incised at the level of the back legs. The posterior part of the spine was removed along with the spinal marrow. DRGs were located closely along the dorsal root of the cord, in the intervertebral foramina. DRGs were isolated with spring scissors and suitable forceps. Isolated DRGs were collected in a Petri dish filled with a drop of Locke's solution. After collecting approximately 30-40 ganglia within 45 minutes the DRGs were transferred into the previously prepared Petri dish with 200 μ L of TrypLE Express solution to allow slow enzymatic dissociation of the DRG

connective tissues. The DRGs were then transferred into a freshly prepared digestion solution (1 mL NBA medium with 2.31 U/mg Liberase, sterile filtered). DRGs were digested at 37°C in a water bath with gentle shaking. After about 6 minutes of digestion, DRGs were triturated five times with a 1 mL pipette tip followed by ten times trituration after around 12 minutes and a final fifteen times trituration at the end of the digestion, which was roughly 18-22 minutes depending on the age of the mouse. Digestion was stopped by adding 100 µL FCS and the cell suspension was centrifuged at 300 rcf for 4 minutes. The cell pellet was washed with 600 µL DPBS and centrifuged again under the same conditions. Afterwards the cell pellet was resuspended in 600 µL NBA medium. 100 µL of cell suspension were plated on each coverslip. After 5 minutes resting under the sterile hood to let the cells settle down, they were put in the incubator (37°C and 5% CO₂). On the next day, the old DRG culture medium was replaced with fresh culture medium.

2.2.5 Primary cell culture of embryonic mouse DRG neurons

Mice with a deletion of CAPS1 are not viable and die shortly after birth. To obtain DRGs from CAPS1 KO or CAPS1/2 dKO mice, it was necessary to prepare embryonic animals. The protocol was very similar to the adult preparation and cell culture. Minor changes are explained below. Pregnant mice were euthanized by CO₂ and sacrificed by cervical dislocation. Embryos were removed by C-section. DRGs were isolated as described previously. 350 µL of TrypLE Express were directly added to the Petri dish with the DRGs in Locke's solution. Afterwards DRGs were transferred to the Liberase Digestion solution. Trituration was required through the entire digestion time of 3 minutes. Digestion was stopped by adding 200 µL FCS. Cells were centrifuged as described before and washed with 700 µL DPBS. Depending on the experiment, cells were either seeded on 25 mm coverslips (in a 6-well plate with 2 mL cell culture medium per well) or on 15 mm coverslips (in a 12-well plate with 1 mL cell culture medium per well). Enough cells for one to two 25 mm coverslips or three 15 mm coverslips were isolated from one embryo.

2.2.6 Primary co-culture of DRG/SC neurons

There is no synapse formation in DRG neurons monocultures (Ransom et al., 1977a; Ransom et al., 1977b; Wake et al., 2015), but they do form synapses onto their natural target cells, the dorsal and ventral horn neurons (Joseph et al., 2010). So, to study synaptic transmission it was necessary to make use of the DRG/SC co-culture system.

The DRG preparation was performed as explained before. On the next day, if appropriate, DRG neurons were infected with a lentivirus containing a protein of interest. On the following day, SC neurons were added to the DRG neurons. For this, P0 to P2 old mice were sacrificed by decapitation. The lower part of the mouse, at the height of the hind legs, was cut off to expose both ends of the SC. The mouse was then sterilized with 70% ethanol. A 2 mL syringe with a 21 G capillary was used to isolate the SC. The syringe was filled with EBS solution, placed on the lower part of the exposed SC and pressure was applied to eject the SC tissue into an ice cold EBS solution, which was before bubbled with carbogen for about 30 minutes to adjust the pH. Next, the SC was transferred into an enzymatic solution with 20 U/mL Papain. The digestion was performed in a water bath at 37°C gentle shaking under constant gassing with carbogen for 30 minutes. To stop the digestion 1 mL of SC neuron cell culture medium was added. The tissue was triturated six to eight times using a 1 mL pipette tip and another 1 mL of SC neuron cell culture medium was added. The tissue was centrifuged at 800 rpm for 5 minutes. The supernatant was removed and 500 µL of 1/1 medium was added to the pellet. The tissue was triturated three times, then the tube was left upstanding to allow remaining fragments to sink by gravity for roughly 1 minute. The supernatant including the cells was collected into 2mL of 10/10medium. The previous step was repeated three times and cells in 10/10 medium were centrifuged again under the same conditions as before. The supernatant was again discarded and the cells were triturated three times in 500 µL SC neuron cell culture medium. Again the tube was left upstanding to allow remaining tissue fragments to sink by gravity flow and the supernatant was transferred into 1 mL of SC neuron cell culture medium. This step was also repeated three times and cells were centrifuged as before. The supernatant was discarded and the cell pellet was resuspended in fresh SC neuron cell culture medium. The cells were plated on the coverslips (100 µL per well) and after 5 minutes of rest under the sterile hood to allow them to settle, the plate was moved to the incubator (37°C and 5% CO₂). On the next day, 2/3 of the old SC neuron culture medium was replaced with fresh culture medium.

2.2.7 Lentivirus production

To produce lentivirus, the plasmids encoding the structural elements, envelope, and transfer gene were transfected into fast growing human embryonic kidney cells with the SV40 large T antigen (HEK293FT) (Vigna and Naldini, 2000). Following transfection, lentiviral particles were released into the cell culture medium (Tang et al., 2015) and were then harvested via ultracentrifugation.

Three days before lentivirus production, about 2×10^6 HEK293FT cells were split into one 150 cm² cell culture flask to reach a confluence on the transfection day of around 80 to 90%. In total four to six flasks were used for the production of one batch of lentivirus. In the morning of the first production day, the medium of the HEK293FT cells was replaced by incomplete DMEM + GlutaMAX to starve the cells. Around six hours later, the calcium phosphate transfection procedure started. The components were added into a 15 mL falcon tube in the following order, sterile 1.8 mL Sigma H₂O, the DNA mixture and 200 μ L of freshly prepared CaCl₂ (2.5 M). The DNA mixture for third generation lentivirus production contained 170 to 180 μ g of transfer vector DNA encoding the gene of interest and 80 μ g of all helper plasmids pMDLg/pRRE, pRSV-REV and pMD2.G. For the production of the second generation, 180 μ g of transfer vector DNA were combined with two helper plasmids pCMV-dR8.2 dvpr (120 μ g) and pCMV-VSV-G (80 μ g).

The Sigma H₂O, DNA and CaCl₂ mixture was then dropped with a glass pipette into another 15 mL falcon tube with 2 mL HBS. In this critical step it was important to drop the DNA solution directly into the middle of the HBS solution without touching the plastic wall of the falcon. The mixture was incubated for 25 minutes at room temperature (RT). After incubation a cloudy mixture appeared which was used to transfect the HEK293FT cells with a glass pipette in a drop wise manner along the entire cell culture flask while moving it gentle in a circular way. Two cell culture flasks were transfected with this 4 mL DNA/CaCl₂/HBS mixture. Cells were incubated at 37°C and 5% CO₂ for at least 5.5 hours before the old medium was replaced with complete DMEM + GlutaMAX (containing 100 mM sodium pyruvate, 10% FCS and 1% NEAA). The cells were kept in the incubator for 36 hours.

Before harvesting the virus, the cells were inspected under the microscope and the change of the cell culture medium from red to yellow was observed. If cells were floating and building clumps the virus harvesting was started. The medium was pipetted out of the flasks into 50 mL falcon tubes and centrifuged at 1800 rpm for 20 minutes. The supernatant was pushed through a cell filter (for a total of about 150 mL 3 filters were needed) and pooled together. Afterwards, the virus containing medium was centrifuged in an Amicon Ultra Centrifugal Filter (7.5 mL per tube and re-used for maximum 5 centrifugation steps) at 1900 rpm for 20 minutes at 4°C. The elution was transferred equally into 2×38.5 mL thinwall polypropylene tubes filled before with 1.5 mL of 20% sucrose (in DPBS sterile filtered) and placed into chilled SW 32 Ti buckets. For ultracentrifugation all six buckets of the SW 32 Ti rotor must be correctly balanced. The buckets that were not filled with virus were filled with water. The virus was centrifuged at 22500 rpm for 2.5 hours at 4°C.

Following ultracentrifugation, the supernatant was poured off gently, ensuring that the virus pellets were not disturbed. To remove as much liquid as possible tubes were put upside down on tissue paper for about 10 minutes. Afterwards, 100 μ L DPBS was pipetted onto the virus pellets and incubated on ice for 30 to 60 minutes. Then, the pellets were resuspended by pipetting up and down and pooled together into one tube. Once resuspended, virus was aliquoted into 2 mL screw cap cryotubes and flash frozen in liquid nitrogen. From six 150 cm² cell culture flasks, 15 cryotubes of virus in DPBS were aliquoted, each with about 15 to 25 μ L volume, depending on how much residual liquid were still in the tubes. Virus was stored at -80°C.

2.2.8 Halo ligand chloroalkane-ATTO590 staining

Cell labelling was performed on day *in vitro* (DIV) 6 or 8 by replacing half of the old DRG cell culture medium with fresh culture medium containing the Halo ligand chloroalkane (CA)-ATTO590 (produced by Alexander Horn). A final concentration of 0.5 μ M was used for confocal and TIRF microscopy and 2.5 μ M for STED microscopy. After 30 minutes of incubation at 37°C and 5% CO₂, cells were rinsed twice with pure NBA medium and incubated in half fresh and half old DRG cell culture medium for overnight or additional three days before they were measured.

2.2.9 Immunocytochemistry

Immunocytochemistry (ICC) is used to visualize proteins of interest in cells by using a specific primary antibody against the target protein. A fluorophore-conjugated secondary antibody is applied against the primary antibody to make the protein visible under a fluorescence microscope.

Before the cells were fixed, they were washed once with PBS. Fixation was performed in 4% paraformaldehyde (PFA) in PBS with a pH of 7.4 for 15 minutes at RT. Then the coverslips were washed three times for 3 minutes with PBS. Samples were quenched for 10 minutes with 50 mM Glycine in PBS followed by three times for 3 minute washes with PBS. Permeabilization was performed for 30 minutes at RT. To prevent nonspecific antibody binding, the coverslips were washed two times for 5 minutes with blocking solution. The primary antibody was diluted in blocking solution to the working concentration. Coverslips were incubated upside down with the cell side in 100 μ L diluted primary antibody solution for 1 hour at RT or overnight at 4°C.

Afterwards the coverslips were washed three times for 3 minutes with permeabilization solution. The secondary antibody was diluted in blocking solution to the working concentration and kept in the dark. The secondary antibody solution was centrifuged for 5-10 minutes at 13000 g and 4°C to avoid high background signals. The samples were then incubated with the secondary antibody for 45 minutes at RT in the dark. Cells were washed four to five times for 3 minutes with permeabilization solution followed by two short washes with PBS. On the microscope slides, 15 µL mounting medium were added for 15 mm coverslips and 25 µL mounting medium were used for 25 mm coverslips. If the samples were used for STED microscopy, they were mounted with the Abberior Solid Mounting Medium, which was put at 50°C for 10 minutes prior to use. Before the coverslips were mounted on the microscope slides, they were shortly dipped in distilled water. Excess water was removed by touching the coverslips gently on a piece of fine tissue paper. The coverslips were then embedded with the cell side facing the mounting medium and left to dry for 10 to 20 minutes at 37°C or for 3 hours at RT. After drying, the edges of the coverslips were sealed with nail polish. Samples were stored at 4°C in the dark and imaged within the next three days.

2.2.10 Double immunocytochemistry

To visualize the localization of two proteins in the sample using primary antibodies raised against the same species, a double ICC with a 'blocking' step in between was required. Blocking of the free epitopes of the antibodies is performed by using unconjugated Fab fragments from the same host species as the secondary antibody. This protocol was divided into three parts. Starting with the labelling of the first protein of interest with its specific primary antibody and a fluorophore-conjugated secondary antibody as described in the previous section (see 2.2.9 Immunocytochemistry). After the last washing step with permeabilization solution and PBS, the free epitopes of the secondary antibody must be blocked before starting with the second primary antibody. For this purpose, the samples were incubated again with blocking solution for 1 hour at RT. After washing three times for 5 minutes with PBS, the samples were incubated with an excess of unconjugated Fab fragments against the host species of the primary antibody diluted in blocking solution. The samples were washed again three times for 10 minutes with PBS. Finally, the samples were incubated with the second primary antibody and then with a secondary antibody according to the protocol described in the previous section (see 2.2.9 Immunocytochemistry).

2.2.11 Preparing protein lysates

Samples (whole brain or cerebellum) were homogenized manually in lysis buffer with 300 mM sucrose using a glass potter. The samples were always kept on ice to minimize degradation of the proteins. The lysates were then rotated at 4°C for 45 minutes to improve cell lysis. This was followed by two centrifugation steps at 2000 rpm and 4°C for 5 minutes to pellet the cell debris and the non-lysed cells. The supernatant contained the final protein lysate, which was stored at -80°C or directly measured for protein concentration using Quick Start Bradford on the Eppendorf BioPhotometer according to the manufacturer's instructions. The system was calibrated by measuring a BSA dilution series. Before the samples were measured, a blank sample containing the dye Coomassie Brilliant Blue G-250 and the lysis buffer was measured at 595 nm as a zero value.

2.2.12 Immunoprecipitation

For immunoprecipitation (IP), whole brain or cerebellar lysates were freshly prepared and Dynabeads protein G were used to pull down the protein of interest with the appropriate antibody. 2 mg of protein lysate were pre-cleared with 25 µL of bead slurry. For that, beads were washed three times for 5 minutes with lysis buffer on a rotator. Lysis buffer was removed using a magnetic stand to hold back the beads. Next, the lysate was added to the beads. The pre-clearance was performed for 1 hour at RT on a rotator. The pre-cleared lysate was removed with a magnetic stand and 20 µL was removed to load on the gel as input. The remaining protein lysate was split into two fractions (1 mg each).

One fraction was incubated with the primary antibody for the protein of interest and the second fraction was incubated with an anti-rabbit IgG control antibody. First, lysate and antibody were incubated for 3 hours at RT on a rotator to allow binding of the antibody to its target protein. Next, 25 µL of prewashed beads were added to the sample and incubated for one more hour or overnight (for CAPS1 or CAPS2 IP, respectively) at RT on a rotator, so the antibody protein complex can bind to the beads. After incubation, the supernatant was collected by using the magnetic stand and the beads were washed three times 7 minutes on a rotator. The antibody protein complex bound to the beads was eluted in 80 µL 1 × LDS sample buffer (4 × LDS sample buffer with 10% β-Mercaptoethanol was diluted with Sigma H₂O to 1 ×) and cooked for 10 minutes at 95°C. Afterwards, beads were removed by using the magnetic stand. The precleared lysate (input), the supernatant and the elution from the beads were tested for protein expression by western blot.

2.2.13 Western blot

The expression of several proteins in the prepared lysates were checked by western blot. First, protein samples were denatured. For that, 10% β -Mercaptoethanol was added to 4 \times LDS sample buffer. Next the LDS sample buffer was added to the desired protein concentration to a final ratio of 1 \times and Sigma H₂O was added if necessary. The samples were boiled at 95°C for 10 minutes. A pre-cast NuPAGE 3-8% tris-acetate gel was used to separate the proteins by mass. The tris-acetate running buffer (20 \times) was diluted with distilled water to obtain 1 \times running buffer. The wells of the gel were washed with the running buffer and the samples together with the Spectra Multicolor Broad Range Protein Marker were loaded. By applying a voltage of 120 V, separation was performed for 1.5 hours at RT.

After gel electrophoresis, the proteins were transferred to a nitrocellulose membrane. Therefore, 20 \times transfer buffer was diluted to 1 \times with 20% methanol and 80% distilled water. Four foam sponges, a Whatman paper, the gel, the nitrocellulose membrane, another Whatman paper and four foam sponges were equilibrated in the transfer buffer and stacked in the above mentioned order in the transfer chamber Minigelsystem XCell. The gel was positioned towards the anode to transfer the proteins to the nitrocellulose membrane at 60 mA and 4°C for 20 hours. In order to check the quality of the transfer, the membrane was stained with Ponceau S solution for 5 minutes and the gel was incubated in Coomassie S solution for 2 hours.

The membrane was washed two times for 5 minutes with TBS and 0.05% Tween 20 (TBST) to wash out the Ponceau S solution and blocked with 7% non-fat dry milk in TBST for 2 hours at RT. Primary antibodies were incubated for 1 hour at RT or overnight at 4°C in TBST with 3.5% milk. Afterwards, the membrane was washed three times for 20 minutes in TBST with 3.5% milk. The secondary antibody coupled to horseradish peroxidase (HRP) was incubated for 1 hour at RT in TBST with 3.5% milk. The membrane was washed again three times for 20 minutes in TBST. After two short washes in TBS, the SuperSignal West Dura Extended Duration Substrate was prepared and added to the membrane to visualize the proteins using the FluorChem M gel imaging system.

2.2.14 Laser scanning microscopy

Laser scanning microscopy (LSM) is suitable for recording living and fixed samples. A fluorescence microscope from Zeiss (LSM 780) scans the sample with a focused laser beam. Scan mirrors deflect the light in x and y and a motor-driven z-drive allows the creation of z-stacks for capturing three-dimensional images. The system has various excitation lasers that

can deliver light of the wavelengths 405, 458, 488, 494, 514, 561 and 633 nm. Images were taken with a 40x or 63x oil objective. For a z-stack, the number and thickness of a single focal plane were defined individually for each image. For acquisition, the scan mode was set to frame and the frame size was adjusted to 1024×1024 . The line step was set to 1 and the speed was 8. To improve the quality, 2 scans of the same region were averaged. The mode of the averaging was set to line and the averaging method was adjusted to mean. The bit depth was 16 bits. Scanning of the laser was set to unidirectional (single arrow). The digital gain was always set to 1 and the digital offset to 0. The amplification voltage of the multiplier (master gain) and the laser power were adjusted individually for each data set. The system-specific imaging software ZEN was used to control the microscope and acquire the data.

2.2.15 Stimulated emission depletion microscopy

Stimulated emission depletion (STED) microscopy is one of several types of super-resolution microscopy techniques recently developed to bypass the diffraction limit of light microscopy and increase resolution (Hell and Wichmann, 1994; Klar and Hell, 1999). It works by deactivating fluorescence from the outer part of the focal spot. While the first laser pulse produces a diffraction-limited distribution of the excited molecules, a spatially offset pulse quenches the excited molecules from the outer part of the focus by stimulated emission. When a fluorophore in the excited state encounters a photon corresponding to the energy difference between the excited and ground state, it can be brought back to the ground state by stimulated emission before spontaneous fluorescence emission occurs. This process effectively depletes fluorophores in the excited state that are capable of fluorescence emission (Figure 7A and B). To use STED to sharpen the excitation point spread function (PSF), the STED laser must have a pattern with a zero intensity at the centre of the excitation laser focus and a non-zero intensity at the periphery. The key to achieve super-resolution is the nonlinear dependence of the depleted population on the intensity of the STED laser as it approaches the level of saturated depletion: if the local intensity of the STED laser is higher than a certain level, essentially all spontaneous fluorescence emission is suppressed. By increasing the power of the STED laser, the range of saturated depletion is extended without greatly affecting the fluorescence emission at the focal point, because the intensity of the STED laser is nearly zero at this point. Consequently, the fluorescence signal can only be observed in a small area around the focal point, which reduces the effective width of the PSF (Figure 7C). Scanning these small effective PSF will then produce super-resolution images.

The STED laser pattern is typically generated by inserting a phase mask into the beam path to modulate its phase-spatial distribution (Huang et al., 2009). Such a phase mask produces a donut-shaped STED pattern in the xy -plane and has provided a lateral resolution of about 30 nm (Westphal and Hell, 2005), whereas axial resolution is not increased above diffraction. This might not be a disadvantage when imaging a correctly oriented, two-dimensional sample. However, when imaging three-dimensional biological structures, e.g. synapses, which extend along the optical axis, the poor axial resolution will drastically affect the image quality. Therefore, dual-colour 3D STED was established by making use of an appropriate beam shaping technique with a specially designed phase mask. While 2D imaging uses a doughnut beam, the introduction of a π -step phase change creates the bottle-beam (Arlt and Padgett, 2000), which depletes out-of-focus light and increases axial resolution to about 100 nm (Klar et al., 2000).

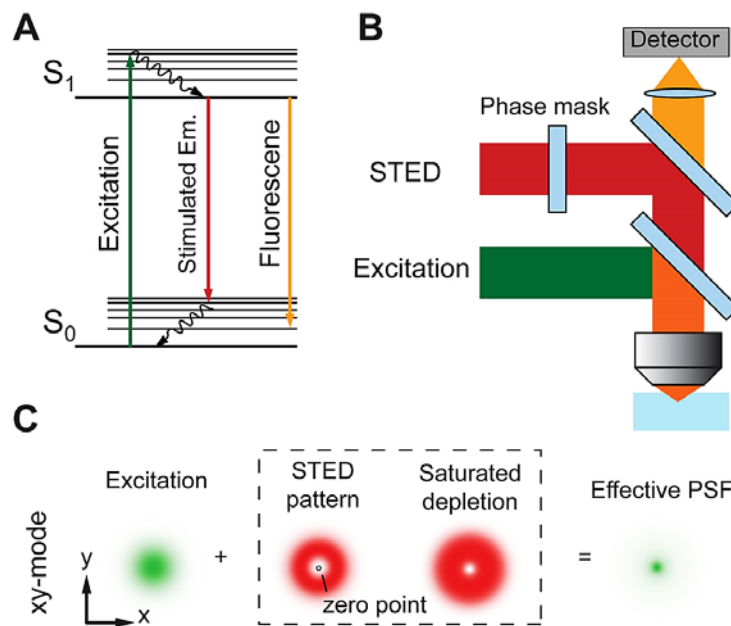


Figure 7: The principle of STED microscopy. (A) The process of stimulated emission. (B) Schematic illustration of a STED microscope. (C) In the xy mode, a donut-shaped STED laser is used, with the zero point overlapping the maximum of the excitation laser focus (Huang et al., 2009).

For STED microscopy, secondary antibodies with specific fluorescent properties were used, which ensure the highest fluorescence intensity and stability. To achieve an optimal result, the samples were mounted with the Abberior Mount Solid Antifade, which is specially designed for confocal and super-resolution 2D and 3D microscopy. Imaging was performed with a four-color STED QuadScan using pulsed excitation lasers at 485 nm, 561 nm and 640 nm and the STED laser at 775 nm. Pinhole size was set to 80 μm (1AU) and the samples were visualized

with a 100x objective. The acquisition protocol was as follows: first, a single confocal section was recorded in confocal mode at 488 nm, 561 nm and 640 nm to visualize Synapsin, CAPS and Bassoon staining. Then a central section of a DRG-SC neuron synapse, identified by its triple labelling, was acquired in 2D STED mode at 561 nm and 647 nm to visualize the CAPS and Bassoon staining. Finally, a stack of about 1 to 1.5 μm depth of the same synapse was recorded in 3D STED mode.

For confocal images, the laser power was 12% at 488 nm and 15% at 561 nm and 640 nm. The pixel size was 80×80 nm. For 2D STED images laser power was 25% and 15% at 561 nm and 640 nm, respectively. The STED laser emitted at 25% of the maximal power of 1250 mW (corresponding to 37.5–42.5 mW in the focus, repetition rate 40 MHz) with a pulse duration of 938 ps. Pixel size was 20×20 nm. For 3D STED images, laser power and pulse duration were identical to 2D STED imaging. However, the STED laser emitted at 40% of the maximal power of 1250 mW (corresponding to 60–68 mW in the focus, repetition rate 40 MHz). Voxel size was $40 \times 40 \times 40$ nm. The settings used to acquire the STED images with Synapsin or the active zone proteins Munc13-1 and Homer1 together with Bassoon were similar to those with CAPS, aside from the laser power which had to be adjusted for the individual staining.

Before analysis and for display purposes, the acquired images were deconvolved with Matlab by Dr Marcel Lauterbach. A linear deconvolution method (according to Wiener filter) was applied, using a theoretical PSF and user-adapted regularization parameters. In 3D stacks each plane was deconvolved individually with a 2D deconvolution. The confocal PSF was modelled as a 2D Gaussian function and the STED PSF as 2D Lorentzian function.

2.2.16 Total internal reflection fluorescence microscopy

Total internal reflection fluorescence (TIRF) microscopy is one of the high-resolution microscopy techniques based on the total internal reflection of an induced evanescent wave between two media having different refractive indices. This technique makes it possible to illuminate fluorescent samples within a close proximity to the glass water interface. Thereby only the plane with which the cell adheres to the coverslip is illuminated. The rest of the cell is not illuminated resulting in an improved signal-to-noise ratio due to the reduction of stray light from objects in the background (Axelrod, 1981). This defined illumination of the sample is achieved by taking advantage of the refraction laws. If light strikes through different media with decreasing refractive indices $n_1 > n_2$, like the coverslip and the extracellular solution, it is completely reflected from the critical angle of incidence θ_c . Nevertheless, a portion of light,

called the evanescent wave, can pass into the extracellular solution and excite fluorescent samples at a distance of approximately 200 nm from the coverslip (Axelrod, 2001). Therefore, TIRF microscopy is a suitable method to observe LDCV fusion events and synaptic transmission with high spatial resolution and fast acquisition rates.

The imaging setup was the same as described previously (Bost et al., 2017; Shaib et al., 2018). Briefly, an Olympus IX70 microscope was equipped with a 100x/1.45 NA Plan Apochromat Olympus objective, a TILL-TIRF condenser, and a QuantEM 512SC or Evolve 512 camera. A multi-band argon laser emitting at 488 nm was used to excite Synaptophysin-pHluorin (SypHy) fluorescent and a solid-state laser 85 YCA emitting at 561 nm was used to excite NPY-pHuji or Halo ligand CA-ATTO590. A dual-view camera splitter was applied to separate the red and green channels. Secretion was evoked by electrical stimulation via a bipolar platinum-iridium field electrode and a pulse stimulator.

2.2.16.1 Recording of LDCV and/or SV evoked release from DRG/SC neuron co-cultures

On DIV1 DRG neurons were double infected with lentiviruses encoding for SypHy to highlight SVs and NPY-pHuji to mark LDCVs. For rescue experiments of synaptic transmission, SypHy was combined with either CAPS1-, CAPS2- or CAPS1/2 chimera-HaloTag (in short Halo). The next day, viruses were removed and SC neurons were added to the infected DRG neurons to ensure synapses marked with SypHy were only formed by DRG neurons on SC neurons and not by SC neurons on each other. The Halo constructs were used to co-express CAPS paralogs with SypHy. The HaloTag is a 33 kDa self-labelling protein tag derived from a bacterial enzyme, created to covalently bind to a synthetic ligand of choice. The synthetic ligands have a reactive chloroalkane (CA) linker, which is bound to a functional group (Los et al., 2008). For visualization of CAPS-Halo in the experiment, the CA linker was fused to the fluorescent dye ATTO590. The choice of fluorophores in the experiment was carefully considered to avoid a spectral overlap during measurements of the co-expressed proteins. Measurements were performed eight or nine days after the addition of SC neurons to the infected DRG neurons. DRG/SC neurons were recorded for 5 minutes. The measurement protocol was 30 seconds without stimulus, followed by a stimulus train of 4 V at 10 Hz for 30 seconds to trigger the exocytosis of SVs. After a resting phase of 10 seconds, a second stimulus train of 4 V at 100 Hz for 60 seconds was applied to trigger the exocytosis of LDCVs. At the end of the measurement, NH_4Cl was applied to visualize the entire SV pool. During the measurement, the bath temperature of the neurons was kept at 32°C by an extracellular solution in a perfusion system with an inline solution heater.

2.2.17 Confocal image analysis

All confocal data were analysed with ImageJ. In a first step the background on the single plane images was subtracted. The co-localization of anti-CAPS1, anti-Munc13-1 antibody and Synaptobrevin2-mRFP was analysed in two different ways: (1) Line profile analyses were performed on heterotypic synapses identified by co-localization of all three proteins. The profiles were determined on three pixel-wide lines of about 2 μm length crossing the synapse along the neurite. The centre of the synapse was defined by the maximum fluorescence intensity of the Synaptobrevin2-mRFP. This Synaptobrevin2-mRFP peak was used to register the individual CAPS1 and Munc13-1 curves of each synapse. (2) Manders' overlap coefficient and Pearson's correlation coefficient (Manders et al., 1993) for co-localization were measured using the JACoP ImageJ plugin (Bolte and Cordelières, 2006) on isolated neurites of DRG neurons. The analysis was limited to neurites that were at least 10 μm long and contained Synaptobrevin2-mRFP puncta, indicating the presence of heterotypic synapses. In addition, co-localization of CAPS1 with Munc13-1 was illustrated by measuring the fluorescence intensity along a three-pixel wide line within the displayed neurite.

To analyse the overexpression levels of CAPS1-, CAPS2- and CAPS1/2 chimera-Halo, the mean fluorescence intensity for CA-ATTO590 and anti-CAPS1 or anti-CAPS2 antibody signals were measured in a region of interest (ROI) that included the cell soma. The distribution of proteins from the cell soma into the neurite was analysed by measuring the fluorescence intensity along a three-pixel wide line of 15 μm length starting in the cell soma and ending in the neurite. The ratio of the average fluorescence intensities over a distance of 2.5 μm at the beginning and end of the line was calculated.

To analyse the accumulation of CAPS1-, CAPS2- and CAPS1/2 chimera-Halo at synapses, the mean fluorescence intensity of a ROI drawn precisely around the synapse was measured. This signal was then normalized to the mean fluorescence intensity of a ROI placed in the neurite right next to the synapse. In addition, the co-localization of CAPS1, CAPS2 or CAPS1/2 chimera to Synapsin was measured with the Pearson's correlation coefficient and the Manders' overlap coefficient using the JACoP plugin in ImageJ. This co-localization analysis was limited to synapse-rich regions in DRG neurites.

2.2.18 3D STED image analysis

The subsynaptic localization of CAPS-Halo proteins in comparison to the active zone protein Bassoon was analysed on the full 3D volume of the synapse using a cluster analysis approach

in Imaris on the deconvolved images. First, protein clusters in each channel (CAPS and Bassoon) were identified with the ImarisCell module using the creation wizard with the following settings: background subtraction width 1.6 μm , smoothing filter 0.04 μm , near automatic threshold and split by seed points (0.2 μm). Other settings were adjusted individually for each image. This module provided the XYZ centre of mass position of the clusters, their volume and their average fluorescence intensity. The position of the centre of mass of the two protein clusters made it possible to measure the distance between Bassoon and CAPS. As most 3D STED images contained more than one active zone defined by a Bassoon cluster, an analysis of the nearest neighbour between the clusters of both proteins was performed. The maximum distance between the clusters was set to 0.3 μm . This nearest neighbour analysis allowed to define pairs between a Bassoon and a CAPS cluster. Individual pairs were selected to perform the overlap analysis. This analysis was repeated with anti-Munc13-1, anti-Synapsin and anti-Homer1 antibodies with similar settings as described above.

2.2.19 TIRF image analysis

The LDCV fusion curves were presented as a cumulative increase of secreted vesicles over the measurement period. The histograms show the number of fused vesicles over time in a 10 second interval. LDCV fusion events were identified when the LDCVs suddenly appeared with a sharp raising fluorescent intensity and then quickly disappeared due to the release of NPY-pHuji (maximum event duration was 5 frames = 500 ms). In some cases, before measuring the sharp increase in fluorescence intensity due to the opening of the fusion pore, a weak fluorescent spot was detected, indicating the presence of a LDCV. The graphs and images in Figure 19Bi and Bii or Figure 21Bi and Bii show representative examples of classical LDCV fusion events. All other forms of LDCV fusion were also included, such as kiss-and-run and kiss-and-stay (Bost et al., 2017). The obtained data were analysed with ImageJ and secretion events with specific ROIs were documented. Synaptic transmission was also analysed with ImageJ. Synapses were defined as SypHy-labelled structures that responded to the electrical stimulus of 4 V at 10 Hz. First, the background of the images was subtracted. Then, synapses were marked by ROIs and the mean grey value was measured as a function of time. The displayed diagrams were normalized to the maximum signal at NH_4Cl application, which was used for deprotonation of the vesicles at synapses and induction of the maximum increase of the fluorescence signal.

2.2.20 Mass spectrometry data analysis

The Scaffold Viewer software was used to analyse the mass spectrometry (MS) data generated by Dr Claudia Fecher-Trost. To ensure significant protein identification the protein probability filter was set to 95% and the peptide probability filter was set to 90%. The identification of 2 unique peptides per protein was set as the minimum for protein identification, resulting in a protein false discovery rate (FDR) of 0.6% and 0.0% decoy and a peptide FDR of 0.1% and 0.0% decoy for CAPS1 and CAPS2, respectively. The total spectra were calculated for each protein and quantitative differences were statistically analysed by a t-test using Scaffold Viewer. Differences with p-values lower than 0.05 were considered statistically significant.

2.2.21 Statistics

In the box plots, the boundaries of the box represent 25th to the 75th percentile, a black line within the box marks the median while the white line corresponds to the average. Whiskers (error bars) above and below the box indicate the 90th and 10th percentile. In all other diagrams, error bars show the standard error of the mean value calculated with Excel or SigmaPlot. The one-way ANOVA, Dunn's post-hoc test and Tukey post-hoc test were calculated using SigmaPlot. A p-value < 0.05 was considered to be significant. N is the number of cultures, while n is the number of measured neurons. Graphs were generated by SigmaPlot, Igor or Excel. The violin plots were generated with the web tool from <http://shiny.chemgrid.org/boxplotr>. The graphs and models were formatted with CorelDRAW.

3 Results

3.1 Sequence alignment of CAPS paralogs reveals heterogeneity in the N-terminus

A comparison of the CAPS1 and CAPS2 sequences showed that they share about 80% sequence identity at the amino acid level (Speidel et al., 2003). Assuming that paralog-specific functions are mediated by protein-protein interactions, it is likely that these interactions are encoded in the most divergent regions of the proteins. Thus, the mouse protein sequences for CAPS1 (Q80TJ1) and CAPS2 (Q8BYR5) were downloaded from the UniProt Knowledgebase (<http://www.uniprot.org/>) and used for further in-depth sequence analysis. For the comparison of both protein sequences, they were entered in FASTA format and aligned with the multiple sequence alignment program Clustal Omega (<http://www.ebi.ac.uk/Tools/msa/clustalo/>). The analysis and manual correction were performed with jalview (<http://www.jalview.org/>). The sequence alignment of CAPS paralogs shows the greatest divergence in the N-terminal domain consisting of approximately the first 120 amino acids (always counted from the CAPS1 sequence). A closer comparison indicates that the N-terminal half of the CAPS paralogs contain highly conserved regions that are interrupted by more divergent regions. As shown in Figure 8, the first 18 amino acids between CAPS1 and CAPS2 are almost identical, as is the amino acid sequence from 69 to 73. Furthermore, the region from 82 to 97 residues is homologous. After amino acid 109 of the CAPS1 sequence, the alignment shows the before mentioned sequence identity of about 80%. However, there are three sections (amino acids 19-68, 74-81 and 98-108) with strongly divergent amino acid sequences. Among them are amino acids that either occur in only one of the two sequences or have completely different chemical-physical properties. The protein sections that show these differences could play a special role in paralog-specific protein interactions.

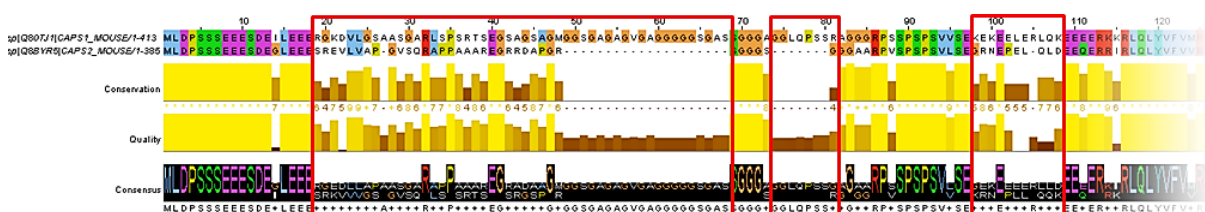


Figure 8: Sequence alignment of the N-terminus of CAPS paralogs. Sequences of about the first 120 amino acids of mouse CAPS1 and CAPS2 paralogs are aligned. Amino acids are coloured by the ClustalX default colour scheme. Conservation, quality and consensus sequence are automatically calculated by jalview and displayed below the sequence alignment. Conservation is visualized as a histogram giving the score for each column. The numbers reflect the conservation of physicochemical properties in the alignment: Identities score highest, and the

next most conserved group contain substitutions to amino acids lying in the same physicochemical class. Conserved columns are indicated by * (score of 11 with default amino acid property grouping), and columns with mutations where all properties are conserved are marked with a + (score of 10, indicating all properties are conserved). The quality is displayed as a histogram under the columns of the sequence alignment giving the probability that the mutations in a particular column of the alignment will be observed. The quality score is inversely proportional to the average cost of all mutation pairs observed in a given column of the alignment, a high quality score of the alignment for a column would suggest that there are no mutations or that most of the observed mutations are favourable. The consensus sequence logo indicates the relative amount of amino acids per column, which can be estimated by its size in the logo. Red rectangles indicate important differences between CAPS paralogs which may account for paralog-specific protein interactions.

To further differentiate which region with differences in the amino acid sequence of CAPS1 and CAPS2 might be important for function, the CAPS1 sequence was compared to its conserved homologs in other species to investigate the conservation and taxonomic range using the Basic Local Alignment Search Tool (BLAST, <https://www.ebi.ac.uk/Tools/sss/ncbiblast/>). The CAPS1 FASTA format sequence was entered and settings were adjusted. The search was started with the UniProt Knowledgebase eukaryota and the parameters SCORES and ALIGNMENT were adjusted to 500. In further steps, taxonomic subsets, for example vertebrates, nematoda, arthropoda, fungi or viridiplantae, were used and the parameters SCORES and ALIGNMENT were set to 50. The protein sequences released by the BLAST search were aligned using Clustal Omega and further analyses and manual corrections were performed with jalview. The multiple sequence alignment revealed that two of the three diverging regions in the N-terminus of CAPS paralogs (Figure 8) were highly conserved in the CAPS1 sequences of vertebrates. Figure 9 shows an example of a multiple sequence alignment between zebrafish (*Danio rerio*), african clawed frog (*Xenopus laevis*), rat (*Rattus norvegicus*), mouse (*Mus musculus*) and human (*Homo sapiens*) with the two unique highly conserved CAPS1 regions highlighted with a red rectangle. In further investigations of these sequences using secondary structure prediction tools provided by SMART (<http://smart.embl-heidelberg.de/>) and Pfam (<http://pfam.xfam.org/>) databases, only one of the two CAPS1 regions conserved between different species is located within a predicted helical structure, which is a valid indication that this region might play an important role in the determination of the global structure of CAPS1 and its function.

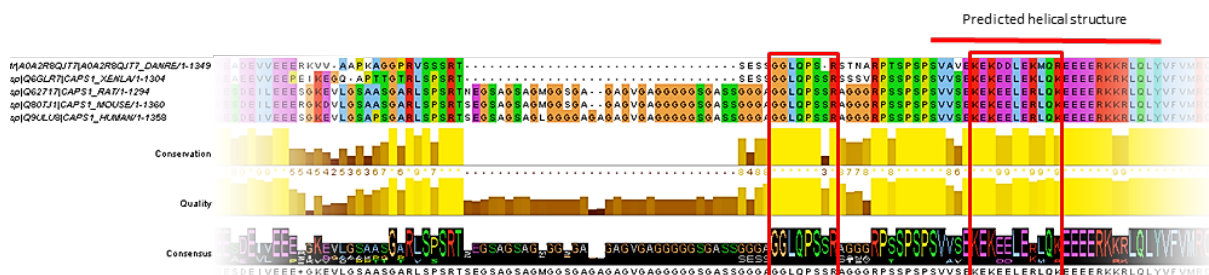


Figure 9: Sequence alignment of the N-terminus of CAPS1 between different species. Sequences from 9 to about 120 amino acids of zebrafish, frog, rat, mouse and human CAPS1 homologs. Amino acids are coloured by the ClustalX default colour scheme. Conservation, quality and consensus sequence are automatically calculated by jalview and displayed below the sequence alignment. Red rectangles indicate conserved regions in CAPS1 within the differences between CAPS1 and CAPS2 sequences (see Figure 7). Note the predicted helical structure between amino acids 93-120, which also contains one of the highly conserved unique CAPS1 regions.

Next, a protein similarity search was performed because it is an effective and reliable tool for identifying related protein sequences with known functions and can be combined with the functional prediction of CAPS sequences. A protein with high sequence similarity in the N-terminal region of CAPS1 (amino acids 84 to 134) was identified. This protein, called Cytohesin-1 or mSec7-1, specifically localizes into presynaptic compartments and improves neurotransmitter release (Neeb A., 1999). It was shown that the N-terminus is important for the localization of Cytohesin-1. This N-terminal region of Cytohesin-1 (amino acids 15 to 25) also shows the strongest similarity to the unique CAPS1 sequence (amino acids 98 to 108), which is indicated in Figure 10 with the red rectangle. Therefore, one could assume that this region has a similar functional importance for the subcellular localization of CAPS1. In addition, analyses to predict the secondary structure of Cytohesin-1 revealed a predicted helical structure within the N-terminus (amino acids 13 to 54), located in the same region as the predicted helical structure in CAPS1, which could therefore be a further indication of a related function.

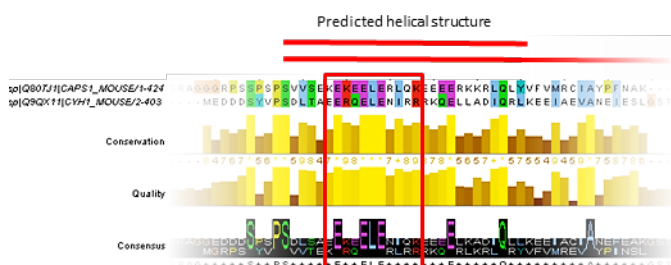


Figure 10: Sequence alignment of the N-terminus of CAPS1 and Cytohesin-1. Sequences from 84 to 134 amino acids for CAPS1 and 1 to 50 amino acids for Cytohesin-1 are shown. Amino acids are coloured by the ClustalX default colour scheme. Conservation, quality and consensus sequence are automatically calculated by jalview and displayed below the sequence alignment. The red rectangle indicates the unique CAPS1 region within the predicted helical structure and the high similarity to Cytohesin-1, which also contains a predicted helical structure from amino acids 13 to 54.

3.2 CAPS1 is present at synaptic and extra-synaptic sites

Recently our group showed a differential role for CAPS1 and CAPS2 in mediating exocytosis of LDCVs and SVs in sensory DRG neurons. The results indicated that CAPS1 mediates SV transmission whereas CAPS2 plays a role in LDCV exocytosis (Shaib et al., 2018). As the availability of CAPS1 at synapses could influence its role in priming of SVs, the synaptic and extra-synaptic localization of CAPS1 in neurites of cultured DRG neurons was investigated in the following experiments. Since DRG neurons *in vivo* or in culture do not build synapses on each other (Ransom et al., 1977a; Ransom et al., 1977b), they were co-cultured with their natural target cells, the dorsal horn neurons of the spinal cord (SC), so that the DRG neurons could form functional synapses (Gu and MacDermott, 1997; Joseph et al., 2010). DRG neurons were isolated from four to six weeks old Synaptobrevin2-mRFP knock-in mice to identify heterotypic synaptic contacts (Matti et al., 2013). The next day, the SC WT cells were added to the DRG neurons and co-cultured for another six to seven days, allowing functional synapses to form. On DIV6 or 7, cells were stained with antibodies against CAPS1 (Farina et al., 2015; Shaib et al., 2018) and Munc13-1 (Farina et al., 2015), which is a well described priming protein for SV and LDCV exocytosis in neurons (Varoqueaux et al., 2002; van de Bospoort et al., 2012) and is specifically localized to active zones (Kalla et al., 2006).

CAPS1 revealed a cytosolic distribution along neurites but in addition was detected in neuritic puncta (Figure 11A). Many of these CAPS1 positive puncta co-localized with the synaptic marker Synaptobrevin2-mRFP and the priming protein Munc13-1, which label synapses in the DRG/SC neuron co-culture (Figure 11B). About 60% of the CAPS1 positive puncta co-localized with the synaptic marker Synaptobrevin2-mRFP in neurites (Figure 11C, Pearson's correlation coefficient: 0.59 ± 0.03). Synaptobrevin2-mRFP immunoreactivity was detectable in approximately 65% of CAPS1 positive spots and approximately 40% of CAPS1 co-localized with Synaptobrevin2-mRFP (Figure 11D, Manders' overlap coefficients for Synaptobrevin2-mRFP in CAPS1: 0.64 ± 0.03 , and CAPS1 in Synaptobrevin2-mRFP: 0.39 ± 0.03). These results indicate that CAPS1 is not present at all synapses in the DRG/SC neuron co-culture, but rather is detected in about half of the Synaptobrevin2-mRFP positive synapses.

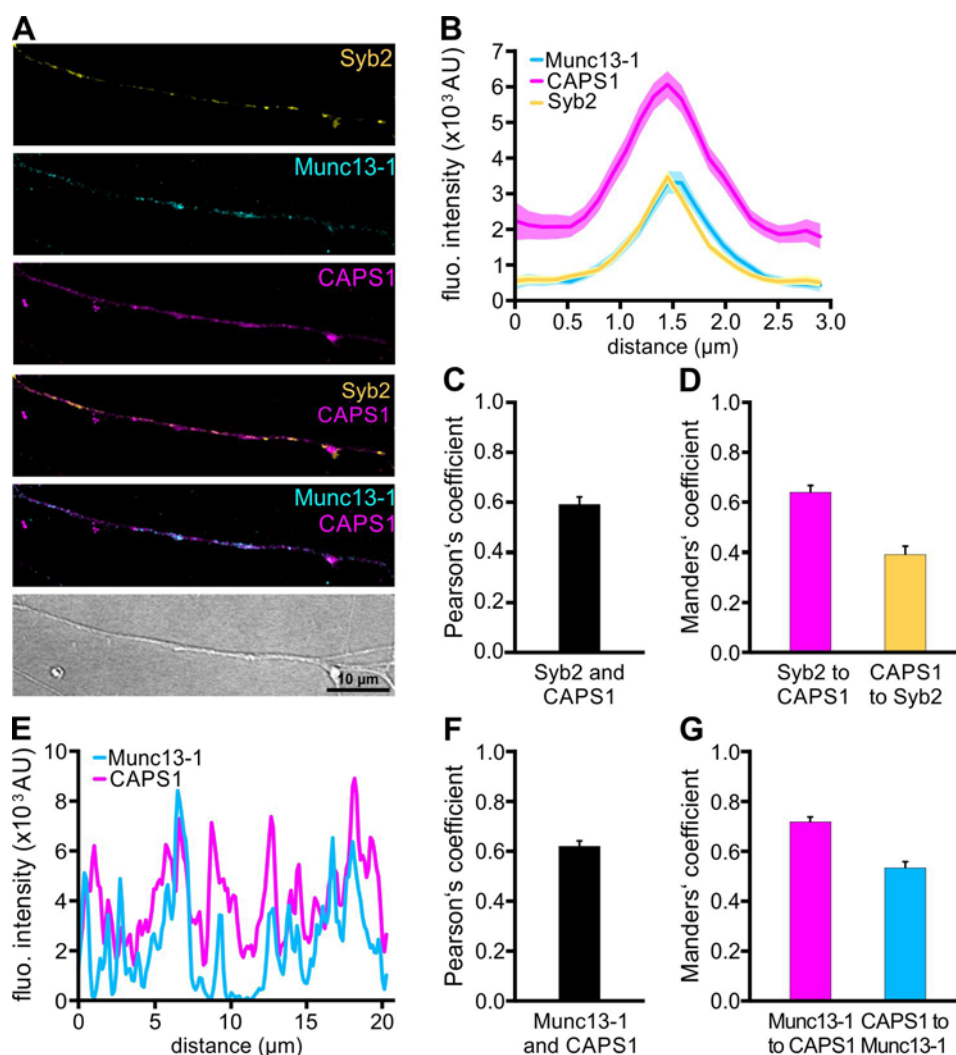


Figure 11: CAPS1 clusters are present at synaptic and extra-synaptic sites. (A) An exemplary neurite of a DRG neuron (DIV6) labelled with synapse marker Synaptobrevin2-mRFP (Syb2, yellow). Endogenous CAPS1 (magenta) and active zone protein Munc13-1 (cyan) were immuno-labelled with specific antibodies. (B) An averaged line profile diagram for CAPS1 over synapses that were selected according to co-localized high fluorescence intensities of the Synaptobrevin2-mRFP and Munc13-1 signals ($n=81$ synapses; $N=3$). (C) Co-localization of CAPS1 with Synaptobrevin2-mRFP was measured on isolated neurites of DRG neurons and quantified by Pearson's correlation coefficient ($n=25$ neurites, $N=3$). (D) Manders' overlap coefficients for the proportion of Synaptobrevin2-mRFP immunoreactivity in CAPS1 positive locations ($n=25$ neurites, $N=3$) or the proportion of CAPS1 immunoreactivity in Synaptobrevin2-mRFP positive locations ($n=25$ neurites, $N=3$). (E) Line profile along the neurite presented in A. Note the good co-localization of CAPS1 with Munc13-1. (F) Co-localization of CAPS1 with Munc13-1 was measured on isolated neurites of DRG neurons and quantified by Pearson's correlation coefficient ($n=31$ neurites, $N=3$). (G) Manders' overlap coefficients for the proportion of Munc13-1 immunoreactivity in CAPS1 positive locations ($n=31$ neurites, $N=3$) or the proportion of CAPS1 immunoreactivity in Munc13-1 positive locations ($n=31$ neurites, $N=3$).

In addition to the synaptic localization, CAPS1 clusters were found at extra-synaptic sites in the entire neurite. The displayed neurite in Figure 11A, indicates a partial co-localization of CAPS1 with Munc13-1 not only at synapses but also at extra-synaptic sites. The line profile of the measured fluorescence intensities of CAPS1 and Munc13-1 (Figure 11E) along the entire neurite shown in Figure 11A supports the visual perception of a co-localization of the two

priming factors at extra-synaptic sites in DRG neurons. Analysing the co-localization of CAPS1 positive puncta with Munc13-1 positive labelling in several neurites revealed that about 60% of the immunofluorescence signal between both proteins was overlapping (Figure 11F: Pearson's correlation coefficient in the entire neurite: 0.62 ± 0.02). In addition, immunofluorescence positive spots for Munc13-1 in CAPS1 and vice versa were calculated by Manders' overlap coefficients. The data in Figure 11G shows approximately 70% of Munc13-1 positive spots co-localizes with CAPS1, whereas the co-localization of CAPS1 positive domains in Munc13-1 was lower, and only reached about 50% (Manders' overlap coefficients in the entire neurite for Munc13-1 in CAPS1 domains: 0.72 ± 0.02 and CAPS1 in Munc13-1 puncta: 0.53 ± 0.02). These differences in Manders' overlap coefficients were not unexpected, because the microscopic images already showed partially different staining patterns of both proteins. Munc13-1 was exclusively punctate, whereas CAPS1 showed a combined cytosolic and punctate signal. In summary the data show that endogenous CAPS1 is present at synapses and at extra-synaptic regions where it partly co-localizes with Munc13-1.

3.3 Functional analysis of a CAPS1/2 chimera in comparison to CAPS1 and CAPS2

After identifying a unique sequence in the N-terminus of CAPS1 that might have functional importance and possibly explain differences between CAPS1 and CAPS2 function in DRG neurons, a chimeric CAPS1/2 mutant construct was designed and analysed. The unique 11 amino acid sequence of CAPS1 N-terminus was introduced into the CAPS2 protein (Figure 12A). To ensure that the cloning was successful, the correct size of the CAPS1/2 chimera was checked against the size of the CAPS2 WT protein in a western blot (Figure 12B). In addition, the functionality of the CAPS1/2 chimera was verified by performing exocytosis rescue experiments in CAPS dKO mouse adrenal chromaffin cells using membrane capacitance measurements (Figure 12C).

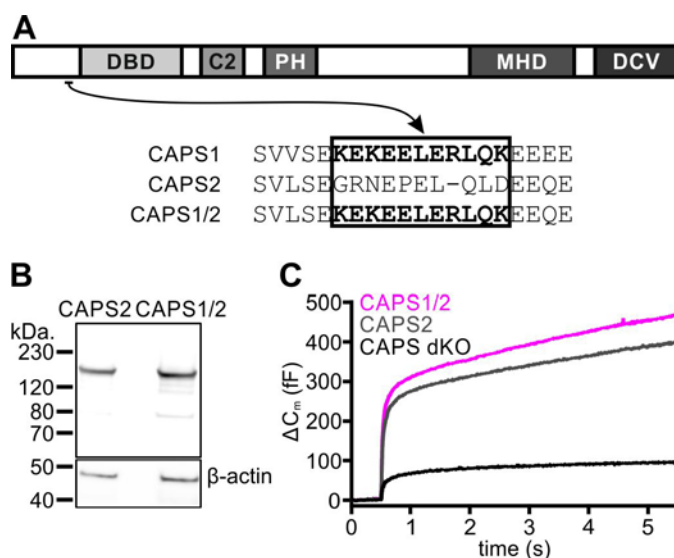


Figure 12: CAPS1/2 chimera is correctly expressed and functional. (A) CAPS domain structure with N-terminal sequence of CAPS1, CAPS2 and CAPS1/2 chimeric mutant. (B) Western blot of CAPS2 and CAPS1/2 chimera. Chromaffin cells transfected with CAPS2-HA or CAPS1/2-HA were lysed and blotted with anti-HA antibody. β -actin was used as a loading control. (C) Averaged membrane capacitance measurements of CAPS dKO mouse chromaffin cells transfected with CAPS2 (light grey, n=20) or CAPS1/2 (magenta, n=22) compared to non-transfected controls (black, n=15).

In these experiments, CAPS1/2 chimera and CAPS2 were overexpressed using the Semliki Forest virus (SFV) expression system. The SFV is well suited for acute expression of recombinant proteins (Knight, 1999). However, there are two major disadvantages associated with this viral expression system. First, the strong cytotoxic effect on host cells and second, the short-term expression pattern (Lundstrom, 2005). To eliminate these problems in further protein localization studies, CAPS1, CAPS2 and the CAPS1/2 chimera were introduced into a lentiviral expression system. Lentiviruses provide an excellent tool for the long-term expression of the desired proteins in non-dividing cells, such as neurons, with the additional benefit of low cytotoxicity (Naldini et al., 1996; Hioki et al., 2007; Lundstrom, 2019). Further, a HaloTag (Los et al., 2008) was attached to CAPS1, CAPS2 and the CAPS1/2 chimera, because the HaloTag (in short Halo) technology has decisive advantages compared to classical fluorophores. First, a variety of fluorescent dyes can be used, providing more freedom in designing the experiments. Second, many of the available dyes are highly stable under high- and super-resolution microscopy and third, they can be applied to live cell imaging.

Before the localization studies of CAPS1, CAPS2 and CAPS1/2 chimera were carried out, the expression level of each construct was tested in order to exclude possible differences in the efficacy of the lentiviruses. For this purpose, DRG neurons were isolated from CAPS dKO mice and infected on the next day with the lentiviruses encoding for either CAPS1-, CAPS2- or CAPS1/2 chimera-Halo. On DIV2, SC neurons from WT mice were added to the culture to

create the same experimental conditions as in the following localization studies. On DIV6, the cells were stained with the Halo ligand CA-ATTO590, directly fixed and immuno-labelled with either anti-CAPS1 or anti-CAPS2 antibody (example images are shown in Figure 13A).

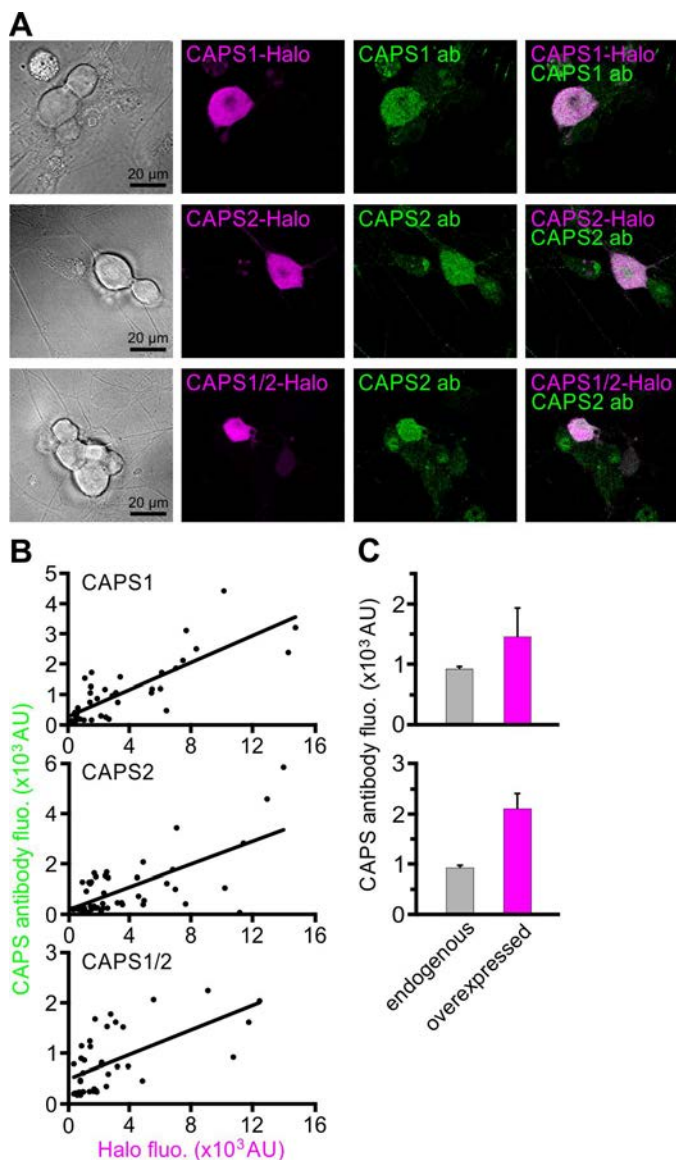


Figure 13: All CAPS-Halo constructs are equally expressed at about twice the endogenous level. (A) Images of DRG CAPS dKO neurons expressing CAPS1-, CAPS2- or CAPS1/2 chimera-Halo co-cultured with SC WT neurons. On DIV6 cells were stained with Halo ligand CA-ATTO590 and immuno-labelled with anti-CAPS1 or anti-CAPS2 antibody. (B) Fluorescence intensities of anti-CAPS1 or anti-CAPS2 antibody and Halo ligand CA-ATTO590 was measured and plotted ($n=42$, 52 and 39 for CAPS1, CAPS2 and CAPS1/2 chimera, $N=3$). Note that all three lentiviruses express proteins in comparable amounts. (C) CAPS endogenous expression level compared to overexpression level. DRG neurons were isolated from WT mice or CAPS dKO mice. CAPS dKO neurons were infected with CAPS1- or CAPS2-Halo on DIV1. The next day, SC WT neurons were added to WT and CAPS dKO neurons. On DIV6 CAPS dKO cells expressing CAPS1- or CAPS2-Halo were stained with Halo ligand CA-ATTO590. The same day, cells were immuno-labelled with anti-CAPS1 or anti-CAPS2 antibody. Fluorescence intensities of endogenous CAPS1 or CAPS2 (grey bars) vs. overexpressed CAPS1- or CAPS2-Halo (magenta bars) were measured ($n=15$ and 8 for endogenous vs. overexpressed CAPS1 and $n=16$ and 18 for endogenous vs. overexpressed CAPS2, $N=1$). Note that, expression level is about twice compared to endogenous protein level.

In the images, the signal of each construct after staining with CA-ATTO590 is shown in magenta and the corresponding signal of the anti-CAPS1 or anti-CAPS2 antibody in green. In addition, the bright field images contain cells that were not infected, which is indicated by lack of signal after staining with ATTO590. This confirms our hypothesis that the virus expresses sufficient protein for detection after 5 days and that the staining protocol is suitable to distinguish between infected cells from non-infected cells. Beyond that, the anti-CAPS1 and anti-CAPS2 antibodies were able to show specific signals of the expressed proteins, although the intensity was not as strong as the Halo ligand CA-ATTO590 staining. The diagrams in Figure 13B show the correlation between the fluorescence intensities of the anti-CAPS1 or anti-CAPS2 antibody and the Halo ligand CA-ATTO590. The dots in the diagrams reflect the signal of individual cells and reveal that the level of expression can be very diverse even within the same construct. However, in about 70% of the cells no more than twice the amount of the endogenous protein level is expressed (Figure 13C). This analysis ensures that the cells are not overloaded with the expressed proteins and that the expression level is very similar between the three different constructs.

3.4 A role for CAPS1 N-terminal sequence in protein distribution

Synapses in neurons are located at a significant distance from the neuronal cell soma and the molecules that are supposed to function at synapses must be transported over long distances before they reach their functional sites. To assess whether there are differences in the distribution of CAPS1, CAPS2 or CAPS1/2 chimera, the spread of the proteins from the cell soma into the neurites was analysed. For this purpose, the DRG neurons of CAPS dKO mice were infected with the lentivirus encoding for either CAPS1-, CAPS2- or CAPS1/2 chimera-Halo and stained with the Halo ligand CA-ATTO590 on DIV6. Afterwards, the cells were kept in culture for another three days before fixation on DIV9. During these three days, between Halo ligand CA-ATTO590 staining and fixation, the stained proteins were given time to localize at their final target position. Example images are shown in Figure 14A and the analysis of the distribution is schematically illustrated in Figure 14B. A line profile measurement was performed over a distance of 15 μm starting in the cell soma and extending into the neurite. The fluorescence intensities were averaged over a distance of 2.5 μm , at the very beginning of the line located in the cell soma and at the very end of the line in the neurite, to calculate a ratio of the protein amount between the cell soma and the neurite. All three proteins were detected diffusely in the cell soma and in the neurite, but CAPS2 was consistently

more abundant in the cell soma than in the neurite (Figure 14C). The mean fluorescence intensity of CAPS2 in the cell soma was three times higher than in the neurite (3.28 ± 0.25). CAPS1 soma versus neurite fluorescent ratio was comparatively lower (2.67 ± 0.22). Interestingly, the CAPS1/2 chimera mimicked the CAPS1 distribution pattern with a mean fluorescence intensity ratio of 2.65 ± 0.21 , which suggests a potential role of the CAPS1 N-terminus, in the distribution of the protein.

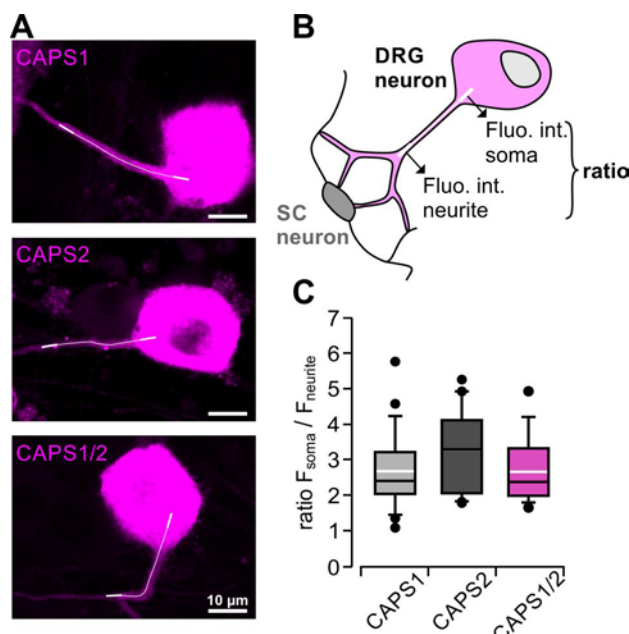


Figure 14: CAPS1/2 chimera mimics the CAPS1 distribution pattern. (A) Example images of DRG CAPS dKO neurons expressing CAPS1-, CAPS2- or CAPS1/2 chimera-Halo co-cultured with WT SC neurons. On DIV6 cells were stained with Halo ligand CA-ATTO590. Fixation was performed on DIV9. Fluorescence intensities were measured along the line profile from the cell soma into the neurite (white line). (B) Schematic representation of the method used to determine the distribution of CAPS-Halo from the soma into the neurite. A fluorescence intensity profile of Halo ligand CA-ATTO590 (magenta) was measured along a 15 μm long line shown in white. The relationship between somatic and neurite fluorescence was calculated as a ratio between the fluorescence intensities over the first and last 2.5 μm on the line (thick ends). (C) Halo ligand CA-ATTO590 soma intensity vs. neurite intensity ratios. Box plot indicate median (black line) and mean (white line) for CAPS1, CAPS2 and CAPS1/2 chimera (n=23, n=20 and n=18, respectively, N=4). The differences between CAPS2 and CAPS1 or CAPS2 and CAPS1/2 chimera are not significant.

3.5 The CAPS1 N-terminal sequence influences localization at synapses

The detection of a potentially different distribution of CAPS1-Halo and CAPS2-Halo and the distinct localization of endogenous CAPS1 at synapses support the described function of CAPS1 in SV exocytosis in DRG neurons (Shaib et al., 2018). However, the contribution of CAPS1 N-terminus remains unknown. Therefore, the localization of overexpressed CAPS1, CAPS2 and the CAPS1/2 chimera at synapses of DRG neurons from CAPS dKO mice was

directly compared. After isolation of DRG neurons on DIV0, lentivirus infection followed on DIV1 and the addition of SC neurons on DIV2. Labelling with the Halo ligand CA-ATTO590 was performed on DIV6. After a further three days in culture (on DIV9), fixation and immuno-labelling was carried out with anti-Synapsin and anti-Bassoon antibodies as synaptic markers (Micheva et al., 2010). Representative images of stained DRG neurites for CAPS1, CAPS2 and CAPS1/2 chimera are shown in Figure 15A.

Co-localization of the proteins in the merged images appears in white. Similar to endogenous CAPS1 protein localization (see Figure 11 on page 60), overexpressed CAPS1 is present in the cytosol and as neuritic puncta. In neurites, CAPS1 shows a high degree of co-localization with the presynaptic markers Synapsin and Bassoon (note the high proportion of the white signal in the merged image). In contrast, CAPS2 is less restricted to synapses and shows a more cytosolic staining pattern across the entire neurite, which is also indicated by the fact that the merged image shows more of the magenta signal in CAPS2 compared to CAPS1. Interestingly, the CAPS1/2 chimera shows a comparable synaptic accumulation as CAPS1, displayed by a less diffuse CAPS1/2 magenta signal in the neurite of the merged image.

The schematic representation of the experimental design in Figure 15B illustrates the synapses analysed, which were identified by a positive CAPS signal and a staining of the synaptic markers Synapsin and Bassoon (shown as white dots). Thus, homotypic synapses of the SC neurons that showed a signal for Synapsin and Bassoon (green dots) but not for CAPS were excluded from the analysis, as well as CAPS-positive domains within the neurite (dots in magenta) that did not have a signal for the synapse markers.

To investigate the synaptic accumulation of CAPS1, CAPS2 and the CAPS1/2 chimera at Bassoon and Synapsin-positive synapses CA-ATTO590 fluorescence intensity was measured at the synapse and normalized it to its fluorescent intensity in the neurite. The summary of the analysis is shown in Figure 15C. The graph shows a significantly higher fluorescence ratio of CAPS1, in comparison to CAPS2 (normalized mean fluorescence intensity ratios: 6.54 ± 0.34 and 4.85 ± 0.30 for CAPS1 and CAPS2, respectively), which indicates a better localization of CAPS1 at synapses. Interestingly, the CAPS1/2 chimera shows an identical synaptic accumulation as CAPS1 (normalized mean fluorescence intensity ratio: 6.29 ± 0.30).

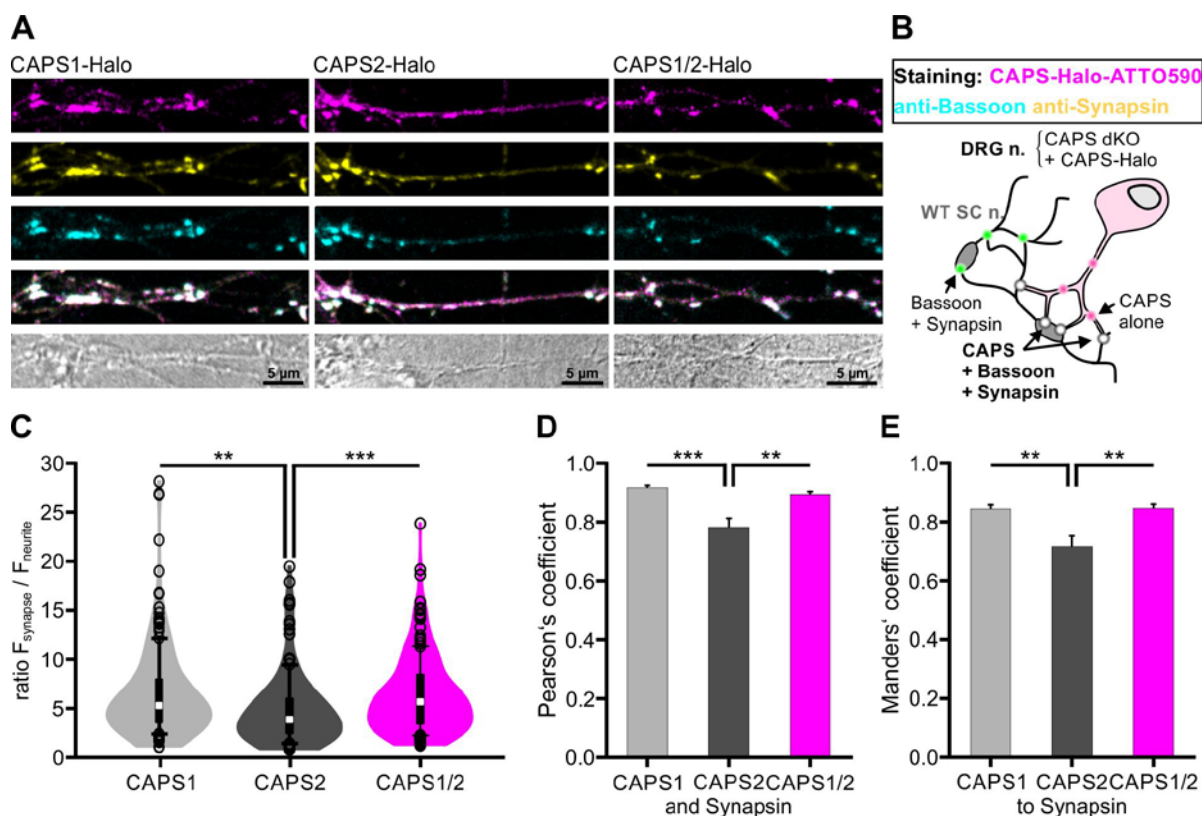


Figure 15: CAPS1 N-terminal sequence determines synaptic localization. (A) Representative neurites of DRG CAPS dKO neurons infected with CAPS1-, CAPS2- or CAPS1/2 chimera-Halo. On DIV2 SC neurons were added to the culture. Halo ligand CA-ATTO590 labelling (magenta) was performed on DIV6. On DIV9 cells were fixed and immuno-labelled with specific antibodies against Bassoon (cyan) and Synapsin (yellow). (B) Schematic representation of the experimental design. Green dots indicate homotypic synapses from SC neurons marked by a positive staining of Synapsin and Bassoon, while co-localization of CAPS-Halo constructs with Synapsin and Bassoon are visualized as white dots. (C) Halo ligand CA-ATTO590 fluorescence intensity at synapses was quantified and normalized to the signal in adjacent areas of the neurites ($n=182$, 148 and 173 synapses for CAPS1, CAPS2 and CAPS2/1 chimera, respectively, $N=3$, $**p<0.01$ or $***p<0.001$ ANOVA on rank with Dunn's post-hoc test). (D) Co-localization of CAPS1, CAPS2 and CAPS1/2 chimera with Synapsin was measured on isolated synapses of DRG neurites and quantified by Pearson's correlation coefficient ($n=24$ neurites, $N=3$, $**p<0.01$ or $***p<0.001$ ANOVA on rank with Tukey post-hoc test). (E) Manders' overlap coefficients for the proportion of CAPS1, CAPS2 and CAPS1/2 chimera immunoreactivity to Synapsin positive locations ($n=24$ neurites, $N=3$, $**p<0.01$ ANOVA on rank with Tukey post-hoc test).

In addition to the analysis of CAPS accumulation at the synapse, a co-localization analysis of CAPS1, CAPS2 or CAPS1/2 chimera with the synaptic marker Synapsin was performed. For this purpose, sections of single DRG neurites with a high number of synapses were used. Calculating the Pearson's correlation coefficient between CAPS and Synapsin revealed a significantly higher degree of co-localization in CAPS1 and CAPS1/2 chimera positive synapses compared to CAPS2 (Figure 15D Pearson's correlation coefficients at synapses: 0.92 ± 0.01 , 0.79 ± 0.03 and 0.90 ± 0.01 for CAPS1, CAPS2 and CAPS1/2, respectively). The Manders' overlap coefficients also confirm a significantly higher co-localization of CAPS1 and CAPS1/2 chimera on Synapsin-positive synapses, which is indicated by higher values compared to CAPS2 (Figure 15E Manders' overlap coefficients at synapses: 0.84 ± 0.01 ,

0.71 ± 0.04 and 0.84 ± 0.01 for CAPS1, CAPS2 and CAPS1/2 to Synapsin). In summary, CAPS1 and CAPS1/2 chimera not only show a significantly higher accumulation, but also a better localization at the synapse compared to CAPS2. Thus, the introduction of the unique CAPS1 N-terminal sequence into the CAPS2 protein (CAPS1/2 chimera) results in a subcellular localization similar to that of CAPS1, rather than that of CAPS2.

3.6 STED microscopy indicates a role of the CAPS1 N-terminus in protein localization near active zones

To assess whether the CAPS1 N-terminus has an influence on subsynaptic localization, STED super-resolution microscopy was performed, because diffraction-limited microscopy lacks the resolution to determine the exact localization of a protein in the synapse. DRG neurons were isolated from CAPS dKO mice, infected with CAPS1- or CAPS1/2 chimera-Halo and co-cultured with SC WT neurons. On DIV6, the neurons were stained with the Halo ligand CA-ATTO590 and cultured for another 3 days before being immuno-labelled with the anti-Synapsin and anti-Bassoon specific antibodies.

In the confocal overview mode, synapses were identified by co-localization of CAPS, Bassoon and Synapsin (Figure 16A). In a next step, smaller regions within the identified synapses were recorded as two colour (CAPS and Bassoon) 2D STED images (Figure 16B), followed by 3D STED imaging of the entire synapse in all three dimensions (Figure 16C). The images nicely resolve the localization of CAPS and Bassoon at synapses. The active zone is exclusively marked by Bassoon, which appears as a narrow band surrounded by the CAPS signal distributed in a much larger portion of the synapse. CAPS and Bassoon protein clusters at synapses were measured and their volume, distance and overlap was calculated (Figure 16D).

In order to put the measured data into perspective, the synaptic distribution of CAPS-Halo was compared with the SV marker Synapsin, the priming factor and active zone protein Munc13-1 and the postsynaptic marker Homer1 (representative 2D and 3D STED images are shown in Figure 16E and F). Analysis of the cluster distance and overlap with Bassoon in the presynapse revealed that Munc13-1 is localized closer to Bassoon and has a significantly higher degree of overlap with Bassoon than with Synapsin (Figure 16G and Figure 16H: 88 ± 4 nm and $35 \pm 2\%$ or 146 ± 8 nm and $23 \pm 2\%$ for distance and overlap). Furthermore, a clear distinction could be made between the presynapse marked by Bassoon and the postsynapse stained with Homer1 (distance of 163 ± 6 nm). By comparing the data with the subsynaptic localization reported for

hippocampal neurons (Grauel et al., 2016), it was concluded that 3D STED acquisition is particularly well suited to resolve subtle differences in the localization of synaptic proteins.

The CAPS clusters had an intermediate position in the synapse between Synapsin and Munc13-1. Interestingly, the CAPS1/2 chimera was significantly closer to the active zone than CAPS1. This conclusion is supported by distance measurements between CAPS and Bassoon clusters, which were smaller in CAPS1/2 chimera than in CAPS1 (Figure 16G: 132 ± 9 nm and 101 ± 8 nm for CAPS1 and CAPS1/2, respectively). By measuring the overlap of CAPS clusters with Bassoon clusters, CAPS1 behaves like the SV-associated protein Synapsin, while the CAPS1/2 chimera resembles the active zone protein Munc13-1 (Figure 16H: $31 \pm 2\%$ and $39 \pm 3\%$ for CAPS1 and CAPS1/2, respectively). These differences between CAPS1 and the CAPS1/2 chimera are not due to significant differences in cluster size (Figure 16I: $0.100 \pm 0.007 \mu\text{m}^3$ and $0.085 \pm 0.006 \mu\text{m}^3$ for CAPS1 and CAPS1/2, respectively).

Taken together, the findings suggest that the unique N-terminal sequence of CAPS1 is not only involved in CAPS1 enrichment at synapses, but also disproportionately increases the localization of CAPS1/2 chimera towards the active zone. Therefore, it is proposed that the CAPS1 N-terminus is involved in the transport and retention of CAPS1 at synapses.

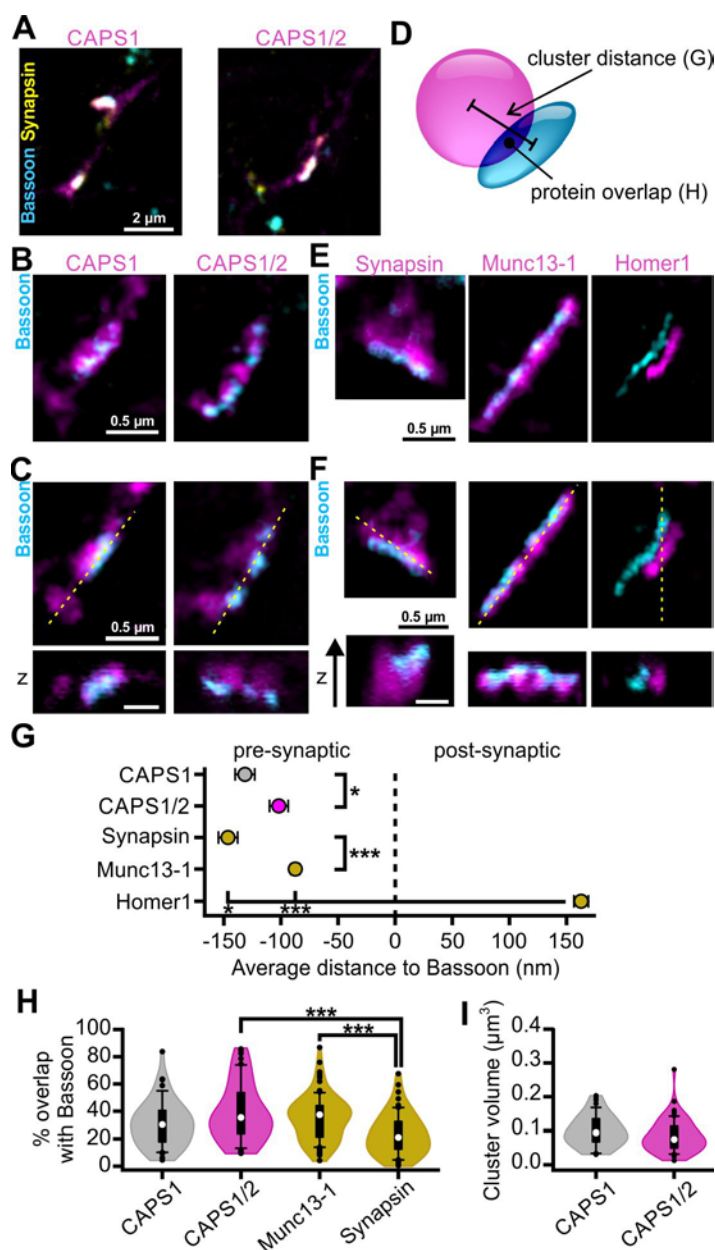


Figure 16: 3D STED microscopy resolves CAPS1 N-terminus function in CAPS1 accumulation near active zones. (A-C) DRG CAPS dKO neurons infected with CAPS1- or CAPS1/2 chimera-Halo. On DIV2 WT SC neurons were added to the culture. Staining of the cells with Halo ligand CA-ATTO590 (magenta) was performed on DIV6 followed by immunostaining for Bassoon (cyan) and Synapsin (yellow) on DIV9. (A) An example confocal overview of a neurite network for each CAPS construct is shown. Enlarged portion of a synapse outlined in (A) acquired with 2D (B) or 3D (C) STED microscopy. The 3D STED images display a sagittal and an axial section of the synapse. The orientation of the axial section is indicated as a dashed yellow line on the sagittal section. Scale bar is 0.5 μm . (D) Schematic representation of image analysis. 3D protein clusters were defined on the 3D STED images. Their centre of mass was used to calculate the distance between CAPS and Bassoon clusters. Further, their degree of overlap and volume was quantified. (E and F) DRG/SC WT neuron co-culture pair-wise immuno-labelled for Bassoon and either Synapsin, Munc13-1 or Homer1. Representative 2D (E) and 3D (F) STED micrographs. Scale bar is 0.5 μm . (G) Distance between the centre of mass of the indicated protein clusters relative to Bassoon cluster. (H) Percentage of indicated protein cluster overlapping with Bassoon. (I) Analysis of CAPS cluster volume. $n=48$, 78 and 59 synapses for CAPS1, CAPS2 and CAPS1/2 respectively, $N=3$; $n=83$, 61 and 64 synapses for Munc13-1, Synapsin and Homer1, respectively, $N=1$. Statistical significance determined by one-way ANOVA followed by Tukey post hoc test (* $p<0.05$, ** $p<0.01$ and *** $p<0.001$). The violin plots include a box plot with the median shown as a white dot.

3.7 Functional analysis of CAPS paralogs in SV and LDCV exocytosis

In the following section, the role of CAPS paralogs in the secretion of LDCVs and SVs was investigated, based on the hypothesis that differential localization leads to specific functions. In previous studies it was shown that CAPS2, in contrast to CAPS1, is the major priming factor for exocytosis of LDCVs in the DRG neuron soma (Shaib et al., 2018). However, it is not known which paralog has the greatest influence on LDCV fusion in DRG neurites. Since localization studies indicate that more CAPS1 is present in the neurites compared to CAPS2, CAPS1 could play a greater role in the fusion of LDCVs in regions further away from the cell soma. Therefore, simultaneous measurements of LDCV and SV fusion in neurites of DRG neurons from CAPS2 KO, CAPS1 KO and CAPS dKO mice were performed and compared to DRG WT neurons.

Secretion was visualized by lentivirus-based co-infection of DRG neurons with SypHy and NPY-pHuji. Synaptophysin-pHluorin (SypHy) is a well-established sensor of SV exocytosis. It was made by fusing superecliptic pHluorin, a pH-sensitive GFP, to the second intravesicular loop of the SV protein Synaptophysin to visualize exocytosis and endocytosis (Miesenbock et al., 1998; Granseth et al., 2006). At an acidic pH inside the vesicle, SypHy is almost non-fluorescent, but when vesicles fuse, it is exposed to a neutral pH in the extracellular space and the presynaptic terminal becomes fluorescent (see illustration in Figure 17A). This cycle can start again after endocytosis and re-acidification of the vesicles. To visualize LDCV fusion, Neuropeptide Y (NPY), a secreted vesicle marker and reporter of dense core granule exocytosis and release, was fused to the fluorophore pHuji (Gandasi et al., 2015). pHuji was made by a single mutation in the fluorophore mApple at the position K163Y, resulting in a high pH sensitivity with a pKa of 7.7 (Shen et al., 2014). Similar to SypHy, NPY-pHuji is almost non-fluorescent at an acidic pH inside the vesicle, but when the vesicle fuses, NPY-pHuji is released and becomes fluorescent.

SV exocytosis was induced by mild stimulation at 10 Hz for 30 seconds, followed by stronger 100 Hz stimulation for 60 seconds to increase the probability of LDCV fusion (Bost et al., 2017). The electrical stimulus was applied by using a bipolar platinum-iridium field electrode at 4 V. Synaptic fluorescence responses were normalized to the entire SV pool by applying 40 mM NH₄Cl to deprotonate the SVs lumen and induce a maximal fluorescence increase. LDCV fusion events were identified as a sudden increase in fluorescence intensity which rapidly dispersed due to the release of NPY-pHuji.

3.7.1 The absence of CAPS2 has no effect on SV or LDCV fusion in DRG neurites

DRG neurons of CAPS2 KO and WT mice were collected on postnatal days 6 to 8 (P6 to P8), because CAPS2 deletion does not affect viability of the animals. The cultures were then infected with the lentivirus encoding for SypHy and NPY-pHuji and co-cultivated with SC WT neurons. The measurements were performed as described above (2.2.16 Total internal reflection fluorescence microscopy, page 51).

Figure 17Bi and Bii show exemplary images of a measurement of the SypHy signal for WT and CAPS2 KO neurons. The images show the intensities of the SypHy signal before stimulation, during the 4 V at 10 Hz stimulation and during the NH₄Cl application. In the images SV exocytosis can be seen at single synapses of WT and CAPS2 KO neurons during stimulation, as they show a strong increase of the SypHy signal intensity. During NH₄Cl application, the individual synapses show variable maximum responses, indicating differences in the SV pool. Therefore, all synapses were normalized to their individual maximum response upon 40 mM NH₄Cl application.

Figure 17 Ci shows the response to the 10 Hz depolarization train of WT and CAPS2 KO neurons and indicates that deletion of CAPS2 has no influence on the normalized maximum increase in SypHy fluorescence. This is confirmed by calculating the difference in SypHy fluorescence before stimulation and at the maximal fluorescence increase during the stimulus, as shown in the box plot in Figure 17 Cii. No significant change is found in the mean and median values between WT and CAPS2. Therefore, synaptic transmission in DRG neurons is not promoted by CAPS2.

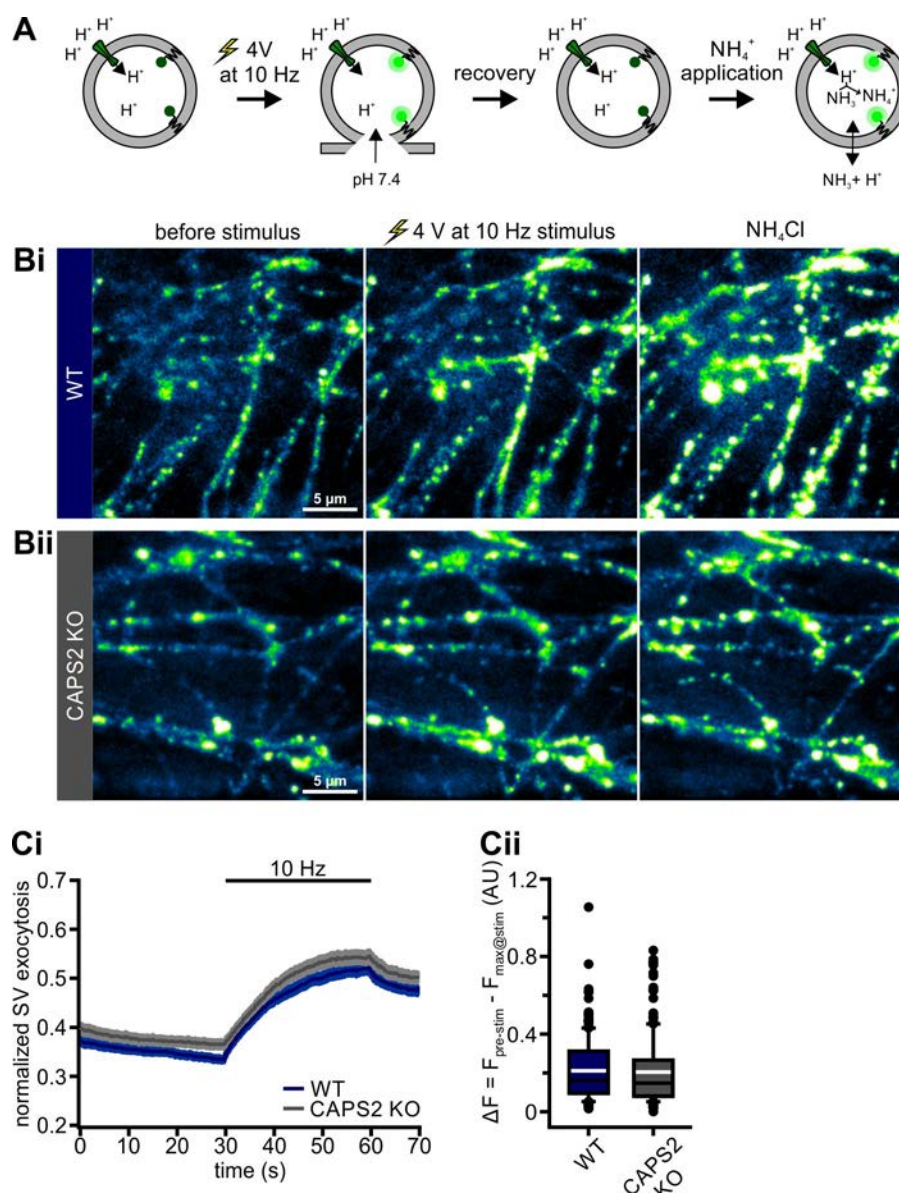


Figure 17: CAPS2 has no effect on SV fusion in DRG neurons. (A) Schematic of imaging exocytosis with SypHy. SypHy is quenched by the low pH inside the vesicle. Upon stimulation, the vesicle fuses with the plasma membrane and the fluorescence of SypHy increases as the pH rises to 7.4. After stimulation, the vesicle is re-acidified and the fluorescence decreases. When NH₄Cl is applied, the NH₃ diffuses into the membrane and deprotonates the lumen of the vesicle by binding the H⁺ ions inside, thus achieving the maximum fluorescence intensity of SypHy. (B-C) WT or CAPS2 KO DRG neurons were isolated from P6 to P8 mice, infected with SypHy and NPY-pHuji and co-cultured with SC WT neurons. Neurons were measured after 10 DIV. Representative images of SV fusion in WT (Bi) and CAPS2 KO (Bii) neurons, visualized by SypHy. (Ci) The normalized average SypHy signal at synapses in response to electrical stimulation for WT neurons (blue) and CAPS2 KO neurons (dark grey). Data are mean \pm SEM. (Cii) Box plot of the maximum normalized fluorescence intensity increase in SypHy elicited by 10 Hz electrical stimulation. Note that CAPS2 deletion did not reduce synaptic transmission. The black and white lines in the box plot correspond to the median and mean fluorescent increase. n=241 and 184 synapses for WT and CAPS2 KO, respectively, N \geq 3.

After finding that CAPS2 deletion had no effect on synaptic transmission, which is consistent with previous observations (Shaib et al., 2018), LDCV fusion visualized by NPY-pHuji and measured simultaneously to SV exocytosis was analysed.

Exemplary maximum intensity projections of NPY-pHuji recordings for WT and CAPS2 KO neurons before and during 4 V at 10 Hz stimulation are shown in Figure 18Ai and Aii. In the images, LDCV fusion events can be recognized by a strong increase in NPY-pHuji fluorescence within the 10 Hz stimulus. For better identification, the fusion events were highlighted with white squares. Figure 18Bi and Bii show an enlargement of a LDCV fusion event from WT and CAPS2 KO DRG neurites presented in Figure 18Ai and Aii, respectively. The images visualize the release of NPY-pHuji over 0.5 seconds before and after secretion. The diagrams below the images display the measured fluorescence intensities of NPY-pHuji with the characteristic peak that indicates the fusion event.

The average cumulative secretion for the analysed movies is shown in Figure 18C and was 9.1 ± 1.1 vesicles in WT cultures and 7.6 ± 1.1 vesicles in CAPS2 KO cultures. The average number of cumulative LDCV fusion events is not significantly different between WT and CAPS2 KO cultures, indicating that CAPS2 deletion has no impact on the number of LDCV fusion events in neurites of DRG neurons.

In addition to the total number of secreted LDCVs, the distribution of fusion events over the measurement period was analysed. Figure 18D shows the number of fusion events within 10 seconds over a total time frame of 170 seconds for WT in blue (top) and CAPS2 KO in dark grey (bottom). The histograms show two peaks within the stimulation at 10 Hz and 100 Hz with no obvious differences in the distribution of fusion events between WT and CAPS2 KO cells.

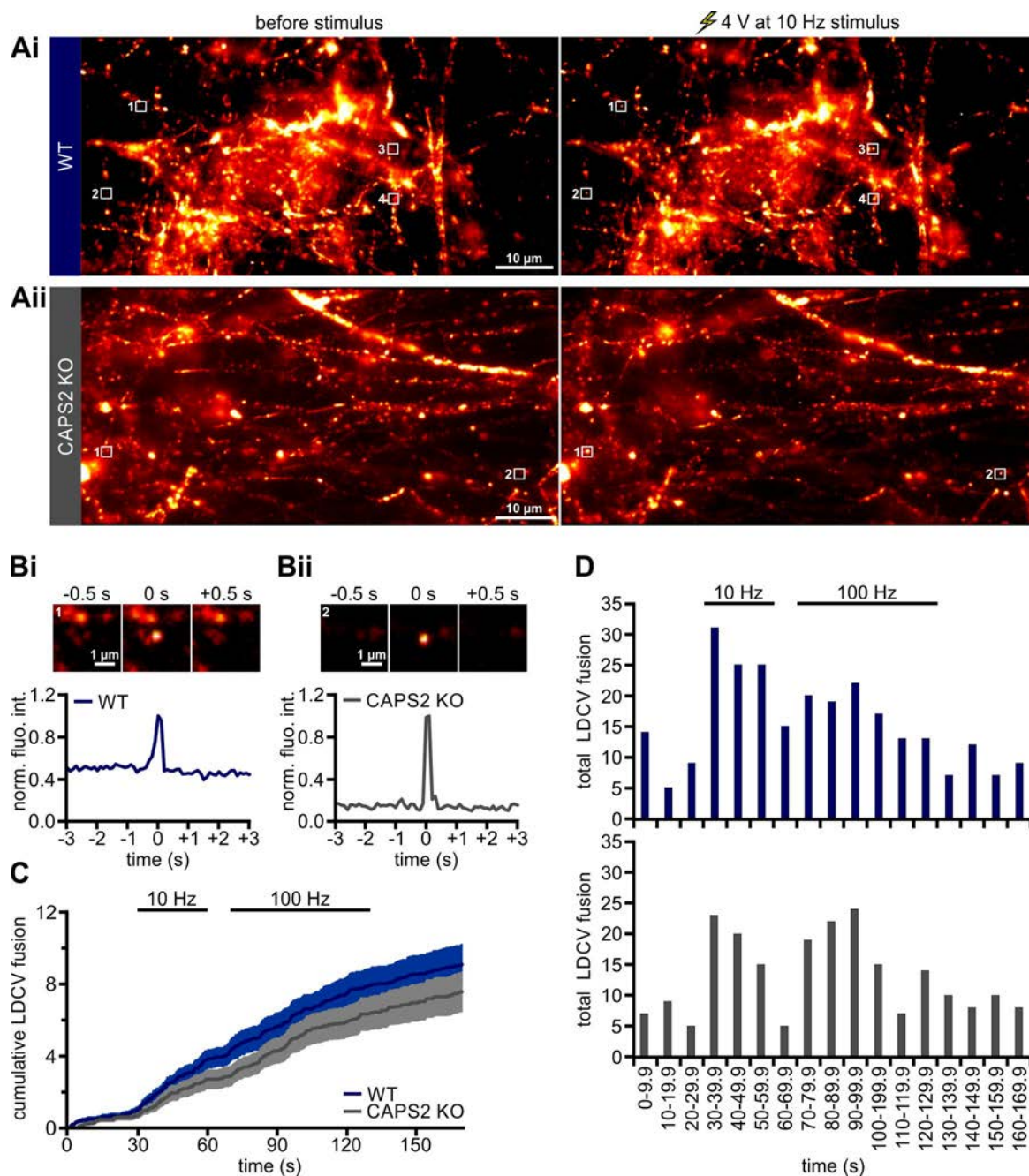


Figure 18: CAPS2 KO has no effect on LDCV fusion in DRG neurites. WT or CAPS2 KO DRG neurons were isolated from P6 to P8 mice, infected with SypHy and NPY-pHuji and co-cultured with SC WT neurons. Neurons were measured after 10 DIV. Exocytosis was evoked via field electrode stimulation. (Ai and Aii) Representative maximum intensity projections of the 30 seconds before stimulus and during 10 Hz stimulation show LDCV fusion in WT (Ai) and CAPS2 KO (Aii) neurons using NPY-pHuji. (Bi and Bii) Example fusion events from images Ai and Aii are magnified for WT (Bi) and CAPS2 KO (Bii). In the upper part of each figure an exemplary image sequence of secreted NPY-pHuji from the LDCV is shown. The lower part demonstrates the fluorescence intensity change over time during LDCV fusion, which was normalized to the maximum value. Fusion events were analysed by drawing a region of interest (ROI) around the LDCV. (C) LDCV fusion is displayed as the average cumulative fusion events for WT (blue) and CAPS2 KO (dark grey). Note that CAPS2 deletion did not reduce the total number of LDCV fusion events after 10 Hz and 100 Hz stimulation. Data are mean \pm SEM. (D) Shown is the frequency of fusion events over the recording time for WT (blue) and CAPS2 KO (dark grey) neurons. $n=29$ movies for WT and CAPS2 KO, $N \geq 3$.

3.7.2 Both CAPS1 KO and CAPS dKO reduce synaptic transmission but only CAPS dKO decreases the total number of LDCV fusion events in DRG neurites

All LDCV and SV release experiments of CAPS1 and CAPS dKO mice were performed on DRG neurons from embryonic day 18 or 19 (E18 or E19) animals because mice lacking either CAPS1 or both CAPS1 and 2 are not viable and die immediately after birth. Furthermore, DRG neurons of WT control mice were also isolated from E18 or E19 animals. The cultures were then infected with SypHy and NPY-pHuji and co-cultivated with SC WT neurons. The measurements were performed in the same way as in the CAPS2 KO experiments (see also 2.2.16 Total internal reflection fluorescence microscopy, page 51).

Figure 19Ai to Aiii show exemplary images of the SypHy signal during measurement of WT, CAPS dKO and CAPS1 KO neurons. The images show the intensities of the SypHy signal before stimulation, during 4 V at 10 Hz stimulation and during 40 mM NH₄Cl application. In the images SV exocytosis is particularly well visualized at single synapses of WT (Ai) neurons during 10 Hz stimulation, because they show a strong increase of the SypHy fluorescence intensity, which is less visible in CAPS dKO (Aii) and CAPS1 KO (Aiii) synapses. As displayed in Figure 19Ai to Aiii, synapses show different maximum responses during NH₄Cl application and were therefore normalized to their individual maximum response.

Figure 19Bi indicates that SypHy fluorescence intensity increase elicited by a 10 Hz depolarization train was maximal in WT neurons and about 35% reduced in CAPS dKO neurons. Similarly, the deletion of only CAPS1 led to an approximately 16% decrease in the SypHy peak response. The box plot in Figure 19Bii represent the difference in the SypHy fluorescence intensity between pre-stimulation and the maximal fluorescence increase upon stimulus. A significant reduction in synaptic transmission was observed in CAPS dKO neurons, when compared to WT neurons. CAPS1 KO neurons also exhibited reduced synaptic transmission, compared to that of WT neurons, although this difference was less pronounced. Hence, in DRG neurons, synaptic transmission seems to be mainly promoted by CAPS1.

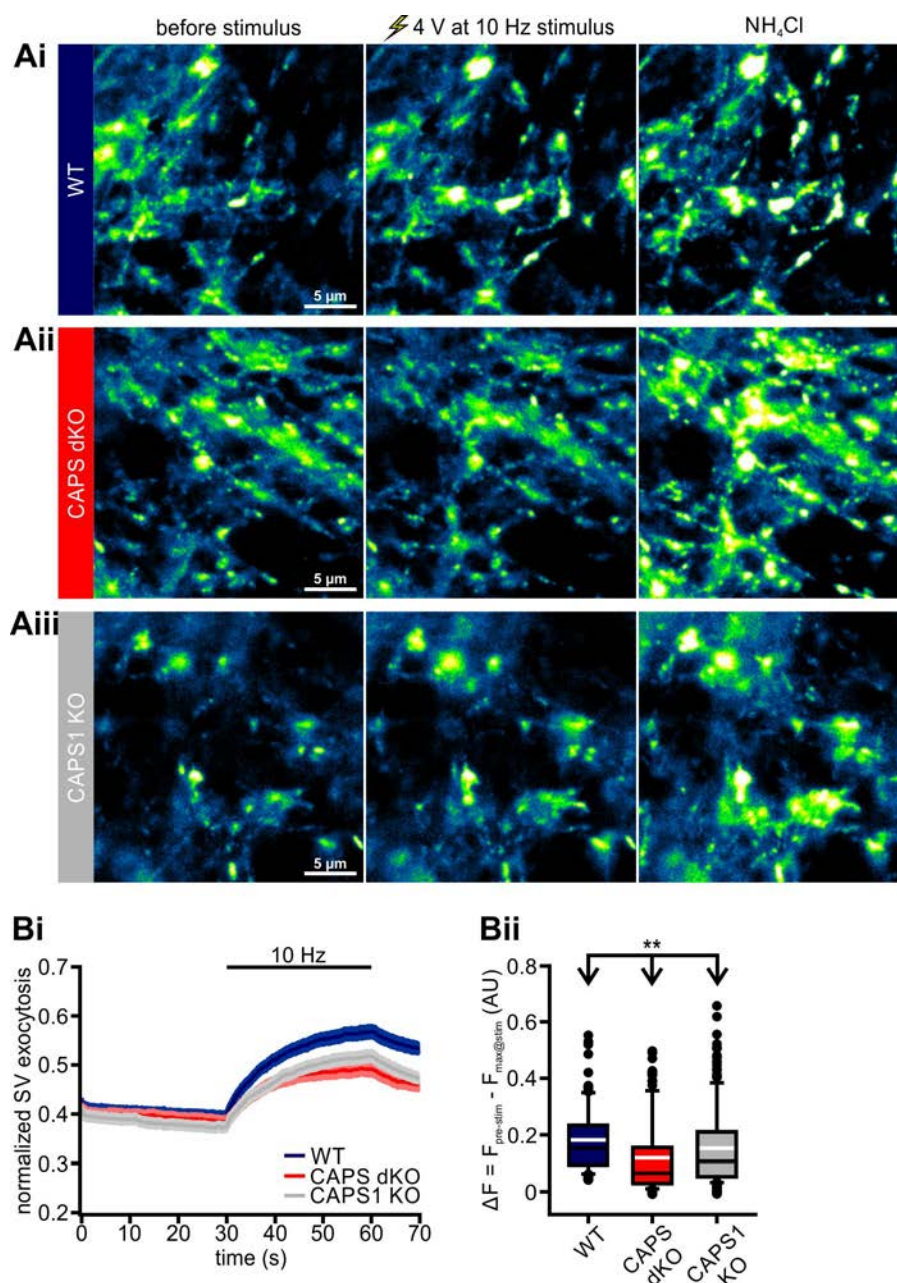


Figure 19: CAPS dKO and CAPS1 KO reduce SV fusion in DRG neurons. WT, CAPS dKO or CAPS1 KO DRG neurons were isolated from E18 or E19 mice, infected with SypHy and NPY-pHuji and co-cultured with SC WT neurons. Neurons were measured after 10 DIV. Representative images of SV fusion in WT (Ai), CAPS dKO (Aii) and CAPS1 KO (Aiii) neurons, visualized by SypHy. (Bi) Normalized average SypHy signal at synapses in response to electrical stimulation for WT (blue), CAPS dKO (red) and CAPS1 KO (light grey) neurons. Data are mean \pm SEM. (Bii) Box plot of the maximum normalized fluorescence intensity increase in SypHy elicited by 10 Hz electrical stimulation. Note that CAPS1 deletion was sufficient to reduce synaptic transmission. The black and white lines in the box plot correspond to the median and mean fluorescent increase. $n=119, 143$ and 171 synapses for WT, CAPS dKO and CAPS1 KO, respectively, $N \geq 3$. $**p < 0.01$ ANOVA on rank with Dunn's post-hoc test.

After confirming that CAPS1 deletion had a similar effect on synaptic transmission as deletion of both CAPS paralogs (Shaib et al., 2018), LDCV fusion measurements visualized by NPY-pHuji were analysed, which were acquired simultaneously with SV exocytosis in DRG neurites.

Figure 20Ai to Aiii show exemplary maximum intensity projections of NPY-pHuji recordings for WT (Ai), CAPS dKO (Aii) and CAPS1 KO (Aiii) neurons before and during 4 V at 10 Hz stimulation. In the images, LDCV fusion events can be recognized by a strong increase in NPY-pHuji fluorescence within the stimulation (right images). The fusion events are highlighted with white squares for better identification. Note that due to reduced LDCV fusion in CAPS dKO neurons, no fusion event can be recognized in the displayed images. Example LDCV fusion events shown in the overview images in Figure 20Ai and Aiii are magnified in Figure 20Bi and Bii for WT and CAPS1 KO, respectively. The images show the neurite 0.5 seconds prior to the release of NPY-pHuji, at the time point of release and 0.5 seconds after secretion. The diagram below the images shows the measured fluorescence intensities of NPY-pHuji with the characteristic peak that indicates the fusion event.

The average cumulative secretion for the analysed movies is shown in Figure 20C. After 170 seconds of measurement including 30 seconds at 10 Hz and 60 seconds at 100 Hz stimulation, the WT neurons secreted, on average, 4.4 ± 1.0 LDCVs. The average secretion of CAPS1 KO cultures was slightly reduced with 2.6 ± 1.0 LDCVs, but LDCV fusion in CAPS dKO neurons was dramatically impaired to an average of 0.5 ± 0.2 LDCVs.

In addition to the total number of LDCV fusion events, the distribution of the fusion events was analysed. Figure 20D indicates the number of fusion events within every 10 seconds over a total time frame of 170 seconds for WT in blue (top), CAPS dKO in red (middle) and CAPS1 KO in light grey (bottom). The top histogram for WT neurons shows a peak during 10 Hz stimulation, at which most LDCVs fuse. The middle histogram indicates the fusion events of CAPS dKO cells, that only occur sporadically. The distribution of the LDCV fusion events in the CAPS1 KO neurons (bottom histogram) shows that LDCV fusion predominantly occurred during the 100 Hz stimulus. Thus, although there is no significant difference in the total number of fusion events between CAPS1 and WT cells after 10 and 100 Hz stimulation, the distribution of LDCV fusion events is changed. While most LDCVs of WT cells fuse at 10 Hz stimulation, in CAPS1 KO neurons LDCV fusion mainly takes place at 100 Hz stimulation. Altogether, LDCV fusion events after 10 and 100 Hz stimulation are significantly reduced only if both CAPS paralogs are absent. Deletion of CAPS1 alone has no significant impact on the total number of LDCV fusion events after the complete measurement, but the likelihood of fusion at mild stimulation is reduced.

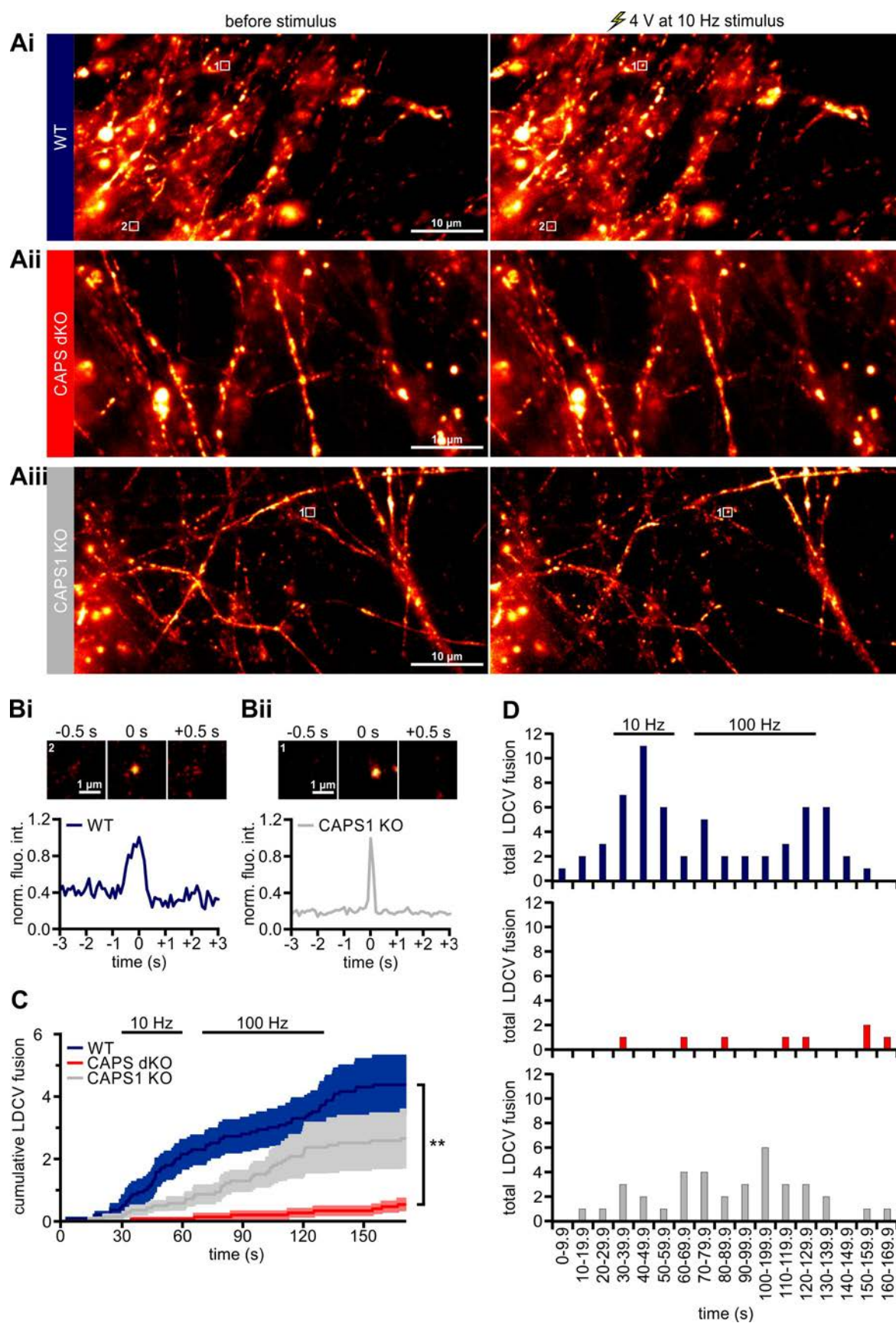


Figure 20: CAPS1 dKO reduces LDCV fusion in DRG neurites. WT or CAPS1 KO DRG neurons were isolated from E18 or E19 mice, infected with SypHy and NPY-pHuji and co-cultured with SC WT neurons. Neurons were measured after 10 DIV. Exocytosis was evoked via field electrode stimulation. (Ai, Aii and Aiii) Representative maximum intensity projections of the 30 seconds before stimulus and during 10 Hz stimulation show LDCV fusion

in WT (Ai) CAPS dKO (Aii) and CAPS1 KO (Aiii) neurons using NPY-pHuji. (Bi and Bii) Example fusion events from images Ai and Aiii are magnified for WT (Bi) and CAPS1 KO (Bii). In the upper part of each figure an exemplary image sequence of secreted NPY-pHuji from the LDCV is shown. The lower part represents the fluorescence intensity change over time during LDCV fusion, which was normalized to the maximum value. (C) LDCV fusion is displayed as the average cumulative fusion events for WT (blue), CAPS dKO (red) and CAPS1 KO (light grey). Note that CAPS1 deletion had no significant effect on the total number of LDCV fusion events, only deletion of both CAPS paralogs resulted in a strong reduction of LDCV exocytosis compared to WT. Data are mean \pm SEM. (D) Shown is the frequency of fusion events over the recording time for WT (blue), CAPS dKO (red) and CAPS1 KO (light grey) neurons, respectively. n=14, 15 and 14 movies for WT, CAPS dKO and CAPS1 KO, respectively, N \geq 3. **p <0.01 ANOVA on rank with Dunn's post-hoc test.

3.8 SV exocytosis is rescued by CAPS1 but not by CAPS2 or CAPS1/2 chimera

The functional roles of CAPS1 and CAPS2 in SV and LDCV exocytosis in the neurites of DRG neurons were investigated using TIRF microscopy. CAPS1, but not CAPS2, was necessary for synaptic transmission, while both paralogs played a redundant role in LDCV fusion. In localization analysis it was shown that CAPS1 localizes better at synapses than CAPS2 due to its unique N-terminal sequence. Therefore, in the following experiments the function of CAPS1, CAPS2 and CAPS1/2 expression in CAPS dKO DRG neurons on SV exocytosis was examined.

As in previous measurements, the SVs were specifically labelled by SypHy expression using a lentivirus and exocytosis was induced by field electrode stimulation at 10 Hz (see 2.2.16 Total internal reflection fluorescence microscopy, page 51 for details). In addition to SypHy expression, the CAPS dKO neurons were infected with a lentivirus encoding for either CAPS1-, CAPS2- or CAPS1/2 chimera-Halo. For visualization of CAPS-Halo in the experiment, the cells were stained with CA-ATTO590 one day before measurement.

In Figure 21Ai to Aiiii exemplary images of the SypHy signal during measurement of CAPS dKO neurons (Ai), CAPS dKO neurons overexpressing CAPS1 (Aii), CAPS2 (Aiii) or CAPS1/2 chimera (Aiiii) are presented. The normalized SypHy fluorescence intensity increase elicited by a 10 Hz depolarization train is shown in Figure 21Bi. The increase was minimal for CAPS dKO neurons and maximal for CAPS1 expressing cells. Expression of CAPS2 or CAPS1/2 chimera in CAPS dKO DRG neurons resulted in a slightly stronger SypHy fluorescence increase (about 28% and 24% for CAPS2 and CAPS1/2, respectively) during stimulus compared to CAPS dKO neurons, but was not as strong as in the CAPS dKO neurons expressing CAPS1 (approximately 45% increase).

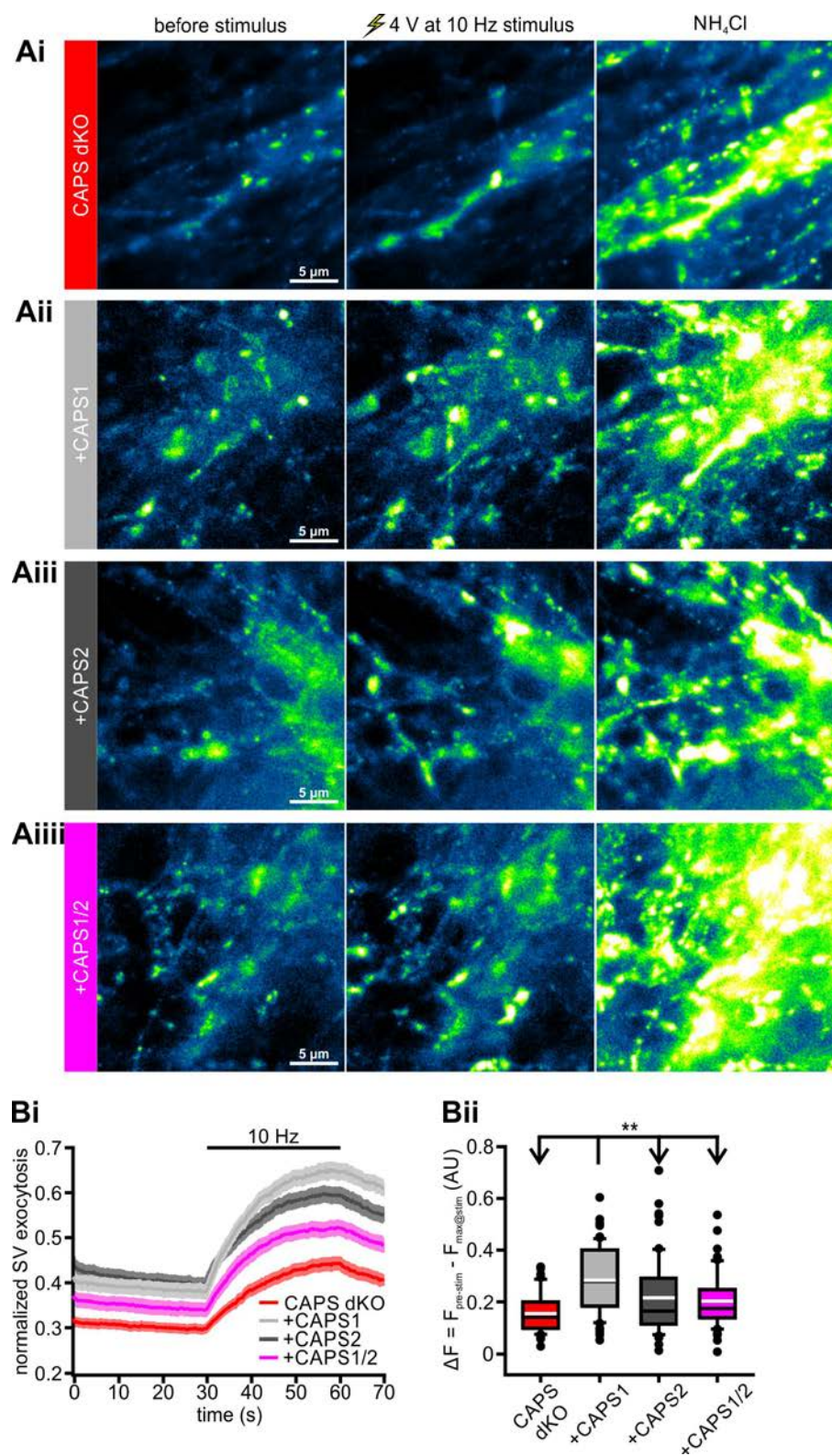


Figure 21: CAPS1 expression rescues SV fusion in DRG CAPS dKO neurons. CAPS dKO DRG neurons were isolated from E18 or E19 mice, infected with SypHy alone or in combination with either CAPS1-, CAPS2- or CAPS1/2-Halo and co-cultured with WT SC neurons. Neurons were stained on DIV9 with Halo ligand CA-ATTO590 and measured on DIV10. Representative images of SV fusion in CAPS dKO (Ai), CAPS dKO + CAPS1 expressing (Aii), CAPS dKO + CAPS2 expressing (Aiii) and CAPS dKO + CAPS1/2 expressing (Aiiii) neurons, visualized by SypHy. (Bi) The normalized average SypHy signal at synapses in response to electrical stimulation for CAPS dKO (red), CAPS dKO + CAPS1 expressing (light grey), CAPS dKO + CAPS2 expressing (dark grey) and CAPS dKO + CAPS1/2 expressing (magenta) neurons. Data are mean \pm SEM. (Bii) Box plot of the maximum normalized fluorescence intensity increase in SyHy elicited by 10 Hz electrical stimulation. Note

that only CAPS1 expression was sufficient to rescue synaptic transmission. The black and white lines in the box plot correspond to the median and mean fluorescent increase. $n=45, 62, 67$ and 63 synapses for CAPS dKO, CAPS dKO + CAPS1 expression, CAPS dKO + CAPS2 expression and CAPS dKO + CAPS1/2 expression, respectively, $N \geq 3$. $**p < 0.01$ ANOVA on rank with Dunn's post-hoc test.

The box plot in Figure 21Bii confirms a significant difference in SypHy fluorescence intensities before and after stimulation between CAPS dKO neurons expressing CAPS1 compared to CAPS dKO control neurons, but also to CAPS dKO neurons expressing either CAPS2 or CAPS1/2 chimera. Therefore, synaptic transmission in DRG neurons is exclusively rescued by CAPS1, but not by CAPS2 or CAPS1/2 chimera. Thus, the unique CAPS1 N-terminal sequence is not responsible for CAPS1 function in synaptic transmission, although a role in localization of the protein to the synapse, was shown.

3.9 Identification of putative CAPS-interacting proteins using immunoprecipitation and mass spectrometry

Prior to this study, CAPS1 was reported to associate with syntaxin-1 (Parsaud et al., 2013), ADP-ribosylation factor 4 and 5 (Sadakata et al., 2010), Septin family proteins (Hosono et al., 2016) and Rabconnectin-3 α and β (Crummy et al., 2019). Although fewer interaction studies have been performed with CAPS2, it is thought to interact with Dynactin subunit 1 (Sadakata et al., 2007b).

For the detection of CAPS1- and CAPS2-specific interaction partners, CAPS1- and CAPS2- antibody immunoprecipitations (IPs) from whole mouse brain lysates for CAPS1 or mouse cerebellum lysates for CAPS2 were performed according to the CAPS1 and CAPS2 tissue-specific distribution (Speidel et al., 2003; Sadakata et al., 2007a). The lysates were immuno-isolated using a specific anti-CAPS1 or anti-CAPS2 antibody bound to magnetic beads for enrichment of CAPS1 or CAPS2, respectively. Bound proteins were eluted from the beads after stringent wash steps. For downstream analysis, eluates were subjected to western blot and mass spectrometry (MS). The membranes in the protein lysates were detergent-solubilized prior to CAPS antibody precipitation to detect proteins that directly associate with CAPS1 or CAPS2. As a consequence, many vesicle-resident proteins may be absent in MS.

3.9.1 CAPS1 IP and MS analysis

The experimental procedure for CAPS1 IP is shown in Figure 22A. The resulting samples were analysed in western blot and MS. The total protein staining confirmed the protein loading for input, supernatant, CAPS1 IP and IgG control IP (Figure 22B). The accumulation of CAPS1 after IP was confirmed in the western blot. The band of the CAPS1 protein was detected at about 145 kDa and its specific accumulation was supported by the absence of the band in the IgG control IP (Figure 22C).

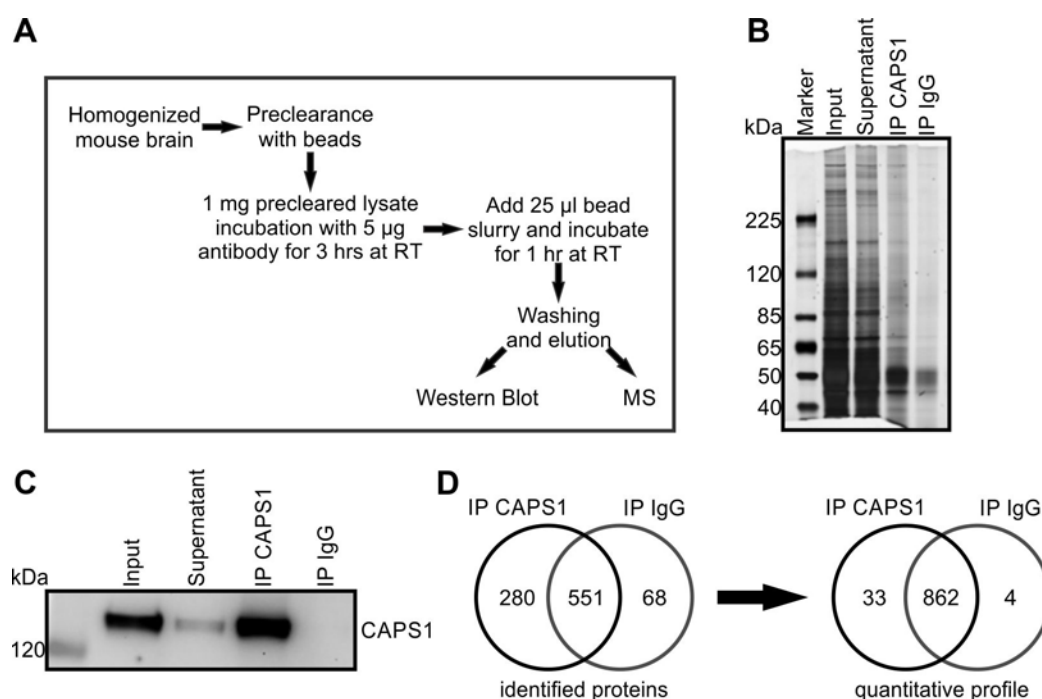


Figure 22: IP and MS analysis of CAPS1 from mouse brain. (A) Schematic of IP protocol to obtain protein samples for western blot and MS. (B) Representative Silver-stained proteins on a SDS gel from input, supernatant, CAPS1 IP and IgG control IP (from left to right). Note the higher protein amount in the CAPS1 IP compared to the IgG control IP. (C) Western blot of input, supernatant, CAPS1 IP and IgG control IP (from left to right) shows that CAPS1 was specifically immunoprecipitated and no labelling occurred in the IgG control IP. (D) Venn diagram of (co-)immunoprecipitated proteins. Number of protein identifications in 3 independent eluates after CAPS1 IPs and IgG control IPs by nano-LC-MS/MS. Total spectrum count analysis with a protein threshold of 95%, a minimum of 2 peptides/protein and a peptide threshold of 90% were set to all MS-identified proteins. Left: number of protein identifications, right: semi-quantitative profile showing proteins significantly enriched ($N=3$ for CAPS1 IP and IgG IP, t -test, $p<0.05$).

Consequently, MS of CAPS1 IP identified CAPS1 as one of the most abundant proteins with a sequence coverage of 54% (Figure 23A) whereas it was completely absent in the IgG control IP. In Figure 23A the protein sequence of mouse CAPS1 is shown in black and the amino acids identified by MS/MS fragmentation are marked in red. As an example of the specificity of peptide recognition, the red underlined tryptic CAPS1 peptide is shown as a collision induced dissociation (CID) MS/MS fragmentation spectra (Figure 23B).

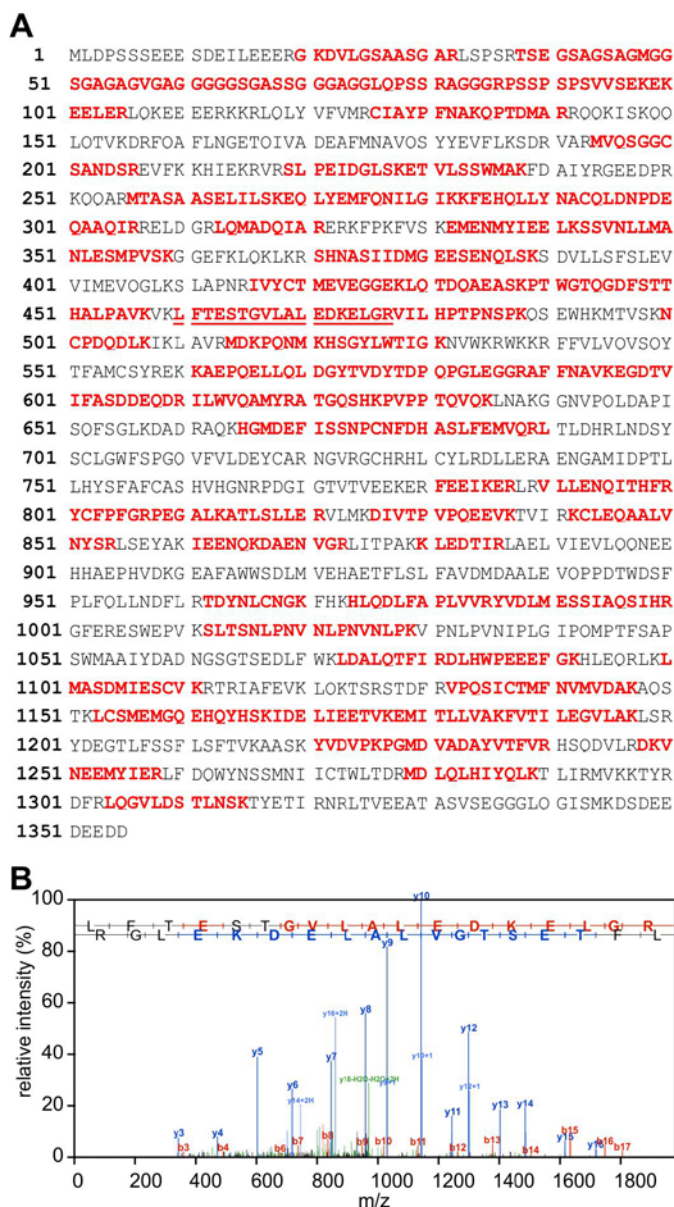


Figure 23: The CAPS1 protein is detected after IP by nano-liquid chromatography (LC)-MS/MS. (A) Protein sequence of mouse CAPS1 (UniProt: Q80TJ1) is shown in black. Amino acids identified by MS/MS fragmentation are shown in red, covering 54% of the protein sequence. (B) Example of CID MS/MS fragmentation spectra (blue: y-ions, red: b-ions, green: $+NH_3$, $+H_2O$, $+2H$, parent) derived from the underlined tryptic mouse CAPS1 peptide in (A) analysed by nano-LC-electrospray ionization (ESI)-MS/MS.

In addition to CAPS1, 898 proteins were identified in MS by analysing the total spectrum counts with a protein threshold of 95%, a minimum of 2 peptides/protein and a peptide threshold of 90%. The volcano plot in Figure 24 shows the result of significantly enriched proteins after IP with the anti-CAPS1 or anti-rabbit IgG antibody (green rectangles and triangles).

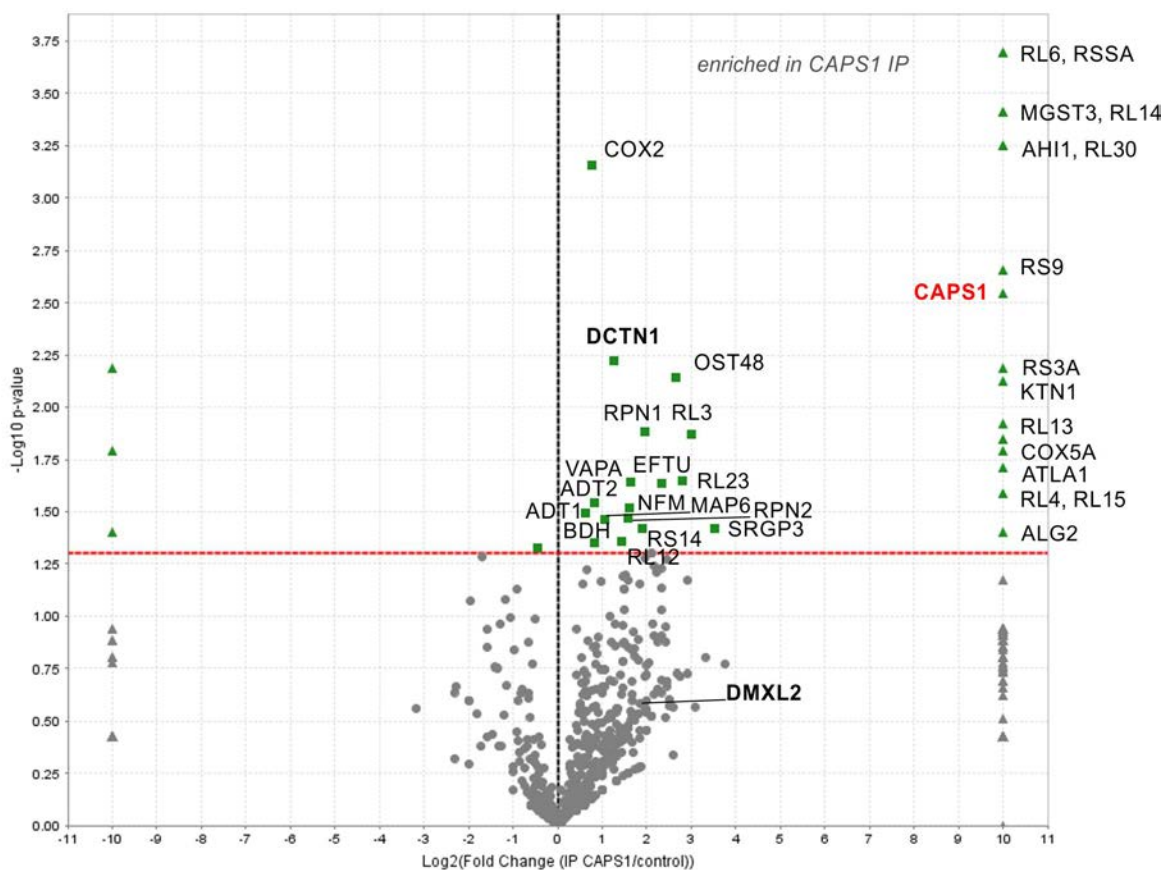


Figure 24: Volcano plot of p-value vs. x-fold change of identified peptide spectrum counts displaying enriched proteins after IP with anti-CAPS1 or anti-rabbit IgG antibodies. Proteins that were significantly enriched with anti-CAPS1 or anti-rabbit IgG antibodies are highlighted in green. The CAPS1 protein (red) is exclusively identified in all CAPS1 IPs from whole mouse brain lysates (N=3 biological replicates for CAPS1 IP and IgG IP, t-test, $p < 0.05$).

Among the 33 significant protein hits found in MS of CAPS1 IP samples (Figure 22D: quantitative profile and Figure 24: volcano plot), there were some interesting candidates, such as Kinectin (KTN1), Microtubule-associated protein 6 (MAP6) and Neurofilament medium polypeptide (NFM), which could be involved in the intracellular localization of CAPS1.

In addition to the new putative CAPS1 interaction partners, MS analysis revealed two CAPS-binding proteins already identified by other groups, which supports this methodological approach to reliably discover new interaction partners. One of the two proteins is the Dynactin subunit 1 (DCTN1), also known as p150Glued, which was described to be involved in intracellular transport by binding both microtubules and Dynein (Zhapparova et al. 2009). However, this interaction was already demonstrated for CAPS2 and influenced axonal protein distribution (Sadakata et al. 2007) and is now suggested to interact with CAPS1 as well. More recently, it has been reported that the DmX-like protein 2, also called Rabconnectin-3, interacts with CAPS1 to recruit soluble CAPS1 to DCV membranes to function in vesicle acidification (Crummy et al. 2019). Although Rabconnectin-3 was not significant in the present study

($p=0.26$), it was found in all three CAPS1 IPs and was highly enriched with a fold change of 3.6 compared to the IgG control. However, further experiments are necessary to obtain detailed knowledge of the molecular CAPS1 interactions and thus to elucidate the specific functions.

3.9.2 CAPS2 IP and MS analysis

The experimental procedure for the CAPS2 IP is described in Figure 25A. Compared to the CAPS1 protocol, only the cerebellum was used to produce the protein lysates and the incubation time of protein with antibody and beads was extended to overnight. The resulting samples were then analysed in western blot and MS. Beforehand, protein loading for input, supernatant, CAPS2 IP and IgG control IP was confirmed by total protein staining (Figure 25B). The accumulation of CAPS2 in the IP was confirmed in the western blot. The band of the CAPS2 protein was detected at approximately 145 kDa, and specific accumulation was supported by the absence of the band in the IgG control IP (Figure 25C).

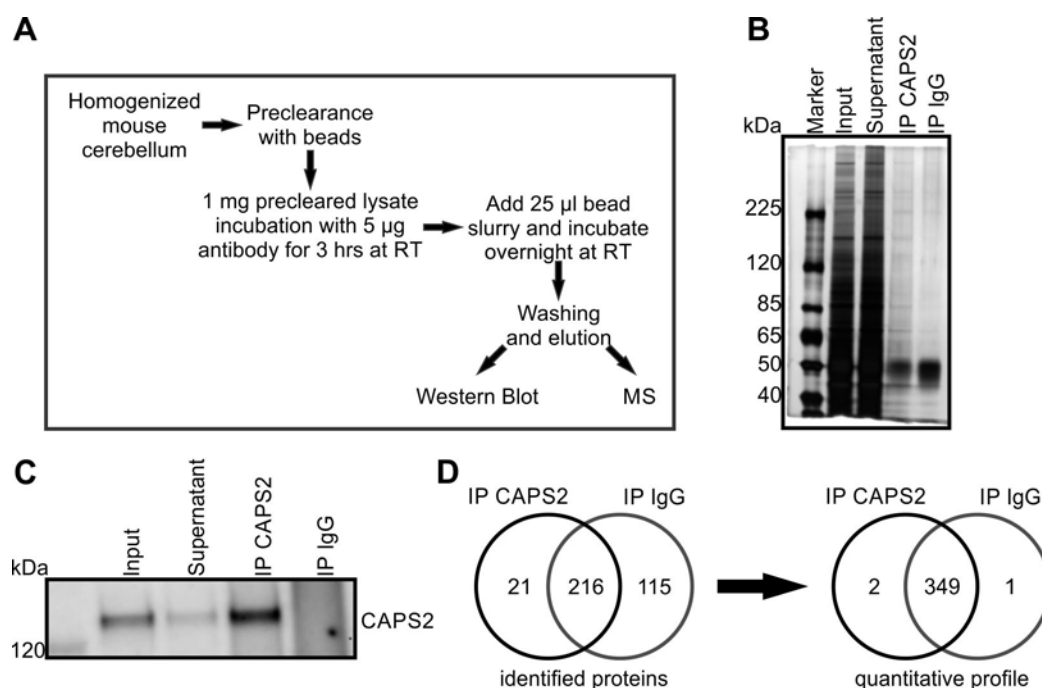


Figure 25: IP and MS analysis of CAPS2 from mouse cerebellum. (A) Schematic of IP protocol to obtain protein samples for western blot and MS. (B) Representative Silver-stained proteins on a SDS gel from input, supernatant, CAPS2 IP and IgG control IP (from left to right). Note the higher protein amount in the CAPS2 IP compared to the IgG control IP. (C) Western blot of input, supernatant, CAPS2 IP and IgG control IP (from left to right) shows that CAPS2 was specifically immunoprecipitated and no labelling occurred in the IgG control IP. (D) Venn diagram of (co-)immunoprecipitated proteins. Number of protein identifications in 3 independent eluates after CAPS2 IPs and IgG control IPs by nano-LC-MS/MS. Total spectrum count analysis with a protein threshold of 95%, a minimum of 2 peptides/protein and a peptide threshold of 90% were set to all MS-identified proteins. Left: number of protein identifications, right: semi-quantitative profile showing proteins significantly enriched ($N=3$ for CAPS2 IP and IgG IP, t -test, $p<0.05$).

Consequently, MS of CAPS2 IP revealed CAPS2 as one of the most abundant proteins with a protein sequence coverage of 16% (Figure 26A), while it was completely absent in the IgG control IPs. However, CAPS2 IPs were not as successful as CAPS1 IPs, which is supported by the lower percent of protein coverage (amino acids in red) of the protein sequence of mouse CAPS2 after MS analyses. As an example of the specificity of peptide recognition, the tryptic CAPS2 peptide underlined in red is shown as a CID MS/MS fragmentation spectrum in Figure 26B.

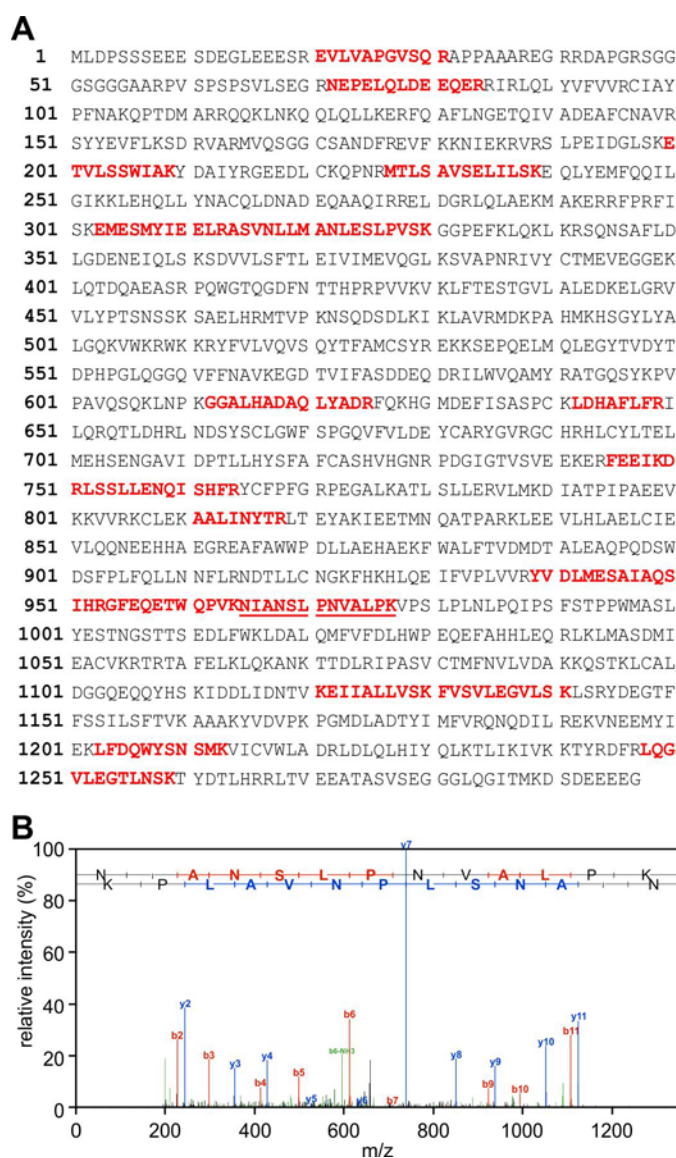


Figure 26: The CAPS2 protein is detected after IP by nano-LC-MS/MS. (A) Protein sequence of mouse CAPS2 (UniProt: Q8BYR5) is shown in black. Amino acids identified by MS/MS fragmentation are shown in red, covering 16% of the protein sequence. (B) Example of CID MS/MS fragmentation spectra (blue: y-ions, red: b-ions, green: $+NH_3$, $+H_2O$, $+2H$, parent) derived from the underlined tryptic mouse CAPS2 peptide in (A) analysed by nano-LC ESI-MS/MS.

In addition to CAPS2, 351 proteins were identified in MS by analysing the total spectrum counts with a protein threshold of 95%, a minimum of 2 peptides/protein and a peptide threshold of 90%. The volcano plot in Figure 27 shows the result of significantly enriched proteins after IP with the anti-CAPS2 or anti-rabbit IgG antibody (green rectangles and triangles). Only CAPS2 itself and Complement C1q subcomponent subunit C (C1QC) were significantly enriched in the CAPS2 IP (Figure 25: quantitative profile and Figure 27: volcano plot). Due to the low yield of co-immunoprecipitated proteins in CAPS2 IP, no speculation can be drawn about molecular interactions leading to specific functions. There are neither known CAPS2 interaction partners among the identified proteins nor specific transport proteins. In order to make reliable statements about CAPS2 specific binding proteins, the IP protocol has to be improved.

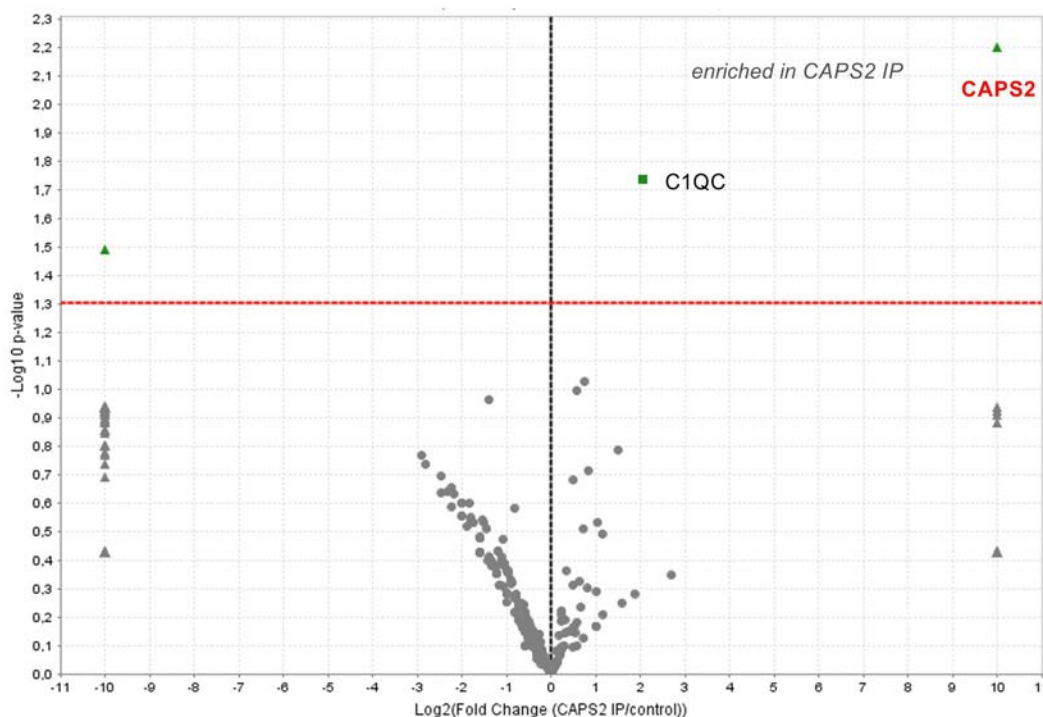


Figure 27: Volcano plot of p-value vs. x-fold change of identified peptide spectrum counts displaying enriched proteins after IP with anti-CAPS2 or anti-rabbit IgG antibodies. Proteins that were significantly enriched with anti-CAPS2 or anti-rabbit IgG antibodies are highlighted in green. The CAPS2 protein (red) is exclusively identified in all CAPS2 IPs from mouse cerebellum lysates (N=3 biological replicates for CAPS2 IP and IgG IP, t-test, $p < 0.05$).

4 Discussion

The main objective of the present work was to define the molecular function of CAPS paralogs and to analyse their role in transmitter release from SVs and in the exocytosis of neuropeptides from LDCVs of mammalian sensory neurons.

The studies described here show that despite a very high sequence identity of 80% at the amino acid level (Speidel et al., 2003) CAPS paralogs exhibit a high heterogeneity in the N-terminus (Figure 8). A region in the N-terminus of CAPS1 is particularly highly conserved between species (Figure 9) and shows sequence similarity with the known presynaptic protein Cytohesin-1, which is involved in neurotransmitter release (Ashery et al., 1999). In addition to the sequence similarity, both proteins show a predicted helical secondary structure in this region, which is a reasonable indication of functional relevance (Figure 10). Subsequent experiments showed a localization of endogenous CAPS1 in the entire neurite with an accumulation at synapses and extra-synaptic sites where it partially co-localized with the priming factor Munc13-1 (Figure 11). Using a suitable system for the exogenous expression of CAPS1 and CAPS2, it was possible to analyse the subcellular localization of both proteins in direct comparison. It was shown that CAPS1 was preferentially present at presynapses, while CAPS2 was more uniformly localized throughout the cell. Interestingly, a CAPS1/2 chimera, in which the unique N-terminal sequence of CAPS1 was transferred into CAPS2, also showed increased presynaptic accumulation, which supports the importance of this domain in the localization of the protein (Figure 15 and Figure 16).

The analysis of the function of CAPS1 and CAPS2 in synaptic transmission as well as in the release of neuropeptides from LDCVs by TIRF microscopy showed that CAPS1 but not CAPS2 mediates synaptic transmission, whereas both CAPS paralogs were able to regulate LDCV fusion in neurites of DRG neurons (Figure 17 to Figure 20). Furthermore, experiments on CAPS dKO cells revealed that LDCV exocytosis depends almost exclusively on the CAPS protein family, while SV fusion is reduced by only one third compared to WT neurons (Figure 19 and Figure 20). In addition, rescue experiments showed that although CAPS1/2 was localized at synapses to a similar degree as CAPS1, synaptic transmission was only rescued by CAPS1 and not by CAPS1/2 or CAPS2 overexpression (Figure 21). Thus, the unique N-terminal sequence of CAPS1 cannot be exclusively responsible for CAPS1 function in synaptic transmission.

By performing CAPS1 and CAPS2 IPs followed by MS analysis, putative CAPS-interaction partners were detected. For CAPS1, 32 co-immunoprecipitated proteins were significantly enriched (Figure 24). Among these, proteins involved in intracellular transport and a previously

detected CAPS2 interaction partner were identified, supporting this approach to discover new binding partners for CAPS1. However, only 1 potential interaction protein was found in the CAPS2 MS analysis and no already known CAPS binding partners were identified (Figure 27), which indicates non-optimal conditions during the CAPS2 IP. Based on the poor yield of proteins found in the CAPS2 IP, no direct comparison with protein hits in the CAPS1 IP can be performed, which also prevents conclusions about unique CAPS1 or CAPS2 interaction partners. Further experiments are required to identify specific binding proteins and the exact mechanism of differential CAPS1 and CAPS2 localization and function.

4.1 Differences in the N-terminus of the CAPS protein family

CAPS was originally identified as a brain protein that stimulates calcium-dependent fusion of secretory vesicles in PC12 cells (Walent et al., 1992). It has been found to have homologues in *C. elegans* (Unc-31) and *Drosophila* (Ann et al., 1997; Renden et al., 2001). In mammals CAPS exists in two paralogs, CAPS1 and CAPS2 (Cisternas et al., 2003; Speidel et al., 2003). While CAPS1 is distributed over a large part of the brain and neuroendocrine cells, CAPS2 is only expressed in restricted areas of the brain such as the granule cells of the cerebellar cortex and in other organs such as the lung, liver and kidney (Speidel et al., 2003).

Functional studies have shown that members of the CAPS family play an important role in preparing the vesicles for exocytosis, a process known as priming (Jockusch et al., 2007; Liu et al., 2008; Liu et al., 2010; Farina et al., 2015). Priming function is mediated by highly conserved functional domains in the central and C-terminal parts of CAPS1 and CAPS2 and has been extensively studied. In analogy to another important priming factor, Munc13-1, the main domain appears to be the Munc homology domain (MHD), which binds to t-SNARE syntaxin-1 and triggers the formation of the SNARE complex (Khodthong et al., 2011). Further support of priming is provided by the C2 domain, by the phosphatidylinositol-4,5-bisphosphate [PI(4,5)P₂]-binding PH domain and by the vesicle-associating DCV domain (Loyet et al., 1998; Grishanin et al., 2002; Grishanin et al., 2004; Petrie et al., 2016).

Interestingly, experiments on non-polarized cells such as adrenal chromaffin cells showed no apparent differences in priming ability between the two paralogs (Liu et al., 2010). However, despite high similarities in their priming domains, there are clear indications for functional differences between CAPS1 and CAPS2. Recent work on DRG neurons expressing both paralogs simultaneously showed that CAPS1 promoted the release of SVs, while CAPS2 mediated exocytosis from LDCVs (Shaib et al., 2018).

Although CAPS1 and CAPS2 are about 80% identical at the amino acid level and have an identical domain structure (Speidel et al., 2003), CAPS1 is larger, mainly due to additional amino acids in the N-terminal sequence. Furthermore, sequence alignment of the murine CAPS1 and CAPS2 paralogs resulted in a sequence unique to CAPS1 in the N-terminus (amino acids 98-108 in Figure 8), which, after further analysis, resulted in a remarkable cross-species conservation (Figure 9). Interestingly, this sequence is located within a predicted coiled coil region. These structures often mediate the physical interaction between proteins and thus have functional significance (Lupas and Gruber, 2005; Watkins et al., 2015). Since this structure is only present in the N-terminus of CAPS1 but not in CAPS2, it could have specific binding partners that lead to functional differences of the paralogs and thus define a unique regulatory role for the N-terminus of CAPS1.

A further indication of the functional importance of this region was the sequence similarity with the protein Cytohesin-1 (Figure 10), which has been shown to be localized at presynapses and increases neurotransmitter release (Ashery et al., 1999). Interestingly, the sequence similarity exists at the N-terminus of Cytohesin-1, where there is also a predicted coiled coil structure. In addition, this region has been identified to interact with Munc13-1 (Neeb A., 1999), a protein that is located at presynaptic active zones and plays a regulatory role in neurotransmitter release (Betz et al., 1998). A similar mechanism of translocation of CAPS1 via specific interaction partners of the N-terminus would thus be conceivable.

4.2 The differential subcellular CAPS localization is determined by its N-terminus

One of the most interesting findings of the present study is the increased presynaptic accumulation of CAPS1, compared to CAPS2 observed in mouse DRG neurons (Figure 15 and Figure 16). In addition, the use of a CAPS1/2 chimera ascribes this property to the specific CAPS1 amino acid sequence in the N-terminus.

First, the endogenous subcellular CAPS1 localization in the neurites was investigated. A presynaptic and extra-synaptic localization of CAPS1 was confirmed by co-localization analysis with the SV protein Synaptobrevin2 and the priming factor Munc13-1 (Figure 11). This specific presynaptic localization of CAPS1 has already been shown in earlier studies on hippocampal neurons (Farina et al., 2015; van Keimpema et al., 2017) and DRG neurons (Shaib et al., 2018), but the underlying mechanism remained unexplained. Although van Keimpema et al. (2017) suggested that the CAPS1 C-terminus regulates synaptic accumulation, this region is

most likely not responsible for a difference in function or localization between CAPS1 and CAPS2, because the C-terminus is highly conserved between both paralogs. One could also speculate that this observed synaptic accumulation is due to the retention of CAPS1 at the synapse, due to its interaction with SNARE proteins such as syntaxin-1 in its C-terminal MHD1. However, this interaction is not responsible for the translocation of the protein from the soma to the synapses.

In order to analyse the influence of the N-terminus on the subcellular localization of CAPS paralogs, a CAPS1/2 chimera was generated in which the specific amino acid sequence of CAPS1 (amino acids 98-108) was introduced into the CAPS2 protein. The CAPS1/2 chimera had the correct size and was functional in membrane capacitance measurements (Figure 12). Lentivirus overexpression levels between CAPS1, CAPS2 and the CAPS1/2 chimera were comparable and could be detected with the corresponding antibodies. Furthermore, after 5 days of virus infection, the overexpressed protein amounts were on average about twice as high as the endogenous protein amounts and thus not far from the physiological range (Figure 13). A detailed confocal study with CAPS1, CAPS2 and the CAPS1/2 chimera at synapses of DRG neurons from CAPS dKO mice showed that the signal from CAPS1, but also from the CAPS1/2 chimera, was much higher at synapses than in neurites and that they differed significantly from CAPS2, which had a lower ratio between fluorescence at synapses and in neurites (Figure 15). An accumulation of CAPS1 at synapses is expected, because it has already been described as a mediator for synaptic transmission in DRG neurons (Shaib et al., 2018), but also in hippocampal neurons (Jockusch et al., 2007). A less pronounced accumulation of CAPS2 is not too surprising either, as functional analyses indicated that CAPS2 plays no role in the exocytosis of SVs (Shaib et al., 2018). However, it is remarkable that the CAPS1/2 chimera accumulates at the synapses just as well as CAPS1, although it contains only 11 amino acids of the N-terminus of CAPS1 and is otherwise identical to CAPS2.

Confocal microscopy is not suitable to show subsynaptic localization due to its resolution limit, therefore the analyses were continued at the STED microscope. First, it was shown that the 3D STED acquisition is appropriate to resolve subtle differences in the localization of synaptic proteins (Synapsin, Munc13-1 and Homer1 to Bassoon) by comparing the data with values already measured in hippocampal neurons (Grauel et al., 2016). The studies revealed that CAPS1 and the CAPS1/2 chimera are centrally located in the synapse between Munc13-1 and Synapsin. This finding is compatible with the fact that CAPS is involved in an early phase of priming, while Munc13-1 plays a role in a late phase of priming (Liu et al., 2010). Interestingly, the CAPS1/2 chimera was significantly closer to the active zone than CAPS1. While the

distribution of CAPS1 within the synapse was more related to the SV-associated protein Synapsin, the CAPS1/2 chimera showed greater similarity in distribution with the active zone protein Munc13-1 (Figure 16).

The data reported here now indicate that the unique N-terminal sequence of CAPS1 is not only involved in CAPS1 accumulation at presynapses, but also disproportionately increases the localization of the CAPS1/2 chimera towards the active zone. It suggests that the CAPS1 N-terminus is involved in the transport and retention of CAPS1 at the presynapses. This scenario is somewhat similar to Munc13s, which are localized to synapses by interactions of their N-termini, either by a RIM-mediated mechanism for the recruitment of ubMunc13-2 and Munc13-1 (Betz et al., 2001; Dulubova et al., 2005; Andrews-Zwilling et al., 2006) or by an ELKS1-dependent targeting process for bMunc13-2 facilitated by a predicted coiled coil region (Kawabe et al., 2017).

4.3 The specific function of CAPS in the exocytosis of LDCVs and SVs

The most significant phenotypic change in CAPS1 KO mice is found in synaptic transmission, while LDCV fusion is only minimally reduced in DRG neurites (Figure 19 and Figure 20). DRG neurons of CAPS2 KO mice show no change in SV exocytosis or LDCV fusion in the cell neurites (Figure 17 and Figure 18). Interestingly, LDCV exocytosis is almost completely eliminated in CAPS dKO mice (Figure 20). The analysis of the simultaneous measurement of SV and LDCV exocytosis in the CAPS deletion mutants confirms the specific function of CAPS1 in synaptic transmission, while the priming of LDCVs in DRG neurites is regulated by CAPS1 and CAPS2. In addition, the investigations show that a deletion of both CAPS paralogs has a stronger effect on the exocytosis of LDCVs than on that of SVs.

The function of CAPS1 for calcium-mediated LDCV exocytosis has already been shown in a large number of studies (Ann et al., 1997; Berwin et al., 1998; Renden et al., 2001; Grishanin et al., 2004; Speese et al., 2007). It was also shown that CAPS2 mediates priming of LDCVs. In chromaffin cells both paralogs have a redundant function (Liu et al., 2008; Liu et al., 2010). In a similar way, both CAPS1 (Farina et al., 2015; Eckenstaler et al., 2016; van Keimpema et al., 2017) and CAPS2 (Shinoda et al., 2011) can promote LDCV secretion in hippocampal neurons. In contrast to the cell types mentioned above, in DRG neurons CAPS paralogs perform partially different functions. In the cell soma CAPS2 is predominantly responsible for LDCV priming, whereas CAPS1 plays a role in synaptic transmission (Shaib et al., 2018). However, it was also shown that the overexpression of either paralog in WT neurons promotes LDCV

fusion to a similar extent and that both paralogs can rescue reduced LDCV secretion in CAPS dKO cells. Therefore, it can be assumed that both CAPS paralogs can act as priming factors for LDCVs in DRG neurons and that a different function is probably due to the localization and thus the availability of the paralogs. Similar to the role of CAPS paralogs in DRG neurons, the individual Munc13 paralogs in chromaffin cells also show differences in their ability to promote LDCV fusion. While a deletion of Munc13-1, Munc13-3 or Baiap3 does not impair LDCV exocytosis, the absence of ubMunc13-2 dramatically reduces LDCV release, which however is rescued by overexpression of not only ubMunc13-2, but also of Munc13-1 and Munc13-4, although with different efficiencies (Man et al., 2015).

In neurons, LDCV exocytosis occurs not only in the cell soma but also in neurites and synapses (Xia et al., 2009; van de Bospoort et al., 2012). In excitatory neurons of the hippocampus, LDCV fusion near synapses is mediated by CAPS1 (Farina et al., 2015), but the expression level of CAPS2 is very low in these cells (Jockusch et al., 2007). In inhibitory neurons of the hippocampus, where the expression pattern of CAPS1 and CAPS2 is inverted (CAPS1 is absent and high concentration of CAPS2), LDCV fusion in neurites is mediated by CAPS2 (Shinoda et al., 2011). The investigations presented here show that in DRG neurons both CAPS paralogs mediate neuropeptide release in the neurites. This finding is also consistent with the localization studies, which show that both CAPS paralogs are localised in the neurites. DRG neurons, however, are highly diverse in their function and only half of the population, the so-called peptidergic neurons, produce a wide variety of neuropeptides that are contained in LDCVs that undergo exocytosis (Bost et al., 2017; Shaib et al., 2018). Nevertheless, overexpressed NPY is detected in peptidergic and non-peptidergic DRG neurons, although non-peptidergic cells usually do not secrete neuropeptides. In addition, it was shown that endogenous CAPS2 is expressed almost exclusively in the peptidergic neurons, while CAPS1 is expressed in all DRG neurons. Only by differentiating between peptidergic and non-peptidergic neurons, a CAPS2-specific role in LDCV exocytosis in the cell body was discovered (Shaib et al., 2018). In the present work, DRG neurons could not be differentiated into peptidergic and non-peptidergic cells when measuring LDCV fusion in the neurites, so that the potential specific effects of CAPS paralogs may not have been recognized.

Initially, CAPS1 was described with a specific function in LDCV exocytosis (Walent et al., 1992; Ann et al., 1997; Tandon et al., 1998; Grishanin et al., 2004), which correlated well with the fact that about 30% of the CAPS protein is membrane-bound and associated with LDCVs but not with SVs in brain homogenates (Walent et al., 1992; Berwin et al., 1998). However, accumulation of both proteins has also been observed in presynaptic compartments of neurons

where SVs predominate and very few LDCVs are present (Speidel et al., 2003; Sadakata et al., 2006; Speese et al., 2007; Farina et al., 2015; van Keimpema et al., 2017). Similarly, in DRG neurons CAPS1 is highly concentrated at synapses, whereas CAPS2, in contrast, is more diffusely distributed in the neurite and a less intense accumulation at synapses was observed (Figure 15 and Figure 16). In line with these localization studies, the functional analyses of SV fusion from this work and previous studies show that CAPS1 and not CAPS2 mediates neurotransmitter release (Figure 17, Figure 19 and (Shaib et al., 2018)). Because, overexpressed CAPS1 and CAPS2 equally promote LDCV secretion from DRG cell bodies (Shaib et al., 2018), a similar redundant function after overexpression of one of the paralogs would also be conceivable in synaptic transmission.

To test this hypothesis, CAPS1 and CAPS2 were overexpressed in DRG neurons of CAPS dKO mice and SV fusion was measured, but no redundancy was detected as only CAPS1 was able to rescue reduced synaptic transmission CAPS dKO cells. In addition, the influence of the CAPS1/2 chimera on synaptic transmission was analysed to verify whether synaptic localization correlates with function. The observation that the CAPS1/2 chimera was not able to rescue reduced synaptic transmission in CAPS dKO DRG neurons, although it reflected the localization phenotype of CAPS1, was somewhat unexpected. Therefore, the results suggest that similar protein localization is not sufficient to enable the same function. One possible explanation is that further differences in the sequence and structure between CAPS1 and CAPS2 are crucial for the unique functional role of CAPS1 as a priming factor for SVs. Therefore, further experiments are necessary to find out which regions in CAPS1 are responsible for its specific role in synaptic transmission. As already started in this study, further targeted mutation analyses could be helpful to address this question.

Although the 11 amino acids in the N-terminus of CAPS1 do not provide a functional rescue, it is still possible that another part of the N-terminal region in CAPS1 plays an important role in the priming process. This hypothesis is supported by studies on chromaffin cells showing that CAPS2 primes vesicles independently of its C-terminal domain, which is important for SNARE interaction. Instead, the PH domain of CAPS2, and thus binding to phospholipids in the membrane, appears to be essential for its priming function (Nguyen Truong et al., 2014). Sequence analysis focusing on already known functional domains of CAPS paralogs may therefore reveal structural evidence for the unique role of CAPS1 in synaptic transmission. A different study by Ratai et al. (2019) showed for example, that the exon 22 in the MHD of CAPS1 and CAPS2 have a low sequence identity, similar to the identified differences in the N-terminus. They reveal a unique function of this exon 22 in CAPS2, which is responsible for

an increased catecholamine load of the LDCVs in mouse chromaffin cells, and that its presence leads to an increased activity of both vesicular monoamine transporters (Ratai et al., 2019). The role of this region in neurons remains unclear, and it would be interesting to investigate whether it provides CAPS1 and CAPS2 with specialized functions that influence the different priming activity of the two proteins for synaptic transmission.

4.4 Identification of putative CAPS-interacting proteins

The data reported here now show a redundant function of CAPS1 and CAPS2 as priming factors for LDCVs in DRG neurites. In contrast, only CAPS1 has the ability to mediate synaptic transmission. It was assumed that this specific function depends on the accumulation of the protein at the presynapse. This characteristic localization of CAPS1 was attributed to a unique region in the N-terminus by comparison with the CAPS1/2 chimera. However, the defect of synaptic transmission in CAPS dKO neurons was only rescued by CAPS1 and not by the CAPS1/2 chimera. Thus, it can be assumed that the N-terminus of CAPS1, which is responsible for the accumulation of the protein at the presynapse, is not exclusively responsible for the specific priming function of SVs. The data strongly suggest that further differences between CAPS1 and CAPS2 are important for the unique role of CAPS1 in the release of neurotransmitters from SVs.

The CAPS1 IP experiments with subsequent MS analysis identified a variety of interesting potential interaction partners (Figure 22D and Figure 24), whereas the efficiency of CAPS2 IP was much lower and only a few proteins were detected in MS (Figure 25D and Figure 27). There are several reasons why only a small number of proteins were co-immunoprecipitated with the anti-CAPS2 antibody. A lower binding affinity of the anti-CAPS2 antibody, non-optimal working conditions (e.g. buffer composition, washing, incubation) during the IP and/or a low protein concentration in the starting material (Moresco et al., 2010; ten Have et al., 2011) are only some of the reasons. However, by comparing the protein content of input and supernatant in the western blots, poor antibody binding can be neglected, because after IP both CAPS1 and CAPS2 show a reduction of protein amount in the supernatant. Nevertheless, the protocol for CAPS2 IP was adapted in that a longer incubation time of the lysate with the antibody and the beads was required to enrich sufficient protein amounts. Longer incubation times can lead to loss of transient or weak protein-protein interactions and increase the chance of breaking down protein complexes. This is supported by the lower protein amount after CAPS2 IP compared to CAPS1 IP detected in silver staining. Furthermore, the endogenous

protein expression of CAPS2 in the brain is much lower compared to CAPS1, and even in the cerebellum, where CAPS2 expression is highest, it is relatively low compared to CAPS1 (Speidel et al., 2003). Thus, a lower CAPS2 protein concentration in the lysate reduces the probability of protein binding to the antibody and leads to less efficient IPs. For these reasons the CAPS2 IP results cannot be directly compared to the CAPS1 IP results.

The CAPS1 IP experiments with subsequent MS analysis identified 33 significantly enriched proteins. Among them are proteins associated with intracellular transport processes, like Neurofilament medium polypeptide (NFM), Microtubule-associated protein 6 (MAP6) and Dynactin subunit 1 (DCTN1), which are potential candidates involved in the localization or transport of CAPS1. NFM is part of the heteropolymeric Neurofilament (NF) complex required in neurons for axon radial growth (Hoffman et al., 1987; Eyer and Peterson, 1994). Similar to many other neuronal proteins, including synaptic proteins, NFs are synthesized in the cell soma and must travel long distances along the axons to reach their functional sites. The molecular motors that control NF transport are believed to be the fast microtubule-based motors Kinesin and Dynein (Pralhad et al., 2000; Sunil et al., 2012) and the microfilament-based motor myosin Va (Alami et al., 2009). Interestingly, NFs also regulate the transport of SVs through their interaction with the molecular motor myosin Va (Rao et al., 2011), which was shown to participate in exocytosis by association with syntaxin-1A in a calcium-dependent manner (Watanabe et al., 2005). One can speculate that CAPS1 interaction with NFM also leads to synaptic targeting, perhaps similarly by association in a complex with other proteins.

Another possible interaction partner for localization of CAPS1 at synapses is MAP6, whose function as a microtubule stabilizer in neurons has been widely studied (Bosc et al., 1996; Guillaud et al., 1998). More recently, studies revealed that MAP6 promotes Kinesin-1 heavy chain (KIF5B)-dependent movement and stimulates cargo transport. In addition, they showed that MAP6 is localized on secretory vesicles and depending on its posttranslational modifications, it is suggested to be shuttled between vesicle membranes and microtubules (Tortosa et al., 2017). Furthermore, MAP6 has been reported to modulate calcium signalling in neurons by regulating the trafficking of Ca_v2.2/N-type calcium channels to presynapses (Brocard et al., 2017).

In addition to the above mentioned new potential CAPS1 interaction partners, Dynactin subunit 1 was identified, which was previously described as a CAPS2 binding protein (Sadakata et al., 2007b) and is now suggested to interact with CAPS1 as well. The protein Dynactin subunit 1 is the most fully characterized subunit of the Dynactin complex (Schroer, 2004), which is associated with axonal transport (Waterman-Storer et al., 1997). In addition, it has

been shown that Dynactin is required not only for the retrograde transport activity of Dynein but also for the anterograde transport activity of Kinesin-2 (Deacon et al., 2003). In *Drosophila*, Dynactin subunit 1 is essential for coordination of bi-directional axonal transport at synaptic endpoints and thereby influences synaptic transmission (Lloyd et al., 2012). However, Dynactin subunit 1 cannot explain the specific synaptic accumulation of CAPS1, because it has already been shown to interact with CAPS2 as well.

Apart from these significantly enriched transport mediating protein hits, another previously described CAPS1 binding protein called Rabconnectin-3 (Crummy et al., 2019) was highly enriched in the CAPS1 IP compared to the IgG control IP. In general, Rabconnectin-3 consists of two subunits, α and β , both associated with SVs. Rabconnectin-3 β has been shown to bind directly to Rab3 GDP/GTP Exchange Protein (Rab3 GEP), allowing it to be recruited from the cytosol to SVs when it functions in calcium-dependent exocytosis of neurotransmitters. Once Rab3 GEP has finished its function, it is released from the vesicles back into the cytosol. Thus, the binding of Rab3 GEP to Rabconnectin-3 can be time-regulated (Nagano et al., 2002; Kawabe et al., 2003). A similar transient interaction would also be conceivable for CAPS1, which interacts with Rabconnectin-3 only depending on its function as a SV priming factor. Interestingly, Crummy et al (2019) identified in their study the N-terminus of CAPS1 (amino acids 1-378) required for the interaction with Rabconnectin-3. This domain also contains the unique CAPS1 sequence, which was shown in this work to be responsible for localization at synapses. Whether this unique CAPS1 sequence mediates the interaction with Rabconnectin-3 remains to be investigated.

In general, there are two different mechanisms proposed to mediate the compartment-specific localization of proteins in neurons: selective sorting and selective retention. While some proteins are specifically sorted to their functional site, others are transported diffusively and are selectively retained in the correct compartment (Sampo et al., 2003). The exact mechanism of differential localization of CAPS proteins is still to be investigated. It is possible that CAPS1 and CAPS2 are selectively localized due to interactions with different transport proteins, but also that specific interactions of CAPS1 with proteins at the presynapse lead to retention of the protein.

5 Outlook

In this work the differential localization and function of CAPS paralogs was elucidated. CAPS is a priming factor for regulated exocytosis of LDCVs and SVs and is therefore crucial for neuronal communication. Disturbances in CAPS functions consequently lead to severe deficiencies in the neurons.

Experiments are required to better understand CAPS function and the associated protein-protein interactions, starting from protein production in the cell soma over intracellular transport and finally during vesicle fusion. Especially with regard to the differential functions of CAPS1 and CAPS2, it would be interesting to identify the specific interaction partners. The experiments concerning this question have already been started in this work. However, due to the inefficient CAPS2 IP, no conclusions could be drawn about specific CAPS1 or CAPS2 binding partners.

In addition, the potential interaction proteins identified in the CAPS1 IP should be confirmed by further analyses, such as Co-IP, Förster resonance energy transfer or proximity ligation assay. Furthermore, it would be conceivable to identify the binding partners of the unique N-terminal CAPS1 domain to reveal the molecular mechanism of CAPS1 accumulation at synapses. The unique CAPS1 sequence can be coupled as a peptide to agarose beads, resulting in specific binding of the interacting proteins, which can then be eluted and analysed by MS.

In addition to the studies to elucidate the molecular interactions, it would also be interesting to investigate the mobility of CAPS1, CAPS2 and the CAPS1/2 chimera in neurites and at synapses in order to check for differences in protein transport and movement. For example, fluorescence recovery after photobleaching can be performed to address these questions. The neurons would be infected with the CAPS-Halo constructs and stained with a photo-bleachable Halo ligand. The kinetics of the proteins in the neurites or at synapses can be measured by photobleaching the signal of the fluorophore at the desired site and then observing the translocation under a fluorescence microscope. The recovery times provide information about the different transport mechanisms of CAPS1, CAPS2 and the CAPS1/2 chimera.

Additional sequence analysis could identify potential regions in CAPS1 and CAPS2 that would provide further information on the differential functions of the proteins. The investigations in this study already revealed heterogeneity in the N-terminus, which led to different subcellular localization of the proteins, but did not explain the unique function of CAPS1 in SV exocytosis.

References

- Abraira VE, Ginty DD (2013) The sensory neurons of touch. *Neuron* 79:618-639.
- Alami NH, Jung P, Brown A (2009) Myosin Va increases the efficiency of neurofilament transport by decreasing the duration of long-term pauses. *J Neurosci* 29:6625-6634.
- Altman J, Bayer SA (2001) *Development of the Human Spinal Cord: An Interpretation Based on Experimental Studies in Animals*: Oxford University Press.
- Andrews-Zwilling YS, Kawabe H, Reim K, Varoqueaux F, Brose N (2006) Binding to Rab3A-interacting molecule RIM regulates the presynaptic recruitment of Munc13-1 and ubMunc13-2. *J Biol Chem* 281:19720-19731.
- Ann K, Kowalchuk JA, Loyet KM, Martin TF (1997) Novel Ca²⁺-binding protein (CAPS) related to UNC-31 required for Ca²⁺-activated exocytosis. *J Biol Chem* 272:19637-19640.
- Arlt J, Padgett MJ (2000) Generation of a beam with a dark focus surrounded by regions of higher intensity: the optical bottle beam. *Opt Lett* 25:191-193.
- Ashery U, Koch H, Scheuss V, Brose N, Rettig J (1999) A presynaptic role for the ADP-ribosylation factor (ARF)-specific GDP/GTP exchange factor msec7-1. *Proc Natl Acad Sci U S A* 96:1094-1099.
- Averill S, McMahon SB, Clary DO, Reichardt LF, Priestley JV (1995) Immunocytochemical localization of trkA receptors in chemically identified subgroups of adult rat sensory neurons. *Eur J Neurosci* 7:1484-1494.
- Avery L, Bargmann CI, Horvitz HR (1993) The *Caenorhabditis elegans* unc-31 gene affects multiple nervous system-controlled functions. *Genetics* 134:455-464.
- Axelrod D (1981) Cell-substrate contacts illuminated by total internal reflection fluorescence. *J Cell Biol* 89:141-145.
- Axelrod D (2001) Total internal reflection fluorescence microscopy in cell biology. *Traffic* 2:764-774.
- Becherer U, Rettig J (2006) Vesicle pools, docking, priming, and release. *Cell Tissue Res* 326:393-407.
- Berwin B, Floor E, Martin TF (1998) CAPS (mammalian UNC-31) protein localizes to membranes involved in dense-core vesicle exocytosis. *Neuron* 21:137-145.
- Betz A, Ashery U, Rickmann M, Augustin I, Neher E, Südhof TC, Rettig J, Brose N (1998) Munc13-1 is a presynaptic phorbol ester receptor that enhances neurotransmitter release. *Neuron* 21:123-136.
- Betz A, Thakur P, Junge HJ, Ashery U, Rhee JS, Scheuss V, Rosenmund C, Rettig J, Brose N (2001) Functional interaction of the active zone proteins Munc13-1 and RIM1 in synaptic vesicle priming. *Neuron* 30:183-196.
- Bolte S, Cordelières FP (2006) A guided tour into subcellular colocalization analysis in light microscopy. *J Microsc* 224:213-232.
- Bosc C, Cronk JD, Pirollet F, Watterson DM, Haiech J, Job D, Margolis RL (1996) Cloning, expression, and properties of the microtubule-stabilizing protein STOP. *Proceedings of the National Academy of Sciences* 93:2125-2130.
- Bost A, Shaib AH, Schwarz Y, Niemeyer BA, Becherer U (2017) Large dense-core vesicle exocytosis from mouse dorsal root ganglion neurons is regulated by neuropeptide Y. *Neuroscience* 346:1-13.
- Brady S, Siegel G, Albers RW, Price D (2012) *Basic Neurochemistry: Principles of Molecular, Cellular, and Medical Neurobiology*: Elsevier Science.
- Brocard J, Dufour F, Gory-Fauré S, Arnoult C, Bosc C, Denarier E, Peris L, Saoudi Y, De Waard M, Andrieux A (2017) MAP6 interacts with Tctex1 and Ca(v) 2.2/N-type

- calcium channels to regulate calcium signalling in neurons. *Eur J Neurosci* 46:2754-2767.
- Brose N, Petrenko AG, Sudhof TC, Jahn R (1992) Synaptotagmin: a calcium sensor on the synaptic vesicle surface. *Science* 256:1021-1025.
- Camacho M, Basu J, Trimbuch T, Chang S, Pulido-Lozano C, Chang SS, Duluvova I, Abo-Rady M, Rizo J, Rosenmund C (2017) Heterodimerization of Munc13 C2A domain with RIM regulates synaptic vesicle docking and priming. *Nat Commun* 8:15293.
- Chapman ER, Hanson PI, An S, Jahn R (1995) Ca²⁺ regulates the interaction between synaptotagmin and syntaxin 1. *J Biol Chem* 270:23667-23671.
- Cisternas FA, Vincent JB, Scherer SW, Ray PN (2003) Cloning and characterization of human CADPS and CADPS2, new members of the Ca²⁺-dependent activator for secretion protein family. *Genomics* 81:279-291.
- Crummy E, Mani M, Thellman JC, Martin TFJ (2019) The priming factor CAPS1 regulates dense-core vesicle acidification by interacting with rabconnectin3 β /WDR7 in neuroendocrine cells. *J Biol Chem* 294:9402-9415.
- Deacon SW, Serpinskaya AS, Vaughan PS, Lopez Fanarraga M, Vernos I, Vaughan KT, Gelfand VI (2003) Dynactin is required for bidirectional organelle transport. *J Cell Biol* 160:297-301.
- Deng L, Kaeser PS, Xu W, Sudhof TC (2011) RIM proteins activate vesicle priming by reversing autoinhibitory homodimerization of Munc13. *Neuron* 69:317-331.
- Dhara M, Yarzagaray A, Schwarz Y, Dutta S, Grabner C, Moghadam PK, Bost A, Schirra C, Rettig J, Reim K, Brose N, Mohrmann R, Bruns D (2014) Complexin synchronizes primed vesicle exocytosis and regulates fusion pore dynamics. *J Cell Biol* 204:1123-1140.
- Dulubova I, Lou X, Lu J, Huryeva I, Alam A, Schneggenburger R, Sudhof TC, Rizo J (2005) A Munc13/RIM/Rab3 tripartite complex: from priming to plasticity? *Embo j* 24:2839-2850.
- Eckenstaler R, Lessmann V, Brigadski T (2016) CAPS1 effects on intragranular pH and regulation of BDNF release from secretory granules in hippocampal neurons. *J Cell Sci* 129:1378-1390.
- Ernsberger U (2009) Role of neurotrophin signalling in the differentiation of neurons from dorsal root ganglia and sympathetic ganglia. *Cell Tissue Res* 336:349-384.
- Eyer J, Peterson A (1994) Neurofilament-deficient axons and perikaryal aggregates in viable transgenic mice expressing a neurofilament-beta-galactosidase fusion protein. *Neuron* 12:389-405.
- Farina M, van de Bospoort R, He E, Persoon CM, van Weering JR, Broeke JH, Verhage M, Toonen RF (2015) CAPS-1 promotes fusion competence of stationary dense-core vesicles in presynaptic terminals of mammalian neurons. *Elife* 4.
- Fernandez-Chacon R, Konigstorfer A, Gerber SH, Garcia J, Matos MF, Stevens CF, Brose N, Rizo J, Rosenmund C, Sudhof TC (2001) Synaptotagmin I functions as a calcium regulator of release probability. *Nature* 410:41-49.
- Fleming MS, Luo W (2013) The anatomy, function, and development of mammalian Abeta low-threshold mechanoreceptors. *Front Biol (Beijing)* 8.
- Fornaro M, Lee JM, Raimondo S, Nicolino S, Geuna S, Giacobini-Robecchi M (2008) Neuronal intermediate filament expression in rat dorsal root ganglia sensory neurons: an in vivo and in vitro study. *Neuroscience* 153:1153-1163.
- Gandasi NR, Vestö K, Helou M, Yin P, Saras J, Barg S (2015) Survey of Red Fluorescence Proteins as Markers for Secretory Granule Exocytosis. *PLoS One* 10:e0127801.
- Goldstein ME, House SB, Gainer H (1991) NF-L and peripherin immunoreactivities define distinct classes of rat sensory ganglion cells. *J Neurosci Res* 30:92-104.

- Granseth B, Odermatt B, Royle SJ, Lagnado L (2006) Clathrin-mediated endocytosis is the dominant mechanism of vesicle retrieval at hippocampal synapses. *Neuron* 51:773-786.
- Grael MK, Maglione M, Reddy-Alla S, Willmes CG, Brockmann MM, Trimbuch T, Rosenmund T, Pangalos M, Vardar G, Stumpf A, Walter AM, Rost BR, Eickholt BJ, Haucke V, Schmitz D, Sigrist SJ, Rosenmund C (2016) RIM-binding protein 2 regulates release probability by fine-tuning calcium channel localization at murine hippocampal synapses. *Proc Natl Acad Sci U S A* 113:11615-11620.
- Grishanin RN, Klenchin VA, Loyet KM, Kowalchuk JA, Ann K, Martin TF (2002) Membrane association domains in Ca²⁺-dependent activator protein for secretion mediate plasma membrane and dense-core vesicle binding required for Ca²⁺-dependent exocytosis. *J Biol Chem* 277:22025-22034.
- Grishanin RN, Kowalchuk JA, Klenchin VA, Ann K, Earles CA, Chapman ER, Gerona RR, Martin TF (2004) CAPS acts at a pre-fusion step in dense-core vesicle exocytosis as a PIP₂ binding protein. *Neuron* 43:551-562.
- Gu JG, MacDermott AB (1997) Activation of ATP P₂X receptors elicits glutamate release from sensory neuron synapses. *Nature* 389:749-753.
- Guillaud L, Bosc C, Fourest-Lieuvin A, Denarier E, Pirollet F, Lafanechère L, Job D (1998) STOP proteins are responsible for the high degree of microtubule stabilization observed in neuronal cells. *J Cell Biol* 142:167-179.
- Hata Y, Slaughter CA, Sudhof TC (1993) Synaptic vesicle fusion complex contains unc-18 homologue bound to syntaxin. *Nature* 366:347-351.
- Hell SW, Wichmann J (1994) Breaking the diffraction resolution limit by stimulated emission: stimulated-emission-depletion fluorescence microscopy. *Opt Lett* 19:780-782.
- Hioki H, Kameda H, Nakamura H, Okunomiya T, Ohira K, Nakamura K, Kuroda M, Furuta T, Kaneko T (2007) Efficient gene transduction of neurons by lentivirus with enhanced neuron-specific promoters. *Gene Ther* 14:872-882.
- Hoffman PN, Cleveland DW, Griffin JW, Landes PW, Cowan NJ, Price DL (1987) Neurofilament gene expression: a major determinant of axonal caliber. *Proc Natl Acad Sci U S A* 84:3472-3476.
- Hosono M, Shinoda Y, Hirano T, Ishizaki Y, Furuichi T, Sadakata T (2016) Interaction of Ca²⁺-dependent activator protein for secretion 1 (CAPS1) with septin family proteins in mouse brain. *Neurosci Lett* 617:232-235.
- Huang B, Bates M, Zhuang X (2009) Super-resolution fluorescence microscopy. *Annu Rev Biochem* 78:993-1016.
- Huang LY, Neher E (1996) Ca²⁺-dependent exocytosis in the somata of dorsal root ganglion neurons. *Neuron* 17:135-145.
- Jahn R, Sudhof TC (1999) Membrane fusion and exocytosis. *Annu Rev Biochem* 68:863-911.
- Ji RR, Berta T, Nedergaard M (2013) Glia and pain: is chronic pain a gliopathy? *Pain* 154 Suppl 1:S10-28.
- Jockusch WJ, Speidel D, Sigler A, Sørensen JB, Varoqueaux F, Rhee JS, Brose N (2007) CAPS-1 and CAPS-2 are essential synaptic vesicle priming proteins. *Cell* 131:796-808.
- Joseph DJ, Choudhury P, Macdermott AB (2010) An in vitro assay system for studying synapse formation between nociceptive dorsal root ganglion and dorsal horn neurons. *J Neurosci Methods* 189:197-204.
- Ju G, Hokfelt T, Brodin E, Fahrenkrug J, Fischer JA, Frey P, Elde RP, Brown JC (1987) Primary sensory neurons of the rat showing calcitonin gene-related peptide immunoreactivity and their relation to substance P-, somatostatin-, galanin-, vasoactive intestinal polypeptide- and cholecystokinin-immunoreactive ganglion cells. *Cell Tissue Res* 247:417-431.

- Kabachinski G, Yamaga M, Kielar-Grevstad DM, Bruinsma S, Martin TF (2014) CAPS and Munc13 utilize distinct PIP2-linked mechanisms to promote vesicle exocytosis. *Mol Biol Cell* 25:508-521.
- Kaeser PS, Sudhof TC (2005) RIM function in short- and long-term synaptic plasticity. *Biochem Soc Trans* 33:1345-1349.
- Kalla S, Stern M, Basu J, Varoqueaux F, Reim K, Rosenmund C, Ziv NE, Brose N (2006) Molecular dynamics of a presynaptic active zone protein studied in Munc13-1-enhanced yellow fluorescent protein knock-in mutant mice. *J Neurosci* 26:13054-13066.
- Kawabe H, Sakisaka T, Yasumi M, Shingai T, Izumi G, Nagano F, Deguchi-Tawarada M, Takeuchi M, Nakanishi H, Takai Y (2003) A novel rabconnectin-3-binding protein that directly binds a GDP/GTP exchange protein for Rab3A small G protein implicated in Ca(2+)-dependent exocytosis of neurotransmitter. *Genes Cells* 8:537-546.
- Kawabe H, Mitkovski M, Kaeser PS, Hirrlinger J, Opazo F, Nestvogel D, Kalla S, Fejtova A, Verrier SE, Bungers SR, Cooper BH, Varoqueaux F, Wang Y, Nehring RB, Gundelfinger ED, Rosenmund C, Rizzoli SO, Südhof TC, Rhee JS, Brose N (2017) ELKS1 localizes the synaptic vesicle priming protein bMunc13-2 to a specific subset of active zones. *J Cell Biol* 216:1143-1161.
- Khodthong C, Kabachinski G, James DJ, Martin TF (2011) Munc13 homology domain-1 in CAPS/UNC31 mediates SNARE binding required for priming vesicle exocytosis. *Cell Metab* 14:254-263.
- Klar TA, Hell SW (1999) Subdiffraction resolution in far-field fluorescence microscopy. *Opt Lett* 24:954-956.
- Klar TA, Jakobs S, Dyba M, Egner A, Hell SW (2000) Fluorescence microscopy with diffraction resolution barrier broken by stimulated emission. *Proc Natl Acad Sci U S A* 97:8206-8210.
- Knight DE (1999) Secretion from bovine chromaffin cells acutely expressing exogenous proteins using a recombinant Semliki Forest virus containing an EGFP reporter. *Mol Cell Neurosci* 14:486-505.
- Koch H, Hofmann K, Brose N (2000) Definition of Munc13-homology-domains and characterization of a novel ubiquitously expressed Munc13 isoform. *Biochem J* 349:247-253.
- Landry M, Vila-Porcile E, Hokfelt T, Calas A (2003) Differential routing of coexisting neuropeptides in vasopressin neurons. *Eur J Neurosci* 17:579-589.
- Le Pichon CE, Chesler AT (2014) The functional and anatomical dissection of somatosensory subpopulations using mouse genetics. *Front Neuroanat* 8:21.
- Li C, Ullrich B, Zhang JZ, Anderson RG, Brose N, Sudhof TC (1995) Ca(2+)-dependent and -independent activities of neural and non-neural synaptotagmins. *Nature* 375:594-599.
- Li CL, Li KC, Wu D, Chen Y, Luo H, Zhao JR, Wang SS, Sun MM, Lu YJ, Zhong YQ, Hu XY, Hou R, Zhou BB, Bao L, Xiao HS, Zhang X (2016) Somatosensory neuron types identified by high-coverage single-cell RNA-sequencing and functional heterogeneity. *Cell Res* 26:83-102.
- Li L, Rutlin M, Abaira VE, Cassidy C, Kus L, Gong S, Jankowski MP, Luo W, Heintz N, Koerber HR, Woodbury CJ, Ginty DD (2011) The functional organization of cutaneous low-threshold mechanosensory neurons. *Cell* 147:1615-1627.
- Liu Y, Schirra C, Stevens DR, Matti U, Speidel D, Hof D, Bruns D, Brose N, Rettig J (2008) CAPS facilitates filling of the rapidly releasable pool of large dense-core vesicles. *J Neurosci* 28:5594-5601.
- Liu Y, Schirra C, Edelmann L, Matti U, Rhee J, Hof D, Bruns D, Brose N, Rieger H, Stevens DR, Rettig J (2010) Two distinct secretory vesicle-priming steps in adrenal chromaffin cells. *J Cell Biol* 190:1067-1077.

- Lloyd TE, Machamer J, O'Hara K, Kim JH, Collins SE, Wong MY, Sahin B, Imlach W, Yang Y, Levitan ES, McCabe BD, Kolodkin AL (2012) The p150(Glued) CAP-Gly domain regulates initiation of retrograde transport at synaptic termini. *Neuron* 74:344-360.
- Lodish H, Berk A, Zipursky SL, Matsudaira P, Baltimore D, Darnell J (2000) *Molecular cell biology* 4th edition. National Center for Biotechnology Information, Bookshelf.
- Los GV, Encell LP, McDougall MG, Hartzell DD, Karassina N, Zimprich C, Wood MG, Learish R, Ohana RF, Urh M, Simpson D, Mendez J, Zimmerman K, Otto P, Vidugiris G, Zhu J, Darzins A, Klaubert DH, Bulleit RF, Wood KV (2008) HaloTag: a novel protein labeling technology for cell imaging and protein analysis. *ACS Chem Biol* 3:373-382.
- Loyet KM, Kowalchuk JA, Chaudhary A, Chen J, Prestwich GD, Martin TF (1998) Specific binding of phosphatidylinositol 4,5-bisphosphate to calcium-dependent activator protein for secretion (CAPS), a potential phosphoinositide effector protein for regulated exocytosis. *J Biol Chem* 273:8337-8343.
- Lu J, Machius M, Dulubova I, Dai H, Sudhof TC, Tomchick DR, Rizo J (2006) Structural basis for a Munc13-1 homodimer to Munc13-1/RIM heterodimer switch. *PLoS Biol* 4:e192.
- Lundstrom K (2005) Biology and application of alphaviruses in gene therapy. *Gene Ther* 12 Suppl 1:S92-97.
- Lundstrom K (2019) RNA Viruses as Tools in Gene Therapy and Vaccine Development. *Genes (Basel)* 10.
- Lupas AN, Gruber M (2005) The structure of alpha-helical coiled coils. *Adv Protein Chem* 70:37-78.
- Ma C, Li W, Xu Y, Rizo J (2011) Munc13 mediates the transition from the closed syntaxin-Munc18 complex to the SNARE complex. *Nat Struct Mol Biol* 18:542-549.
- Ma C, Su L, Seven AB, Xu Y, Rizo J (2013) Reconstitution of the vital functions of Munc18 and Munc13 in neurotransmitter release. *Science* 339:421-425.
- Malet M, Brumovsky PR (2015) VGLUTs and Glutamate Synthesis-Focus on DRG Neurons and Pain. *Biomolecules* 5:3416-3437.
- Man KN, Imig C, Walter AM, Pinheiro PS, Stevens DR, Rettig J, Sørensen JB, Cooper BH, Brose N, Wojcik SM (2015) Identification of a Munc13-sensitive step in chromaffin cell large dense-core vesicle exocytosis. *Elife* 4.
- Manders EMM, Verbeek FJ, Aten JA (1993) Measurement of co-localization of objects in dual-colour confocal images. *Journal of Microscopy* 169:375-382.
- Marieb EN, Hoehn K (2007) *Human Anatomy & Physiology*: Pearson Benjamin Cummings.
- Martin TF (1994) The molecular machinery for fast and slow neurosecretion. *Curr Opin Neurobiol* 4:626-632.
- Martin TF (2003) Tuning exocytosis for speed: fast and slow modes. *Biochim Biophys Acta* 1641:157-165.
- Mason P (2017) *Medical Neurobiology*: Oxford University Press.
- Matti U, Pattu V, Halimani M, Schirra C, Krause E, Liu Y, Weins L, Chang HF, Guzman R, Olausson J, Freichel M, Schmitz F, Pasche M, Becherer U, Bruns D, Rettig J (2013) Synaptobrevin2 is the v-SNARE required for cytotoxic T-lymphocyte lytic granule fusion. *Nat Commun* 4:1439.
- Maximov A, Tang J, Yang X, Pang ZP, Sudhof TC (2009) Complexin controls the force transfer from SNARE complexes to membranes in fusion. *Science* 323:516-521.
- McCoy ES, Taylor-Blake B, Street SE, Pribisko AL, Zheng J, Zylka MJ (2013) Peptidergic CGRPalpha primary sensory neurons encode heat and itch and tonically suppress sensitivity to cold. *Neuron* 78:138-151.

- Micheva KD, Busse B, Weiler NC, O'Rourke N, Smith SJ (2010) Single-synapse analysis of a diverse synapse population: proteomic imaging methods and markers. *Neuron* 68:639-653.
- Miesenbock G, De Angelis DA, Rothman JE (1998) Visualizing secretion and synaptic transmission with pH-sensitive green fluorescent proteins. *Nature* 394:192-195.
- Mills DS, Marchant-Forde JN (2010) *The Encyclopedia of Applied Animal Behaviour and Welfare*: CABI.
- Moresco JJ, Carvalho PC, Yates JR, 3rd (2010) Identifying components of protein complexes in *C. elegans* using co-immunoprecipitation and mass spectrometry. *J Proteomics* 73:2198-2204.
- Nagano F, Kawabe H, Nakanishi H, Shinohara M, Deguchi-Tawarada M, Takeuchi M, Sasaki T, Takai Y (2002) Rabconnectin-3, a novel protein that binds both GDP/GTP exchange protein and GTPase-activating protein for Rab3 small G protein family. *J Biol Chem* 277:9629-9632.
- Naldini L, Blomer U, Gallay P, Ory D, Mulligan R, Gage FH, Verma IM, Trono D (1996) In vivo gene delivery and stable transduction of nondividing cells by a lentiviral vector. *Science* 272:263-267.
- Neeb A. KH, Schurmann A., Brose N. (1999) Direct interaction between the ARF-specific guanine nucleotide exchange factor msec7-1 and presynaptic Munc13-1. *Eur J Cell Biol* 78:533-538.
- Nguyen Truong CQ, Nestvogel D, Ratai O, Schirra C, Stevens DR, Brose N, Rhee J, Rettig J (2014) Secretory vesicle priming by CAPS is independent of its SNARE-binding MUN domain. *Cell Rep* 9:902-909.
- Pang ZP, Shin OH, Meyer AC, Rosenmund C, Sudhof TC (2006) A gain-of-function mutation in synaptotagmin-1 reveals a critical role of Ca²⁺-dependent soluble N-ethylmaleimide-sensitive factor attachment protein receptor complex binding in synaptic exocytosis. *J Neurosci* 26:12556-12565.
- Parsaud L, Li L, Jung CH, Park S, Saw NM, Park S, Kim MY, Sugita S (2013) Calcium-dependent activator protein for secretion 1 (CAPS1) binds to syntaxin-1 in a distinct mode from Munc13-1. *J Biol Chem* 288:23050-23063.
- Perin MS, Fried VA, Mignery GA, Jahn R, Sudhof TC (1990) Phospholipid binding by a synaptic vesicle protein homologous to the regulatory region of protein kinase C. *Nature* 345:260-263.
- Petrie M, Esquibel J, Kabachinski G, Maciuba S, Takahashi H, Edwardson JM, Martin TF (2016) The Vesicle Priming Factor CAPS Functions as a Homodimer via C2 Domain Interactions to Promote Regulated Vesicle Exocytosis. *J Biol Chem* 291:21257-21270.
- Pope JE, Deer TR, Kramer J (2013) A systematic review: current and future directions of dorsal root ganglion therapeutics to treat chronic pain. *Pain Med* 14:1477-1496.
- Prahlad V, Helfand BT, Langford GM, Vale RD, Goldman RD (2000) Fast transport of neurofilament protein along microtubules in squid axoplasm. *Journal of Cell Science* 113:3939-3946.
- Purves D, Fitzpatrick D, Katz LC, Lamantia AS, McNamara JO, Williams SM, Augustine GJ (2000) *Neuroscience*: Sinauer Associates.
- Ransom BR, Christian CN, Bullock PN, Nelson PG (1977a) Mouse spinal cord in cell culture. II. Synaptic activity and circuit behavior. *J Neurophysiol* 40:1151-1162.
- Ransom BR, Neale E, Henkart M, Bullock PN, Nelson PG (1977b) Mouse spinal cord in cell culture. I. Morphology and intrinsic neuronal electrophysiologic properties. *J Neurophysiol* 40:1132-1150.
- Rao MV, Mohan PS, Kumar A, Yuan A, Montagna L, Campbell J, Veeranna, Espreafico EM, Julien JP, Nixon RA (2011) The myosin Va head domain binds to the neurofilament-L

- rod and modulates endoplasmic reticulum (ER) content and distribution within axons. *PLoS One* 6:e17087.
- Ratai O, Schirra C, Rajabov E, Brunk I, Ahnert-Hilger G, Chitirala P, Becherer U, Stevens DR, Rettig J (2019) An Alternative Exon of CAPS2 Influences Catecholamine Loading into LDCVs of Chromaffin Cells. *J Neurosci* 39:18-27.
- Reim K, Mansour M, Varoqueaux F, McMahon HT, Sudhof TC, Brose N, Rosenmund C (2001) Complexins regulate a late step in Ca²⁺-dependent neurotransmitter release. *Cell* 104:71-81.
- Renden R, Berwin B, Davis W, Ann K, Chin CT, Kreber R, Ganetzky B, Martin TF, Broadie K (2001) *Drosophila* CAPS is an essential gene that regulates dense-core vesicle release and synaptic vesicle fusion. *Neuron* 31:421-437.
- Rhoades R, Bell DR (2009) *Medical Physiology: Principles for Clinical Medicine*: Lippincott Williams & Wilkins.
- Richmond JE, Weimer RM, Jorgensen EM (2001) An open form of syntaxin bypasses the requirement for UNC-13 in vesicle priming. *Nature* 412:338-341.
- Rizo J, Sudhof TC (1998) C2-domains, structure and function of a universal Ca²⁺-binding domain. *J Biol Chem* 273:15879-15882.
- Rizo J, Rosenmund C (2008) Synaptic vesicle fusion. *Nat Struct Mol Biol* 15:665-674.
- Sadakata T, Washida M, Furuichi T (2007a) Alternative splicing variations in mouse CAPS2: differential expression and functional properties of splicing variants. *BMC Neurosci* 8:25.
- Sadakata T, Itakura M, Kozaki S, Sekine Y, Takahashi M, Furuichi T (2006) Differential distributions of the Ca²⁺-dependent activator protein for secretion family proteins (CAPS2 and CAPS1) in the mouse brain. *J Comp Neurol* 495:735-753.
- Sadakata T, Mizoguchi A, Sato Y, Katoh-Semba R, Fukuda M, Mikoshiba K, Furuichi T (2004) The secretory granule-associated protein CAPS2 regulates neurotrophin release and cell survival. *J Neurosci* 24:43-52.
- Sadakata T, Shinoda Y, Sekine Y, Saruta C, Itakura M, Takahashi M, Furuichi T (2010) Interaction of calcium-dependent activator protein for secretion 1 (CAPS1) with the class II ADP-ribosylation factor small GTPases is required for dense-core vesicle trafficking in the trans-Golgi network. *J Biol Chem* 285:38710-38719.
- Sadakata T, Washida M, Iwayama Y, Shoji S, Sato Y, Ohkura T, Katoh-Semba R, Nakajima M, Sekine Y, Tanaka M, Nakamura K, Iwata Y, Tsuchiya KJ, Mori N, Detera-Wadleigh SD, Ichikawa H, Itohara S, Yoshikawa T, Furuichi T (2007b) Autistic-like phenotypes in *Cadps2*-knockout mice and aberrant *CADPS2* splicing in autistic patients. *J Clin Invest* 117:931-943.
- Sampo B, Kaech S, Kunz S, Banker G (2003) Two distinct mechanisms target membrane proteins to the axonal surface. *Neuron* 37:611-624.
- Schroer TA (2004) Dynactin. *Annu Rev Cell Dev Biol* 20:759-779.
- Shaib AH, Staudt A, Harb A, Klose M, Shaaban A, Schirra C, Mohrmann R, Rettig J, Becherer U (2018) Paralogs of the Calcium-Dependent Activator Protein for Secretion Differentially Regulate Synaptic Transmission and Peptide Secretion in Sensory Neurons. *Front Cell Neurosci* 12:304.
- Shen Y, Rosendale M, Campbell RE, Perrais D (2014) pHuji, a pH-sensitive red fluorescent protein for imaging of exo- and endocytosis. *The Journal of Cell Biology* 207:419-432.
- Shinoda Y, Sadakata T, Nakao K, Katoh-Semba R, Kinameri E, Furuya A, Yanagawa Y, Hirase H, Furuichi T (2011) Calcium-dependent activator protein for secretion 2 (CAPS2) promotes BDNF secretion and is critical for the development of GABAergic interneuron network. *Proc Natl Acad Sci U S A* 108:373-378.

- Sollner T, Bennett MK, Whiteheart SW, Scheller RH, Rothman JE (1993a) A protein assembly-disassembly pathway in vitro that may correspond to sequential steps of synaptic vesicle docking, activation, and fusion. *Cell* 75:409-418.
- Sollner T, Whiteheart SW, Brunner M, Erdjument-Bromage H, Geromanos S, Tempst P, Rothman JE (1993b) SNAP receptors implicated in vesicle targeting and fusion. *Nature* 362:318-324.
- Solomon E, Martin C, Martin DW, Berg LR (2014) *Biology*: Cengage Learning.
- Speese S, Petrie M, Schuske K, Ailion M, Ann K, Iwasaki K, Jorgensen EM, Martin TF (2007) UNC-31 (CAPS) is required for dense-core vesicle but not synaptic vesicle exocytosis in *Caenorhabditis elegans*. *J Neurosci* 27:6150-6162.
- Speidel D, Varoqueaux F, Enk C, Nojiri M, Grishanin RN, Martin TF, Hofmann K, Brose N, Reim K (2003) A family of Ca²⁺-dependent activator proteins for secretion: comparative analysis of structure, expression, localization, and function. *J Biol Chem* 278:52802-52809.
- Speidel D, Bruederle CE, Enk C, Voets T, Varoqueaux F, Reim K, Becherer U, Fornai F, Ruggieri S, Holighaus Y, Weihe E, Bruns D, Brose N, Rettig J (2005) CAPS1 regulates catecholamine loading of large dense-core vesicles. *Neuron* 46:75-88.
- Sudhof TC (2004) The synaptic vesicle cycle. *Annu Rev Neurosci* 27:509-547.
- Sudhof TC, Rothman JE (2009) Membrane fusion: grappling with SNARE and SM proteins. *Science* 323:474-477.
- Sunil N, Lee S, Shea TB (2012) Interference with kinesin-based anterograde neurofilament axonal transport increases neurofilament-neurofilament bundling. *Cytoskeleton (Hoboken)* 69:371-379.
- Tandon A, Bannykh S, Kowalchuk JA, Banerjee A, Martin TF, Balch WE (1998) Differential regulation of exocytosis by calcium and CAPS in semi-intact synaptosomes. *Neuron* 21:147-154.
- Tang Y, Garson K, Li L, Vanderhyden BC (2015) Optimization of lentiviral vector production using polyethylenimine-mediated transfection. *Oncol Lett* 9:55-62.
- ten Have S, Boulon S, Ahmad Y, Lamond AI (2011) Mass spectrometry-based immunoprecipitation proteomics - the user's guide. *Proteomics* 11:1153-1159.
- Tortosa E, Adolfs Y, Fukata M, Pasterkamp RJ, Kapitein LC, Hoogenraad CC (2017) Dynamic Palmitoylation Targets MAP6 to the Axon to Promote Microtubule Stabilization during Neuronal Polarization. *Neuron* 94:809-825.e807.
- Usoskin D, Furlan A, Islam S, Abdo H, Lonnerberg P, Lou D, Hjerling-Leffler J, Haeggstrom J, Kharchenko O, Kharchenko PV, Linnarsson S, Ernfors P (2015) Unbiased classification of sensory neuron types by large-scale single-cell RNA sequencing. *Nat Neurosci* 18:145-153.
- van de Bospoort R, Farina M, Schmitz SK, de Jong A, de Wit H, Verhage M, Toonen RF (2012) Munc13 controls the location and efficiency of dense-core vesicle release in neurons. *J Cell Biol* 199:883-891.
- van Keimpema L, Kooistra R, Toonen RF, Verhage M (2017) CAPS-1 requires its C2, PH, MHD1 and DCV domains for dense core vesicle exocytosis in mammalian CNS neurons. *Sci Rep* 7:10817.
- Varoqueaux F, Sigler A, Rhee JS, Brose N, Enk C, Reim K, Rosenmund C (2002) Total arrest of spontaneous and evoked synaptic transmission but normal synaptogenesis in the absence of Munc13-mediated vesicle priming. *Proc Natl Acad Sci U S A* 99:9037-9042.
- Vigna E, Naldini L (2000) Lentiviral vectors: excellent tools for experimental gene transfer and promising candidates for gene therapy. *J Gene Med* 2:308-316.

- Wake H, Ortiz FC, Woo DH, Lee PR, Angulo MC, Fields RD (2015) Nonsynaptic junctions on myelinating glia promote preferential myelination of electrically active axons. *Nat Commun* 6:7844.
- Walent JH, Porter BW, Martin TF (1992) A novel 145 kd brain cytosolic protein reconstitutes Ca(2+)-regulated secretion in permeable neuroendocrine cells. *Cell* 70:765-775.
- Wang H, Rivero-Melian C, Robertson B, Grant G (1994) Transganglionic transport and binding of the isolectin B4 from *Griffonia simplicifolia* I in rat primary sensory neurons. *Neuroscience* 62:539-551.
- Watanabe M, Nomura K, Ohyama A, Ishikawa R, Komiya Y, Hosaka K, Yamauchi E, Taniguchi H, Sasakawa N, Kumakura K, Ushiki T, Sato O, Ikebe M, Igarashi M (2005) Myosin-Va regulates exocytosis through the submicromolar Ca²⁺-dependent binding of syntaxin-1A. *Mol Biol Cell* 16:4519-4530.
- Waterman-Storer CM, Karki SB, Kuznetsov SA, Tabb JS, Weiss DG, Langford GM, Holzbaur EL (1997) The interaction between cytoplasmic dynein and dynactin is required for fast axonal transport. *Proc Natl Acad Sci U S A* 94:12180-12185.
- Watkins AM, Wuo MG, Arora PS (2015) Protein-Protein Interactions Mediated by Helical Tertiary Structure Motifs. *Journal of the American Chemical Society* 137:11622-11630.
- Westphal V, Hell SW (2005) Nanoscale resolution in the focal plane of an optical microscope. *Phys Rev Lett* 94:143903.
- Xia X, Lessmann V, Martin TF (2009) Imaging of evoked dense-core-vesicle exocytosis in hippocampal neurons reveals long latencies and kiss-and-run fusion events. *J Cell Sci* 122:75-82.
- Zhou KM, Dong YM, Ge Q, Zhu D, Zhou W, Lin XG, Liang T, Wu ZX, Xu T (2007) PKA activation bypasses the requirement for UNC-31 in the docking of dense core vesicles from *C. elegans* neurons. *Neuron* 56:657-669.

Publications and Conferences

Staudt A, Ratai O, Bouzouina A, Fecher-Trost C, Shaaban A, Bzeih H, Horn A, Shaib AH, Klose M, Flockerzi V, Lauterbach MA, Rettig J, Becherer U. Localization of CAPS1 and CAPS2 in mouse sensory neurons is determined by its N-terminus. (Submitted for publication).

Shaib AH, Staudt A, Harb A, Klose M, Shaaban A, Schirra C, Mohrmann R, Rettig J, Becherer U (2018) Paralogs of the Calcium-Dependent Activator Protein for Secretion Differentially Regulate Synaptic Transmission and Peptide Secretion in Sensory Neurons. *Front Cell Neurosci* 12:304.

Dinkel H, Van Roey K, Michael S, Kumar M, Uyar B, Altenberg B, Milchevskaya V, Schneider M, Kuhn H, Behrendt A, Dahl SL, Damerell V, Diebel S, Kalman S, Klein S, Knudsen AC, Mader C, Merrill S, Staudt A, Thiel V, Welti L, Davey NE, Diella F, Gibson TJ (2016) ELM 2016-data update and new functionality of the eukaryotic linear motif resource. *Nucleic Acids Res* 44: D294-300.

Poster: Staudt A, Shaib AH, Ratai O, Shaaban A, Bzeih H, Mohrmann R, Rettig J, Becherer U (2018) Mechanism of CAPS1 and CAPS2 differential subcellular localization. *Europhysiology*, London, UK.

Poster: Staudt A, Shaib AH, Ratai O, Shaaban A, Bzeih H, Mohrmann R, Rettig J, Becherer U (2019) Functional analysis of calcium-dependent activator protein for secretion 1 and 2 differential subcellular localization. *Neuroscience*, Chicago, USA.

Aus datenschutzrechtlichen Gründen wird der Lebenslauf in der elektronischen Fassung der Dissertation nicht veröffentlicht.

